REMOTE SENSING LEAF AREA INDEX (LAI) DATA ASSIMILATION WITH CROP MODEL FOR YIELD PREDICTIONS IN RICE

A Thesis

Submitted to

Centurion University of Technology and Management

In partial fulfillment of the requirements for the award of the degree of

DOCTOR OF PHILOSOPHY (AGRICULTURE)
IN
AGRONOMY

By

MANDAPATI ROJA

(Registration No. 190506192004)

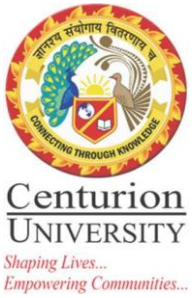

Department of Agronomy and Agroforestry

M. S. Swaminathan School of Agriculture

Centurion University of Technology and Management, Paralakhemundi

Dist.: Gajapati – 761211, Odisha, India

www.cutm.ac.in

May, 2024

REMOTE SENSING LEAF AREA INDEX (LAI) DATA ASSIMILATION WITH CROP MODEL FOR YIELD PREDICTIONS IN RICE

A Thesis

Submitted to

Centurion University of Technology and Management

In partial fulfillment of the requirements for the award of the degree of

DOCTOR OF PHILOSOPHY (AGRICULTURE)
IN
AGRONOMY

By

MANDAPATI ROJA

(Registration No.190506192004)

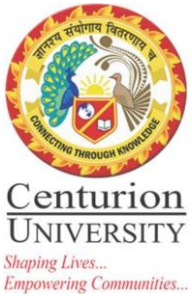

Department of Agronomy and Agroforestry

M. S. Swaminathan School of Agriculture

Centurion University of Technology and Management, Paralakhemundi

Dist.: Gajapati – 761211, Odisha, India

www.cutm.ac.in

May, 2024

DECLARATION

I, declare that the thesis entitled **"Remote sensing leaf area index (LAI) data assimilation with crop model for yield predictions in rice"** is my own work conducted under the supervision of **Dr. M. Devender Reddy, Professor and Dean, Department of Agronomy and Agroforestry,** M. S. Swaminathan School of Agriculture, Centurion University of Technology and Management, Paralakhemundi, Odisha and approved by Research Advisory Committee.

I, further declare that this thesis does not contain any part of any work which has been submitted for the award of any degree either in the University or in any other University without proper citation.

Place: Paralakhemundi **(Mandapati Roja)**

Date: **Signature of the Candidate**

CERTIFICATE - I

This is to certify that the thesis entitled **"Remote sensing leaf area index (LAI) data assimilation with crop model for yield predictions in rice"** Submitted to M. S. Swaminathan School of Agriculture is a piece of research work done by **MANDAPATI ROJA** with **Registration No. 190506192004** under my guidance and supervision for the partial fulfilment of the degree of **Doctor of Philosophy (Agriculture) in Agronomy.**

To the best of my knowledge and belief the thesis

1. Embodies the work of candidate himself.
2. Has duly been completed.
3. Fulfils the requirement of the ordinance relating to the **Doctor of Philosophy (Agriculture) in Agronomy** degree of the University.

Place: Paralakhemundi

Date:

M. Devender Reddy
Chairperson
Professor and Dean
Department of Agronomy and Agroforestry
M. S. Swaminathan School of Agriculture
Centurion University of Technology and Management
Paralakhemundi, Odisha

CERTIFICATE – II

This is to certify that the thesis entitled **"Remote sensing leaf area index (LAI) data assimilation with crop model for yield predictions in rice"** has been prepared and submitted by **Mandapati Roja** with **Registration No. 190506192004** in partial fulfilment of the requirements for the award of degree of **Doctor of Philosophy (Agriculture) in the discipline of Agronomy** has been examined and approved by the Evaluation Committee after viva-voce.

External Examiner signature:
Name:
Designation:

Research Advisory Committee

Chairperson **Dr. M. Devender Reddy**
Professor and Dean
Department of Agronomy and Agroforestry
M. S. Swaminathan School of Agriculture
Centurion University of Technology and
Management, Odisha

Co-Chairperson **Dr. Murali Krishna Gumma**
Cluster Leader and Principal Scientist
Geo-Spatial and Big Data Sciences
International Crop Research Institute for
the Semi-Arid Tropics (ICRISAT)
Patancheru, Hyderabad, Telangana

Member **Dr. Sagar Maitra**
Professor and Head
Department of Agronomy and Agroforestry
M. S. Swaminathan School of Agriculture
Centurion University of Technology and
Management, Odisha

Member **Dr. Soumik Roy**
Assistant Professor and Head
Department of Statistics
M. S. Swaminathan School of Agriculture
Centurion University of Technology and
Management, Odisha

Date of final viva-voce: _____

Head
Department of Agronomy and Agroforestry
M. S. Swaminathan School of Agriculture
Centurion University of Technology
and Management, Odisha

Dean
M. S. Swaminathan School of Agriculture
Centurion University of Technology
and Management, Odisha

Dedicated
to
my family

ACKNOWLEDGEMENT

I wish to start by expressing my profound gratitude to the Almighty for bestowing upon me the strength and blessings to complete this thesis.

The depth of my appreciation for those who have significantly influenced my research journey is beyond words. I am genuinely thankful to all of them. This project is the result of years of dedicated effort, and I am deeply indebted to the numerous individuals who have directly and indirectly supported me in its successful completion.

My deepest gratitude goes to ***Dr. M. Devender Reddy*** *, Professor and Dean, M.S. Swaminathan School of Agriculture, Centurion University of Technology and Management, Paralakhemundi, Odisha for serving as my primary advisor and for your invaluable guidance, encouragement, and unwavering support throughout this project. Your expertise and mentorship have been instrumental in shaping my research and keeping me motivated.*

It is a remarkable chance to convey my profound gratitude for this momentous occasion to my major advisory person ***Dr. Gumma Murali Krishna****, Cluster Leader and Principal Scientist, Geo-spatial and Big Data Science, ICRISAT. I am incredibly grateful to you for providing me with the exceptional opportunity to conduct research at ICRISAT. Your leadership, vision, and ongoing support have been a source of immense inspiration.*

I would like to thank ***Dr. Sagar Maitra****, Professor and Head, Department of Agronomy and* ***Dr. Soumik Roy****, Assistant Professor and Head, Department of Statistics, M.S. Swaminathan School of Agriculture for your valuable feedback, suggestions, and insights on my research. Your contributions significantly enhanced the quality and refinement of my work.*

My sincere thanks to ***Mr. Pranay, Mr. B. Pavan Kumar,*** *and* ***Md. Rafi Ismail*** *each of you for your invaluable support during field data collection. Your dedication and hard work were essential to this crucial aspect of my research. I would like to express my appreciation to the entire team of Geo-spatial and Big Data Science, ICRISAT Remote Sensing, especially* ***Mr. Ishrad, Snigdha, Rajani,*** *and* ***Vineetha*** *for your assistance and collaboration throughout the research process.*

I would like to thank ***S.P Nanda*** *(CUTM) and* ***Dr.K. Dhakshina Murthy*** *(ANGRAU) your support and guidance during my studies and Research. My heartful thanks to Learning System Unit -* ***Pratap*** *and* ***Nalini*** *for your assistance with the intake process at ICRISAT.*

Words cannot express my heartfelt gratitude to my Parents ***M. Prasada Rao*** *and* ***M. Padmavathi****, In-Laws* ***P. Siva Prasad*** *and* ***Annapurna****, Husband* ***P. Chaitanya Kumar*** *and Son* ***Manvik*** *for their unwavering love, support, and encouragement throughout my academic journey. Your sacrifices and understanding allowed me to focus on my research and complete this project.*

*As members of my maternal and extended family **P. Krishna Kishore, M. Venkatesh, and M. Sravanthi,** your unwavering support has been greatly appreciated. Your encouragement and belief in me have been a source of strength throughout this journey.*

*I appreciate **Ramalaxmi, Deepayan, Sagar,** and **Sairam** for the camaraderie and support we shared during our studies. Thank you for **Karimnagar Agricultural Extension Officers** by providing timely input data, which was crucial for my research.*

My thanks to the entire department of Agronomy, MSSSOA, CUTM for creating a supportive learning environment.

*Thank you **Deepu, Raghuveer, Parvathi, VM Rao, VB Rao, Preethi, Priya, Rahul, Bujji, Srinu, Praneeth, Sai, Chandu, Suneetha, Eswari and Shivansh** for your friendship and for believing in me.*

In addition, I would like to acknowledge the many supporters and critics who have accompanied me throughout this journey. While I may not be able to name each one of you, please know that your contributions, whether they were words of encouragement or constructive criticism, have been invaluable to my growth and the successful completion of this thesis. Thank you.

In conclusion, I am incredibly fortunate to have such a wonderful network of support. This thesis would not have been possible without your contributions.

MANDAPATI ROJA

LIST OF CONTENTS

LIST OF TABLES

LIST OF FIGURES

LIST OF PLATES

LIST OF ABBREVIATION

Abbreviation	Words
%	Per cent
*.prn	Formatted Text (Space delimited)
<	Less than
>	More than
=	Equal to
℃	Degree Celsius
ICAR	Indian Council of Agricultural Research
USDA	United States Development Authority
t ha–1	Tonn per hectare
Kg ha-1	Kilo grams Per hecatre
DSSAT	Decision Support System for Agro Technology Transfer
APSIM	Agricultual Production System SIMulator
CSM	Cropping System Model
CERES	Crop Environment Resource Synthesis
LAI	Leaf Area Index
NDVI	Normalized Difference Vegetation Index
CCE	Crop Cutting Experiment
FAO	Food and Agricultural Organization
IASRI	Indian Agricultural statistics Research Institute
NDWI	Normalized Difference Water Index
SAE	Small Area Estimation
GCE	General Crop Estimation Survey
GLF	Gravimetric Leaf and Foliage
PASTIS-57	PAI Autonomous System from Transmittance Instantaneous Sensors oriented at 57°
cm2	Centimeter Square
R2	Corelation
SML	Supervised Machine Learning
SMT	Spectral Matching Technique
RF	Random Forest
SVM	Support Vector Machine
CART	Classification and Regression Trees
VV	Vertical transmit and Vertical receive
VH	Vertical transmit and Horizontal receive
DCRF’s	Dynamic Conditional Random Fields
UAVSAR	Uninhabited Aerial Vehicle Synthetic Aperture Radar
MODIS	Moderate Resolution Imaging Spectroradiometer
GEE	Google Earth Engine

MLA’s	Machine Learning Algorithms
ETM	Enhanced Thematic Mapper
LULC	Land Use/Land Cover Classifications
GIDA	Ghana's Irrigation Development Authority
MSI	Multispectral Sensor
SVM	Support Vector Machines
FFE	Feature Filtering And Enhancement
SPOT	Satellite for Observation of Earth
MACCS	Multi-Sensor Atmospheric Correction And Cloud Screening
ACCA’s	Automated Cropland Classification Algorithms
ESA	European Space Agency
ISODATA	Iterative Self-Organizing Data Analysis Techniques
ERDAS	Earth Resources Data Analysis System
RMSE	Root Mean Square Error
ET	Evapo Transpiration
RCP	Representative Climate
NSE	Nash–Sutcliffe Efficiency
CO2	Carbon Dioxide
PJTSAU	Professor Jayashankar Telangana State Agricultural University
N ha-1	Nitrogen Per Hectare
SEBAL	Surface Energy Balance Algorithm For Land
MPAE	Mean Absolute Percentage Error
LCC	Leaf Chlorophyll Content
CCC	Canopy Chlorophyll Content
WDVI	Weighted Difference Vegetation Index
SAVI	Soil Adjusted Vegetation Index
OLI	Operational Land Imager
EVI-1	Enhanced Vegetation Index
CV	Coefficients of Variations
FPAR	Fraction of Photo Synthetically Active Radiation
GEPIC	GIS-Based Environment Policy Integrated Climate
OSAVI	Optimal Soil-Adjusted Vegetation Index
CI	Chlorophyll Index
SI	Stress Index
WOFOST	World Food Studies
MSR	Modified Simple Ratio
NDRE	Normalized Difference Red Edge
EPIC	Erosion Productivity Impact Calculator
MSR	Modified Simple Ratio
NDRE	Normalized Difference Red Edge

PSO	Particle Swarm Optimization
NRMSE	Normalized Root Mean Square Error
KLIP	Kaleshwaram Lift Irrigation Project
NBSSLUP	National Bureau of Soil Survey and Land Use Planning
CHIRPS	Climate Hazards Group Infrared Precipitation With Station Data
DEM	Digital Elevation Model
PAR	Photosynthetically Active Radiation
GPS	Global Positioning System
AOI	Area of Interest
.WTH	Weather
CSV	Comma Separated Values
EC	Electrical Conductivity
Ph	Potential of Hydrogen
ISRIC	The International Soil Reference And Information Centre
RCN	Runoff Curve Number
GDD	Growing Degree Days
GLUE	Generalized Likelihood Uncertainty Estimation
ME	Modeling Efficiency
NIR	Near Infra Red
SAR	Synthetic Aperture Radar
IW	Interferometric Wide
ESRI	Environmental System Research Institute
GIS	Geographic Information System
ID	Identification
Ha	Hectares
ML	Machine Learning
DL	Deep Learning

ABSTRACT

MANDAPATI ROJA **Registration No - 190506192004**

Year of Admission - 2019 **Degree - Doctor of Philosophy (Agriculture) Agronomy**

Crop yield estimation has gained prominent importance due to its vital significance for policymakers and decision-makers in enacting schemes, ensuring food security, and assessing crop insurance losses due to biotic and abiotic stress. Precise and timely crop yield estimates at regional, national and international levels is essential for making policy to overcome food security worldwide and helping farmers for crop insurance through insurance premium pricing by the companies. Rice is considered the major staple food which is having highest area and production in India. Telangana contributes to 4.49 % of rice area (1.9 million ha) and 5.54 % of production (6.25 million tons) with a productivity of 3176 kg ha-1.

Several studies revealed that remote sensing technology had resulted in higher accuracy in crop growth monitoring with added advantage of high revisit frequency and precision. On the other hand, crop simulation models were also been recognized to assess the effects of different scenarios like climate change, drought, stress etc., on crop yield under varied climatic conditions. LAI is main criterion for evaluating the grain yield as it shows good correlation with the grain yield. There are lack of studies on comparing the ceptometer LAI to any crop model simulated LAI and also yields estimation at local level though they were done at a broad level like state or district. Hence this research was focused on rice yield estimation at the field level in the Karimnagar district of Telangana during 2021 and 2022 by employing the leaf area index (LAI) as the primary criterion for integrating remote sensing technology and crop simulation models.

Optimization of crop cutting experiments were performed based on the criterion encompassing a wide range of potential combinations, further four villages each in Kharif and Rabi were selected for study and 15 fields were selected in each village for study. Ground data visits were planned according to the satellite passing dates and during the visits LAI readings in each field were collected using the LP-80 ceptometer. Supervised classification was performed using the ERDAS imagine. It has been noted that most of the area in the district was occupied by rice in both the seasons. Accuracy showed that

overall accuracy of 94.23% and 88.5% was recorded, while kappa coefficient of 0.89 and 0.85 was resulted in kharif and rabi season respectively.

On an average, kharif and rabi rice grain yields were 5324 kg ha-1 and 6436 kg ha-1 respectively in selected villages. The average simulated rice grain yield in kharif and rabi were 5339 kg ha-1 and 6858 kg ha-1 respectively with DSSAT model which considered sentinel-2 satellite for estimation of LAI. The R2 values of above 0.72 in kharif and above 0.85 in rabi, D index of 0.70 in both the seasons in all the villages showed the model is accurate for predicting yields.

In both the seasons, correlation of above 0.8 was observed between observed rice grain yield with the quantity of nitrogen applied, whereas above 0.77 was noted between ceptometer measured and model simulated LAI. However LAI showed a good R2 of above 0.75 with the grain yield. Due to its strong correlation with LAI of above 0.80, the Normalized Difference Vegetation Index (NDVI) was selected as the critical element for integration with the model. Hence, it can be noted that NDVI is one among the important parameter which can be used to integrate with LAI for grain yield estimation. By utilizing the linear equation generated between the NDVI and model LAI a spatial LAI map was generated for the Karimnagar district. Further the linear equation developed between the model LAI and model grain yield, spatial yield map was generated. From the spatial yield map, it can be concluded that most of the areas fall under the rice grain yield range of 5700 to 6000 kg ha-1 in kharif, while in rabi in the range of 6500 to 7000 kg ha-1. These spatial mean yields for kharif and rabi were 5300 kg ha-1 and 6458 kg ha-1 which were then compared with the Telanagana government statistics and it has been noted that a deviation of less than 10 %. Therefore, this study’s findings show that assimilating remote sensing data with crop models enhances the precision of rice yield prediction for insurance companies and policy- and decision-makers.

Chapter I

INTRODUCTION

In India, of the 328.73 million ha of land area, 197.05 million ha is the gross cropped area. Cereals occupy 51.33 % of the gross cropped area and out of which 22.30 % comes under rice (ICAR agricultural research data book 2020). Rice is considered the major staple food which is having highest area and production in India. In India, during 2020-21, the cultivated area, production, and productivity under rice is around 44 million ha, 121 million tons, and 4.1 metric tons per hectare respectively (USDA 2021- Department of agriculture and cooperation).

Telangana comes under the southern plateau and hills agro-climatic zone. Rice is one of the major crops grown in this state. Telangana contributes to 4.49 % of rice area (1.9 million ha) and 5.54 % of production (6.25 million tons) with a productivity of 3176 kg ha^{-1}. With the development of irrigation resources, there has been a remarkable increase in rice-cultivable areas in the state during the last few years.

Prediction of crop area and yield before harvest will be useful in estimating loss determination for crop insurance schemes. This is required more for countries like India as the economy depends on agriculture and its allied sectors. Crop yields depend on multiple factors like genotype, environment, and their interactions hence, understanding these relations is of top priority for yield predictions. For effective agricultural land management, policymaking, and long-term agricultural food production, precise and timely crop yield estimation is vital (Masson-Delmotte *et al.* 2018). Traditional methods like crop cutting can be used for yield estimation as they are more effective for agricultural management policies (Dwivedi *et al.* 2019), but they are expensive, time-consuming, and error-prone and the availability of information from these is not up-to-date. Monitoring and estimating yields promptly plays a crucial role in decision-making and pricing insurance premiums, as it protects farmers with small holdings from risk and influences markets, export-import decisions, and farm income planning (Choudhury & Jones, 2014 Zhao *et al.* 2020). Many methods, such as empirical formulae, remote sensing, and modeling have been used to estimate yield. Remote sensing has shown to be quite useful in monitoring agricultural crop growth and scheduling irrigation. All of these methods have pros and cons, such as the lack of accurate data from the beginning

to the end of the crop season for running models and the availability of satellite data during cloud periods.

During recent years, crop yield predictions have used empirical formulae, remote sensing, and simulation models. Although studies have been conducted to validate the use of remote sensing data in calculating crop yields, the majority of them have used empirical methodologies for specific locations, crops, cultivars, and crop growth phases. Similarly, researchers used crop models to simulate crop development and production on a regional scale. Using accurate, cost-effective, and easy methods for crop yield estimation at local scales is the main objective of remote sensing agricultural applications (Ahmed *et al.* 2014; Dong *et al.* 2016; Mosleh, 2015; Noureldin *et al.* 2013). Integration of these two technologies results in an increase in output efficiency (Fang et al. 2011; Pitman, 2000; Muslim et al. 2015; Schut *et al.* 2009).

Remote sensing (RS) technologies offer a diagnostic tool that can serve as an early warning system, enabling the agricultural community to respond early to manage possible problems before they spread widely and severely affect crop yield. By employing space-borne sensors, remote sensing acquires synoptic (local to regional coverage) and repetitive (minutes to days) data regarding the spectral performance of crops in dynamic environments (soil and atmosphere). Timely monitoring is dependent on remote sensing methods, which furnish a precise image of the crops with a high frequency of revisits and precision (Shanmugapriya et al. 2019).Remote sensing has a wide range of applications which can be used to estimate yield (Doraiswamy *et al.* 2004; Bernerdes *et al.* 2012), crop phenological information (Sakamoto *et al.* 2005), identify stress circumstances (Gu *et al.* 2007), and detect disruptions (Bellam *et al*., 2023).

Crop models are a set of empirical equations that examine crop growth and development by incorporating crop, weather, soil, and management strategies that have been introduced since the 1960s. They have a wide range of applications since they will replace the time required to conduct expensive and time-consuming field experiments with a greater number of iterations that can be pre-evaluated within minutes (Steduto *et al.* 2009). Crop models are essential for analyzing how climate variability and management practices affect crop yield and environmental performance to encourage better and more sustainable agriculture (Xiong *et al.* 2014). Among the wide range of crop simulation models DSSAT (Ray *et al.* 2018; Alejo *et al.* 2020), APSIM

(Amarasingha et al. 2015 and Yang *et al.* 2021), Infocrop (Kaur and Kaur 2022), Aquacrop (Kumar et al. 2014 and Gebreselassie et al. 2015) and Oryza (Yuan et al. 2017 and Lu et al. 2020) were used for predicting yield.

The Cropping System Model (CSM)-Crop Environment Resource Synthesis (CERES) model, which can be used for 42 crops, is part of the Decision Support System for Agro-technology Transfer (DSSAT), a computer program that forecasts crop growth, development, and yield based on interactions between soil, water, weather, atmosphere, plants, and crop management (Jones *et al.* 2003). CERES modules included in DSSAT which replicate key crop growth and development processes such as phenological development, canopy leaf area increase, dry matter accumulation, and grain production. Past findings at various locations evaluated the CERES-Rice and Maize models, showing high agreement between predicted and observed findings (Gumma *et al.* 2022, Mirakhori et al. 2017, Kadiyala et al., 2015; Alejo et al. 2020; Timsina and Humphreys, 2006; Behera and Panda, 2009; Liu *et al.* 2017; He *et al.* 2012; Ngwira *et al.* 2014). DSSAT is one of the crop models that has been widely used for yield gap analysis (Singh *et al.* 2008 ; Balderama *et al.* 2016). Even though there are often some uncertainties in the simulation findings due to inputs and model parameters, simulation models can still be successfully used as a scientific tool to improve cropping system resource use efficiency (Timsina *et al.* 2008). In comparison to various other crop models, DSSAT can operate effectively with few input parameters. Scanty research has been conducted in a selected area using the DSSAT model for yield estimation in rice.

Remote sensing and crop growth models are two distinct technologies that can solve many field and regional agronomic issues (Batchelor *et al.* 2002). Leaf area is defined as leaf area per unit ground area which is considered as the chief parameter for plant growth and productivity that is directly related to the yield of the crop and used for biophysical modeling (Parker 2020, stark *et al.* 2012 and Yan *et al.* 2019). The leaf area index can be calculated by direct and indirect methods. To overcome the limitations, indirect methods of leaf area measurement can be done by use of an LP-80 ceptometer which measures photosynthetically active radiation by non-destructive sampling. Several investigations have derived biophysical variables from satellite images and included them in simulation models (Hui & Yao, 2018; Yu *et al.* 2019).

The augmented data collection frequency of satellites, coupled with their capability to acquire data over a broad area, has contributed to the growing utilization of integrative approaches that combine remotely sensed data with crop simulation models for the estimation of crop yields. To accomplish this goal, the LAI that is derived from satellite data is subjected to daily interpolation to supply daily observations that are compatible with the interactive time-step of crop models. For modeling crop growth and yield, there is a need to take into account the various elements that can affect the outcome of the projection. In order to estimate crop yields through modeling, meteorological and climate data (including rainfall, sunshine hours and surface temperature), soil properties, and management strategies are integrated with spatially explicit remote sensing-derived data, including vegetation and slope indices (NDVI). This information is used to create a crop growth model (Dorigo *et al.* 2007).

By taking the above-targeted research areas on yield estimation, the study on "**Remote sensing leaf area index (LAI) data assimilation with crop model for yield predictions in rice"** was designed with the following objectives.

1. Optimization of crop cutting experiments (CCE) locations for the respective study area.
2. Crop yield estimation based on the DSSAT model.
3. Comparison of simulated LAI from remote sensing satellite data and DSSAT model.

Chapter II

REVIEW OF LITERATURE

An effort has been made to collect and present the available literature related either directly or indirectly to the present research on assimilation of remote sensing data into crop simulation models for rice yield estimation under the following subheadings.

2.1 Optimizing the CCE locations

Subjective crop yield estimation methods include farmers' judgments and expert views which are not so accurate. Objective yield measurement approaches like whole-plot harvesting are costly and time-consuming. This led to the development of the Crop Cutting Experiment (CCE) in India as a method for estimating crop yield based on sampling small subplots within cultivated fields by pioneers in sampling and survey design.

Ahmad *et al.* (2021) designed a sample approach for estimating harvest and post-harvest losses of crops/commodities using CCE methodologies for actual measurement-based primary data collection, which was approved by FAO in Rome. The established methodology was field tested in two FAO-identified countries, one in Africa and one in the Latin America/Caribbean region, namely Zambia and Mexico. Enumerators, Supervisors/Master trainers, and nominated authorities in both countries received

classroom and field instruction for filling up schedules and different techniques for performing Crop Cutting Experiments from ICAR-IASRI personnel.

Kabir *et al.* (2016) formulated a protocol for conducting CCEs under different crop cut methods in Bangladesh and suggested performing at least two cuts per plot to minimize error regarding over and under estimation with a circle radius of 178.5 cm covering $10m^2$ for easy conversion.

The remote sensing products like NDVI, NDWI, were combined with CCEs conducted through crop-cutting experiments under Pradhan Mantri Fasal Bima Yojana in Orissa to inspect whether CCE points contributing to high yields fall under the good NDVI zone or not (Dubey *et al.* 2019). NDVI data and CCEs data have been sub-grouped into 4 classes with a certain range and it has been noticed that there was a 75 % similarity between the CCE and vegetation index strata.

Aditya *et al.* (2020) showed reduced number of crop-cutting experiments and estimation of crop yield at the district level using Aggregate level Small Area Estimation (SAE). Results from SAE were compared with the GCEs and found that similar yields were seen with SAE with the added advantage of reduced sample size.

Gumma *et al.* (2022) validated crop yields with crop-cutting experiments based on the optimization techniques. Crop-type map data, availability of rain gauges, soil types, and area statistics of each crop in each specified location were considered as the prime criteria for optimization of CCE's.

2.2 Methods of Leaf Area Index Estimation

LAI is the ratio between leaf area and ground surface area (Watson, 1947). LAI is the key input bio-physical parameter for assessing yield as it is directly related to the growth of the plant. It has been extensively used in agriculture and remote sensing studies including smart agriculture and crop models. LAI can be estimated by two methods either directly or indirectly. Direct method like the gravimetric method and planimetric method involves the destruction of leaves which is laborious, time-consuming and costly compared to other methods. Based on the correlation between leaf dry weight and leaf area (wet leaf to dry leaf ratio) gravimetric method is used (Jonckheere *et al.* 2004). The planimetric method of LAI estimation is the correlation between individual leaf area measured by the device and this method is considered as the most accurate method which is used to validate other

methods but the only constraint with this is its implementation over large scale which is not feasible. Indirect methods involve a sequence of readings with specific instruments based on light transmittance.

Aschonitis *et al.* (2014) using the gravimetric leaf and foliage (GLF) method estimated the LAI of rice in an evapotranspiration experiment using lysimeter and concluded that LAI estimations were significantly correlated (R^2= 0.86) with grain yields and other crop factors. It has been reported that this method can be used for crop modelling studies as frequent destruction of samples is not possible in the fields and the variability between replications in experimental plots is not accepted.

Campose Taberner *et al.* (2015) compared indirect LAI estimates collected from three pieces of equipment such as LAI-2000, Pocket LAI, and digital cameras. Pocket LAI is a smartphone application used for measuring LAI based on the segmentation of images taken at 57.5^0 below the canopy. In digital photography, computation of LAI is done by gauging gap fraction. Photographs were taken downward looking and a minimum of 1m distance was set between the camera and the top canopy and the photographs were processed using CAN-EYE3 software to estimate LAI from gap fraction measured at an angle of 57.5^0 because at this angle the information acquired is independent of leaf angle distribution and clumping effect will be minimized. LAI-2000 and DHP outcomes were then compared with pocket LAI during the growing period. LAI values from all three were well correlated. Pocket LAI was correlated with LAI 2000 and DHP. It has been concluded that pocket LAI is an alternative to classical instruments.

Fang *et al.* (2018) evaluated the performance of automatic instrument (PASTIS-57) and smart phone applications (LAI smart and Pocket LAI) to estimate LAI in maize, soybean, and sorghum throughout the growing season. These results were validated against LAI-2000, DHP, and destructive sampling methods. A relative error of <5%, < 20%, -20 to -30 % were observed with PASTIS -57, LAI smart and pocket LAI over LAI 2200 and DHP. It has been concluded that PASTIS-57 can be used for continuous LAI estimation in agricultural crops over the other methods.

Casa *et al.* (2019) estimated LAI in maize, wheat, alfa alfa and broad beans using a sun-scan ceptometer, LAI 2000, DHP and pocket LAI. R^2 of 0.54, 0.62, 0.82 and 0.62 were observed under sun-scan ceptometer, LAI 2000, DHP and pocket LAI. In terms of

accuracy, the hemispherical photography-based method, which was subsequently followed by LAI-2000, exhibited the highest performance among the employed methods.

Wilhelm *et al.* (2000) used three different LAI meters (AccuPAR, LAI-2000, and SunScan) to estimate the LAI in maize at Shelton and this was compared with the destructive sampling. A correlation was observed with individual meter with the field LAI (Destructive LAI). R^2 value of 0.94, 0.93, 0.79 was observed under LAI 2000, Accupar and sun-scan meter respectively. It has been concluded that a proper selection of instruments is to be done before estimating the LAI.

Sone *et al.* (2009) used destructive and non-destructive sampling (LAI 2000 meter and sun scan meter) for estimating LAI in upland rice for different cultivars. Sampling was done between 21 to 56 days after sowing. LAI recorded with these meters were compared with the non-destructive sampling and a correlation of 0.96 was observed with the sun scan meter while, a correlation of 0.95 was observed under LAI -2000. The results indicate that both instruments were effectively indicated the LAI during the crop growth stages.

Stroppiana *et al.* (2006) used LAI -2000 meter to estimate the accuracy of the instrument in calculating the LAI as compared to destructive sampling. The findings of the comparison indicate a strong positive correlation ($R^2 > 0.8$) between destructive LAI measurements and LAI-2000 estimates; however, this correlation weakens as LAI values approach zero ($R^2 < 0.6$). Hence, when the range of practicality is limited to LAI values exceeding one, the LAI-2000 proves to be a suitable tool for the in situ estimation of LAI in rice fields.

2.3 Crop type mapping using algorithms

Crop classification is an utmost measure to quantify the amount of agriculture production season-wise and helps to assess food security. There are a variety of ways used to update crop classifications by government agencies, but they are labour-intensive, expensive and difficult to compare between nations and continents because different systems have been used around the globe. Food scarcity in low-income nations can only be alleviated if accurate and timely crop production information is available. In order to provide this timely update, remote sensing must be used, which provides timely and extensive data.

Land cover mapping and characterization are essential for resource planning and management (e.g., development and conservation), environmental modelling, and habitat distribution (Gumma *et al.*, 2024). Remote sensing and digital image processing can map, appraise, and monitor land cover at multiple spatial, temporal, and thematic scales (Rogan and Chen, 2004). Land cover categories are used to construct thematic maps and establish a monitoring baseline.

In addition, it is difficult to generate consistent and inter-comparable data between countries or even continents in consideration of the different ground field survey methods adopted (Ozdogan and Woodcock, 2006).

In their study, Gumma *et al.* (2020a) assessed the strengths and limitations of mapping cultivated areas during the rabi season and to compare the cropping patterns by utilizing sentinel 2 data. It was revealed that an accuracy level of 84% has been observed for wheat, mustard and chickpea by using spectral Matching Technique approach.

Panjala *et al.* (2022) classified the crop types in Rajasthan with sentinel -2 data by using supervised machine learning (ML) and Spectral Matching Technique (SMT), Supervised classifiers including Random Forest (RF), Support Vector Machine (SVM), and Classification and Regression Trees (CART) achieved the following accuracies: RF - 81.8%, SVM - 68.8%, CART - 64.9%, and SMT - 88%. The results of the RF classifier and the SMT classification map showed a high level of consistency. It was revealed that the RF classification outperforms the rest of the classifiers.

Raman *et al.* (2019) utilized sentinel- 1 A SAR data with VV and VH polarization to measure rice crop area in Tamil Nadu. Results reveal 79.5% accuracy and 0.59 kappa index under VV polarization, while 82.1% accuracy and and 0.64 kappa coefficient under VH polarization. The reduced precision observed in VV and VH polarisation can be attributed to an underestimate of the area sown with direct seeds and transplanted conditions.

Kenduiywo *et al.* (2018) showcased the functionality of Sentinel-1 multi-temporal data in the mapping of various crops. The framework applied was dynamic conditional random fields (DCRFs), a cost-effective, dependable, and adaptable method of categorizing entities. An ensemble classifier was employed to determine the optimal map by considering the historical probability of each class as represented by a series of images.

The accuracy of the results was greater when high-dimensional images were utilized in conjunction with reduced training data compared to the MLC stack.

Li *et al.* (2020) utilized L-band fully-polarimetric Uninhabited Aerial Vehicle Synthetic Aperture Radar (UAVSAR) data to classify eleven crop groups using the Random Forest (RF) technique. It was discovered that polarimetric parameters gave significantly greater classification accuracy than linear polarisation and the combination of all variables, i.e., linear and polarimetric parameters, yielded an accuracy of 90.50 % in 2011 and 84.96 % in 2014.

Gumma *et al*. (2011a) utilized MODIS time series data from 2000 and 2001 to cartographically represent the extent of rice cultivation in six South Asian nations. Data was collected between 2000 and 2001 utilizing spectrum matching algorithms, decision trees, and ideal temporal profile data banks to identify and categorize rice areas across vast regions. In addition, they have utilized MODIS sensor composite pictures to generate rice maps and assess rice attributes, such as cropping intensity and the crop calendar. An accuracy of 67% to 100% was attained for rice, with a total precision of 80% for all classes.

Gumma *et al*. (2014) employed hyper-temporal MODIS data to map the increase and coverage of rice crops during different seasons in Bangladesh. Throughout all three seasons, a 90% accuracy rate was observed when comparing rice and non-rice maps in matched field plots. The rice area estimates produced from MODIS were 6% more than the sub-national figures during the boro season, 7% higher during the aus season, and 3% more during the aman season. The sub-national areas calculated from MODIS data accounted for 9%, 9%, and 96% of the variability at the district level during the boro, aus, and aman seasons, respectively.

Gumma *et al.* (2020b) utilized Landsat satellite time-series big data and machine learning algorithms (MLAs) on Google Earth Engine (GEE) to develop a detailed agricultural extent product for South Asia. The product had a high resolution of 30 meters or greater. The agricultural product from South Asia achieved a producer accuracy of 89.9%, a user accuracy of 95.3%, and a total accuracy of 88.7%. The agricultural extent product provided a comprehensive representation of both national and sub-national (districts) areas. It accounted for 80-96% of the variability in South Asian national data.

Gumma *et al.* (2016) mapped rainfed and irrigated rice-fallow fields in South Asia using MODIS 250 m time-series data to identify areas where a short-duration crop might enhance agriculture. The maps were assessed using independent ground survey data and sub-national statistics. Agricultural fallow groups are 75–82% accurate for producers and users. Rice classes had approximately 82% accuracy and 0.79 kappa coefficient. South Asia had 22.3 million hectares of optimum rice-fallow land, including 88.3% in India, 8.7% in Bangladesh, 1.4% in Nepal, 1.1% in Sri Lanka, 0.5% in Pakistan, and 0.2% in Bhutan.

Gumma *et al.* (2011b) used Landsat Enhanced Thematic Mapper (ETM+) and time-series Moderate Resolution Imaging Spectroradiometer (MODIS) data to map irrigated agricultural areas and other land use/land cover (LULC) classifications in Ghana. The accuracy of the classification for irrigated classes ranged from 67% to 93%. The remote sensing-derived irrigated areas were found to be 20% to 57% larger (32421 ha) than the statistics disclosed by Ghana's Irrigation Development Authority (GIDA).

Sonobe *et al.* (2018) used vegetation indices from the Sentinel 2 multispectral sensor (MSI) to classify crops in Japan. The accuracy and suitability of vegetation indices based on reflectance data from the Sentinel 2 MSI were evaluated. For cropland classification from MSI data, random forests (RF) and support vector machines (SVM) were used. Overall, SVM was more accurate, with an accuracy of between 89.3% and 92%.

Saini and Ghosh (2018) used single-date Sentinel-2 images and algorithms called random forests (RF) and support vector machines to classify crops in the Indian state of Uttarakhand. It has been found that random forest is more accurate than SVM by 84.22 %, and that sentinel 2 is very good at crop mapping in remote sensing.

Zheng *et al.* (2015) used time-series Landsat NDVI data and a stratified random and intelligent selection method to classify the types of irrigated crops in central Arizona. With an overall accuracy of >86% for both, nine major crops have been found. It has been decided that the intelligent selection approach is better than the stratified random approach because it reduces the amount of training data and improves the accuracy of classification as a whole.

Kobyashi *et al.* (2020), evaluated 91 spectral indices in a single image from the Sentinel 2 MSI to classify crops in Hokkaido, Japan. When spectral indices and reflectance are

used together, the accuracy drops from 93.1 to 92.4 percent. This is based on the reflectance at 4 bands and 8 spectral indices.

Wang *et al.* (2019) used a composite enhanced feature image and the feature filtering and enhancement (FFE) method to find soybean and maize in Northeast China. The results of the FEE method were compared with the results of the support vector machine, the maximum likelihood classification, and the random forest. It was found that the FEE method had an overall accuracy of 90.2 and a kappa coefficient of 0.846, which shows that the FEE method is a good way to classify crops and identify crops with similar phenology.

The sentinel 2 random forest algorithm was used to classify crops by Yi *et al.* (2020). Four different experiments (single band, multispectral, selection of optimal temporal window, and early identification of crop) were used to find the most accurate one. For crop identification, combining RE1 and SWR-1 with images taken in the middle of the crop is useful. An accuracy of 90% has been found with the assimilation of sentinel 2 data with Random forest algorithm crop identification.

Inglada *et al.* (2015) conducted a study to evaluate the effectiveness of an Operational System for Crop Type Map Production using high spatial and temporal resolution satellite imagery. They utilized data from SPOT-4 and Landsat 8 satellites and applied the Multi-Sensor Atmospheric Correction and Cloud Screening (MACCS) processor. The study involved multiple sites worldwide and aimed to classify different types of crops based on various factors such as climate, crop type, and agricultural practices. Random forest classifier has been reported to achieve an accuracy of 80 %. Two of the locations performed poorly due to a smaller land area and a mixture of crops and trees in the field.

In their study, Teluguntla *et al*. (2017) employed automated cropland classification algorithms (ACCAs) and spectral matching techniques (SMTs) to map the agricultural land of Australia using MODIS 250-m time-series data spanning the years 2000 to 2015. The overall accuracy of 89.4% with a kappa coefficient of 0.81, producer's accuracy of 72 and 90%, and user's accuracy of 79 and 90%. The ACCA algorithm effectively represented the magnitude and vitality of Australian croplands in comparison to cropland fallows during the period from 2000 to 2015. This underscores the significance of the research in the advancement of food security analysis.

Cai *et al.* (2018) identified corn and soybean crops based on Landsat image and used common land units to separate spectral information of each field in central Illinois based on the Landsat image to prevent cloud contamination during use of a machine learning model based on deep neural network. Short-wave infrared bands showed superior performance over visible and near-infrared bands in classifying corn and soybean. The overall accuracy of 96 % has been found compared to the USDA crop data layer and concluded that this methodology is accurate, cost-effective and can be used for larger extent area.

Arias *et al.* (2020) classified crops in Spain based on temporal signature extracted from sentinel 1. In this study, 14 crops were taken for classification and concluded that overall accuracy of 70% was obtained with combined use of VV, VH and VH/VV. Rice, wheat, barley, and corn have been identified easily with F1 scores > 75% due to crops exhibiting singularities in temporal signatures. 14% higher classification was obtained in larger fields (>1ha) compared to smaller fields (< 0.5 ha). From this study, it has been observed that areas with high diversity in crops, management techniques and fallow lands showed lower accuracy.

Son *et al.* (2018) used a random forest algorithm (RF) and support vector machines (SVM) for rice crop classification in South Vietnam using multi-temporal sentinel 1A. Results indicate that VH backscatter profiles reflected the temporal characteristics of rice cropping patterns in study. It has been concluded that overall accuracy and kappa coefficient resulted from random forest was more accurate (86.1 % and 0.72), compared to SVM (83.4 % and 0.67) and the results were also on par with the government statistics with an error of 0.2 % (RF) and 2.2 % (SVM), respectively.

Enderle *et al.* (2005) used Landsat 7 enhanced thematic mapper plus satellite imagery (ETM) images to integrate supervised and unsupervised classification to increase LULC accuracy in Arkansas. Maximum likelihood was used for supervised classification, while unsupervised classification employed an Iterative Self-Organizing Data Analysis Techniques (ISODATA) algorithm. The overall accuracy of the supervised classification was 74.85%, compared to 40.94% for the unsupervised classification. The dense canopy pine plantation was better identified under the unsupervised (64.29%) than the supervised (43.86%) classification. Unsupervised classification of dense canopy pine plantation was then combined with supervised classification to boost overall accuracy to 76.61%.

Hasmadi *et al*. (2009) assessed supervised and unsupervised algorithms for land cover mapping in Ayer Hitam Forest Reserve using remote sensing data and spot 5 data satellite image. The land cover classes for the research area were categorized to vegetation, urban area, water body, grassland, and desert. Maximum likelihood was used for supervised classification, while an Iterative Self-Organizing Data Analysis Techniques (ISODATA) algorithm was implemented in ERDAS for unsupervised classification. The results indicated that the overall accuracy of the supervised classification was 90.28 % with a Kappa statistic of 0.86, whereas the accuracy of the unsupervised classification was 80.56 % with a Kappa statistic of 0.73. The outcome of this study is that supervised classification appears to be more precise than unsupervised classification.

2.4 Yield Estimations

2.4.1 Rice yield estimation using crop simulation models

Amarasingha *et al.* (2015) utilized the APSIM model to simulate crop and water productivity in Sri Lanka under a variety of agro-climatic conditions and water management techniques (rainfed with supplemental irrigation). According to the findings, the model predicted grain yield with R^2 value of 0.97 and RMSE of 484 kg ha-^{1}. When the commencement of rainfall is prolonged, crop modelling simulations using the validated APSIM model revealed that rice production is more dependent on supplemental irrigation. In contrast, in years with an early onset, late planting in the season reduced the consumption of rainwater by 95% while increasing the irrigation water demand by 11% compared to planting at the onset of rainfall.

Yuan *et al.* (2017) evaluated the ORYZA rice model to estimate the grain yield of rice under different management practices (varied nitrogen levels and planting densities) in central China. The model is being calibrated using the weather data from 1986-2015. The calibrated values model has been validated. Results from the study reveal that the statistical results for grain yield and biomass were reliably simulated by the model. Correlation of 0.79, 0.99, 0.98 was observed for LAI, total biomass and grain yield respectively.

Kaur and Kaur (2022) used info crop to estimate the rice yield under varied agronomic management practices (different varieties and dates of sowing) in Punjab. Results from the model reveal that there was a good correlation between the observed and simulated results. A correlation 0.94, 0.82 and 0.84 was observed for days to anthesis, days to

maturity and grain yield respectively . This study has proven that info crop can be used for rice yield estimation under different cultivable conditions.

2.4.2 DSSAT crop simulation model and calibration

Liu *et al*. (2017) used the DSSAT model to simulate wheat yield and soil organic carbon under different fertilizer conditions in wheat- maize cropping system and this model has shown the effect of nitrogen on crop growth, yield and grain N concentration. R^2 values for grain yield (0.72 and 0.45) and grain N concentration (0.62 and 0.24) were noticed. It ha been suggested that model can be used effectively after proper calibration for better results.

Ray *et al.* (2018) estimated rice yield (Swarna) in Orissa under changing climatic conditions by use of the DSSAT model. There was decrease in Model simulated yields with an increase in maximum and minimum temperature. There is much effect of minimum temperature on the yield compared to maximum temperature. Simulated yield for rise in maximum temperature for $+1^{o}$ C (5712 kg ha^{-1}) to $+5^{o}$ C (3711 kg ha^{-1}). It has been concluded that the model can be used for projections in climate change.

Akinbile *et al.* (2013) simulated rice yield under different irrigation regimes with the use of the CERES-Rice model. The irrigation treatments were 100% ET, 75% ET, 50% ET and 25% ET. The measured yield (2.41 t ha^{-1}) and LAI were compared with the model-simulated yield (2.63 t ha^{-1}) and LAI. Findings reveal that model-simulated yields were on par with the observed yields with R^2 of 0.99, and RMSE of 0.16 for grain yield. Though the model has simulated slightly higher values for LAI and yield, there is no significant difference between them. It has been found that this model can be used to estimate rice yield with differences in irrigation levels, but recalibration and validation under different fertilizer levels and soil situations will lead to better usage of the model.

Mirakhori *et al.* (2017) conducted an experiment to assess the CERES rice model under different fertilizers (nitrogen) and irrigation levels on crop growth. Three levels of irrigation and four levels of fertilizer have been considered. Measured yields were compared with the model-simulated yield with no significant difference. The coefficient of determination for LAI, grain yield, and biomass yield from the model was 0.76-87 %, 0.82-0.95 %, and 0.85-87 % respectively and it was concluded that CERES rice can be used under different management strategies.

Kadiyala *et al.* (2015) used the CERES rice and maize model to identify best management practices in rice - maize cropping system in Hyderabad and observed that 180 kg N ha^{-1} in rice followed by 120 kg N ha^{-1} in maize resulted in stable yield under aerobic and flooded rice conditions. It has been concluded that DSSAT can be used as a tool for recognizing the best alternative management practices for saving water and maintaining optimum yields.

Alejo *et al.* (2020) conducted an experiment in Isabela, the Philippines with different fertilizer rates in dry and wet seasons. Projected climate change data of RCP 4.5 and 8.5 were collected. It has been concluded that Ceres rice has been used to assess the effects of climate change on aerobic rice production with R^2 value ranging from 0.87 -0.96, nRMSE of 17-29, and NSE of 0.77 - 0.92 under wet, dry and different fertilizers conditions of 0%, 50%, and 100% RDF respectively.

Nyangau *et al.* (2014) opted for four different irrigation schemes in Kenya with two rice varieties basmati 370 and IR 2793-80-1 as an experimental treatment. Sensitivity analysis was performed using the CERES rice model where calibration and validation were performed. The observed grain yield was compared with the model simulated yields where R^2 value of 0.786 have been observed during 2011. An increase in temperature and CO_2 concentration affected grain yield for both varieties. Thus, the study's findings indicate that it is important to take into account Kenya's climatic conditions while determining rice yields in order to increase food security and also dependency on the model for estimating rice yields.

Deka *et al.* (2016) conducted a seven-year field experiment from 1998-2005 in the upper Brahmaputra valley of Assam, India and the same package of practices for the Ranjit cultivar was fed into the DSSAT model. Calibration was performed with 3 years of data followed by validation, where the variation in yields was ± 16%, with an RMSE value of 401 kg/ha, nRMSE <10%. The model's predictions ranged from 85% to 107% of the reported grain output. The enhanced capability of the model to accurately replicate the total grain production of the crop will enable policy makers and planners to make smart agricultural based economic decisions in the upper Brahmaputra valley.

Ahmad *et al.* (2012) assessed the performance of the model in estimating rice yield under irrigated conditions in a semi-arid environment in Pakistan using DSSAT Ceres Rice. The researchers also investigated the influence of plant density and irrigation regime on

grain yield and economic returns. The findings demonstrate that the model effectively predicted the development and productivity of rice under irrigated semiarid conditions, with an average discrepancy of 11% between the cereal yields simulated and observed. It can be inferred that the CERES-Rice model has the potential to serve as a decision aid tool for resource-constrained farmers cultivating irrigated rice in semiarid regions, offering them alternative and integrated management strategies.

In their study, Sudarshan *et al*. (2013) conducted a comparison between two distinct rice simulation models—the Simulation Model for RIce-Weather Relations [SIMRIW] and the Decision Support System for Agro-technology Transfer [DSSAT]—in order to estimate rice crop production in the southern semi-arid tropics of India using agrometeorological data and agronomic parameters. The application of linear regression models revealed a strong correlation between predicted DSSAT and observed yield. NSE of 0.73 was observed in DSSAT, while 0.62 in SIMRIW. It is concluded that DSSAT is mor accurate than SIMRIW as it will consider more input parameters for simulation.

Vilayvong *et al.* (2015) used the DSSAT ceres rice model to determine the management practices like different cultivars and planting dates for low-land rice production in Thailand. The model achieved satisfactory accuracy for grain yields, as indicated by normalized root mean square error values ranging from 1% to 16%. The recommended management approach for enhancing lowland rice production in Laos involves transplanting irrigated rice on January 15th with 5 seedlings per hill and using 120 kg of N-fertilizer per hectare. The CSM-CERES-Rice model is a useful tool for predicting rice crop management techniques.

2.5 Relation between Fertilizer and Yield

Chamely *et al*. (2015) revealed that applying 200 kg ha^{-1} recorded highest grain yield (5580 kg ha^{-1}) compared to the rest of the varied nitrogen level treatments during boro season at Bangaldesh. This was due to the contribution of higher straw yield, harvest index and yield attributing characters.

Rajesh *et al.* (2017) conducted experiment to know the effect of varied nitrogen levels (120 kg N ha^{-1} and 60 kg N ha^{-1}) and genotypes (26) on morpho-physiological and yield of rice in college farm of PJTSAU, Hyderabad. Applying nitrogen at the rate of 120 kg N

ha^{-1} recorded highest yields and MTU1010 genotype recorded higher yields (5338 kg ha^{-1}) compared to the rest of treatments and cultivars.

Pooja *et al*. (2018) noticed that increase in nitrogen levels from 0 to 150 kg ha^{-1} there was an increase in the grain yield. The grain yields under different nitrogen application rates were1676.76, 3395.28, 3870.70 and 4001.34 kg ha^{-1} respectively at 0, 90, 120 and 150 kg N ha^{-1}. All the treatments showed a comparable result in respect of grain yield except with the 0 kg N ha^{-1} at Varanasi, Uttar Pradesh.

Ramulu *et al.* (2020) studied on the effect of different establishing methods and nitrogen levels on grain yield of rice at Regional Agricultural Research Station, Warangal. It was found that with raise in nitrogen levels, the grain yield and yield attributes increased up to application of 200 kg N ha^{-1} but the yield under 200kg N ha^{-1} was on par with the application of 160 kg N ha^{-1}. Hence, it can be concluded that applying 160 kg N ha^{-1} produces reliable yield.

Mrudhula and Suneetha (2020) applied seven levels of nitrogen (80, 120, 160, 200, 240, 280 and 320 kg N ha^{-1}) to know the effect on grain yield in Bapatla. It was observed that among all the levels of nitrogen, 320 kg N ha^{-1} recorded highest grain yield (5288 and 5325 kg ha^{-1}) in both the seasons which might be due to the greater number of filled grain per panicle and test weight. It was concluded that application of 200 kg N ha^{-1} is more feasible in terms of economical grain yield.

2.6 Derivation and Integration of Remote sensing products

Using Sentinel 2 data, Ali *et al.* (2021) identified rice regions and predicted rice yield in the Nile region. The multi-temporal NDVI produced from Sentinel-2 satellite data was found to be crucial for crop classification. The LAI was computed utilizing the Surface Energy Balance Algorithm for Land (SEBAL) model was used to assess the LAI and further it was compared with the measure LAI to know the accuracy level. Using NDVI and LAI calculated from Sentinel 2 to predict yield resulted in an average inaccuracy of 0.66 t/ha. MPAE was determined to be 6.76%, and 6.53 % with a high correlation 0.94 and 0.95 in the case of LAI and Yield. It was revealed that the followed procedure can be employed for estimating rice are and yield.

Remote sensing products such as VV, VH, and VV/VH were generated by Bhargav (2021) using Sentinel-1, while NDVI was derived using Sentinel-2, for the purpose of distinguishing amongst rice ecosystems in the Jogulamba Gadwal district of Telangana. Among the leaf area index (LAI) and NDVI maximum a linear regression analysis has been performed and results reveal that a correlation of 0.79 and 0.86 was found for transplanted and direct sown rice scenarios.

Fan *et al.* (2009) conducted research in semi-arid grassland China, using in-situ measurements to know the relationship between NDVI and LAI. It was concluded that there has been linear relationship between LAI and NDVI. A correlation of 0.79 was observed with the measured NDVI and LAI values.

An investigation that was conducted by Goswami *et al.* (2015) studied to find out the relationship between NDVI, LAI and biomass near Barrow, Alaska. It was found that NDVI shows a good correlation with the LAI for all the selected crops. A correlation of 0.70 was observed between NDVI and LAI.

In their study, Clevers *et al*. (2017) employed Sentinel-2 satellite imagery to examine whether vegetation indices could be utilized to calculate LAI, leaf chlorophyll content (LCC), and canopy chlorophyll content (CCC) of a potato crop. In order to achieve this, a LAI prediction was generated utilizing Sentinel-2 TOC spectral observations in conjunction with WDVI calculations. The findings from the Sentinel-2 mission indicate that the leaf area index (LAI) can be estimated using the weighted difference vegetation index (WDVI), which comprises bands with a spatial resolution of 10 meters (R2 value of 0.809; RMSEP of 0.36).

Xavier and Vettorazzi (2004) conducted a study to find out the link between LAI and Spectral Vegetation Indices under different land covers in a subtropical rural watershed of Brazil. NDVI, Soil Adjusted Vegetation Index (SAVI), and Simple Ratio (SR) were calculated utilizing Landsat-7 ETMz data. A correlation of 0.72 was found under LAI-NDVI, while 0.70 was observed under LAI-SR and 0.56 was noticed under LAI-SAVI.

In their study, Ines *et al.* (2013) devised a framework for data assimilation-crop modeling that integrates remotely sensed soil moisture and leaf area index (LAI) via MODIS leaf area. LAI was processed between 2003 and 2009 for the purpose of verifying and evaluating crop assimilation and modeling. The integration of MODIS-LAI resulted in

enhanced simulated yields ($R^2 = 0.51$) in comparison to open-loop simulation ($R^2 = 0.47$), with a minor decrease in systematic error. Absorption of LAI solely may be desirable in excessively damp conditions, whereas under nominal conditions, integration of soil moisture along LAI may be more effective.

Aboelghar *et al.* (2011) assessed rice yield in the Egyptian Nile Delta based on the LAI computed from SPOT data obtained during two crop seasons. In the present study, red and near-infrared bands alone or in the form of vegetation indices and LAI are treated as spectral variables. LAI and Infrared models showed a considerably greater advantage over the other models, with 0.061 and 0.090 standard errors of estimate and 0.945 and 0.883 coefficients of determination between predicted and observed yield, respectively. It is concluded that a month before harvest, the models are suitable for similar regions and conditions.

Kross *et al*. (2015) utilized fast eye vegetation indices to estimate the leaf area index and biomass in corn and soybean crops. Between 2011 and 2013, seven vegetation indices were calculated using combinations of reflectance in green, red, red-edge, and near infrared bands using Rapid Eye data. The NDVI, edge NDVI, and green NDVI exhibited low sensitivity to crop type. The coefficients of variation (CV) for these indices ranged from 19% to 27%, whereas the coefficients of determination ranged from 86% to 88%. Continuous monitoring of agricultural Leaf Area Index (LAI) at the field level can be accomplished by combining data from Rapid Eye, Landsat, and SPOT satellites, together with sensor-specific best-fit functions.

2.7 Integration of remote sensing products with crop simulation model

The combination of remote sensing and crop growth models has become an effective tool for yield estimation and a potential method for grain quality estimation.

For monitoring crop growth and LAI estimation in sugar beet crops Clevers *et al.* (1994) applied optical and microwave remote sensing data using an optical reflectance model and a radar backscattering model. To calibrate the crop growth model to actual growing conditions, remote sensing models were inverted to estimate LAI during the growing season. LAI estimates were not improved by concurrent radar and optical observations in comparison to optical data alone.

Hong *et al.* (2004) used image-derived vegetation indices to estimate leaf area index (LAI) in corn and soybean in two central Missouri experimental fields. Comparison of crop model results with measured and the simulated LAI has been performed. Measured and estimated LAI have been compared with crop model simulation results. The CERES-Maize and CROPGRO-Soybean models accurately reproduced Leaf Area Index (LAI) during the whole crop growth period using data on soil moisture and crop production. CERES-Maize over predicted LAI at all corn sites (R^2 = 0.59-0.61) while CROPGRO-Soybean (R^2= 0.66-0.68) had predicted similar results to that of observed LAI. It can be concluded that image-estimated LAI may improve crop growth model forecasts.

Fang et al. (2011) conducted a study where they used MODIS LAI and vegetation index products with the CERES-Maize model to estimate maize production in Indiana, United States. The CSM-CERES Maize model's parameters have been generated using data obtained from remote sensing. According to this study, the model predicted maize yield was consistent with the United States Department of Agriculture (USDA). The MODIS vegetation index and the LAI products yielded the most accurate outcomes, exhibiting discrepancies of less than 3.5% compared to the USDA data. The EVI was deemed unacceptable due to a variance of 21%.

Milesi *et al.* (2022) conducted research in Uttar Pradesh and Odisha to evaluate crop yields at village level by assimilating weather and satellite data with crop simulation models. Using cloud-screened MODIS 250-m data from Terra and Aqua satellites and a modified MOD15 LAI/FPAR backup method, crop biophysical estimates of LAI and FPAR were obtained. Results reveal that there was similarity between the crop simulation yields and CCE yields. Correlation of 0.80 and 0.84, RMSE of 411 and 309 $kgha^{-1}$ and MAE of 359 and 262 $kgha^{-1}$ respectively was observed under rice and bajra.

GIS-based Environment Policy Integrated Climate (GEPIC) model has been used by Muslim *et al. (*2015) to predict paddy yield at regional level. The predicted yield is 4305.55 kg ha^{-1}. A mean yield of 4783.3 kg ha^{-1} was observed under plain areas with cultivars like China-107, Jhelum, K-39, China 1039, and Chenab and Shalimar rice-1, while cultivars like K-78 and K -332 grown under high altitude resulted a yield of 4102.2 kg ha^{-1}. Predicted results were compared with the measureed yields where correlation of 0.95 and yield variation of 132.24 kg ha^{-1} was noticed which shows that crop models can be integrated with remote sensing.

Dryland wheat yields of North-eastern Australia at field scale has been estimated by Zhao *et al.* (2020) using sentinel -2 data and incorporating model crop water stress index (SI) with the data from 2016-17 crop seasons. The integration of the model with the optimal soil-adjusted vegetation index (OSAVI), chlorophyll (CI), and stress index (SI) resulted in a good correlation of 0.91 and a root mean square error (RMSE) of 0.54 t ha^{-1}. The study has determined that sentinel-2 vegetation indicators effectively forecasted crop yield.

Tripathy *et al.* (2013) estimated wheat yield in Punjab by integrating remote sensing data into the World Food Studies (WOFOST) mechanistic crop simulation model. NDVI data using SPOT satellite (SPOT-VGT). LAI derived from remote sensing was fed into the model. Comparison between simulated and government statistics has been made for three crop seasons and the findings reveal that this methodology resulted a RMSE of < 0.4 t ha^{-1} which can be implemented for spatial yield estimation at regional level.

Doraiswamy *et al*. (2004) utilized LANDSAT and MODIS to observe variations in vegetation, enabling the indirect estimation of crop growth and yields at the individual field level. The spatial distribution of Leaf Area Index (LAI) was mapped for the Walnut Creek watershed in Ames, Iowa, with the purpose of estimating agricultural yields. The results showed that the average simulated yields for soybeans was approximately 6.6% higher than the NASS stated yields, while the average simulated yields for corn were about 3% lower than the reported stats.

Priya and Shibasak (2001) estimated the spatial crop yield for rice, maize and wheat. using spatial EPIC which was generated from an EPIC (Erosion productivity Impact Calculator) model. An R^2 value of 0.74, 0.68 and 0.59 was observed respectively for maize, wheat and rice under varied locations across India. Validation results in case of wheat and maize yield estimation found to be effective under coarse resolution. It has been concluded that model can be used in predicting yields in any area as India is one among the country showing wide diversity in-terms of climate. This will help in taking national policy decisions.

Ali *et al.* (2021) assimilated NDVI multi-temporal data derived from sentinel -2 satellite with LAI to estimate grain yield of rice. LAI is evaluated by use of the Surface Energy Balance Algorithm for Land (SEBAL) model followed by validating with measured LAI values. Yield is being calculated by use of NDVI and LAI. A good correlation has been

observed in LAI and grain yield with 0.94 and 0.95 as the coefficient of determination among measured and simulated values respectively.

Son *et al.* (2016) conducted a trial to estimate rice yield considering principle objective as to build up a technique by assimilating satellite data into DSSAT model. Particle swarm optimization (PSO) algorithm was used for yield estimation. The variation among the MODIS LAI and simulated LAI was used to develop cost function. It has been found that estimation of yield for large areas can be obtained accurately with less error by integration of DSSAT with satellite data.

Fang *et al.* (2011) assimilated satellite data (MODIS LAI and vegetation indices) with the CSM–CERES–Maize model for estimating maize yield by taking principle aim as to predict the yield by the mid of the crop growth period. Integration of MCRM model and CSM-CERES maize was done during the process. Solitary use of LAI, NDVI and EVI and combinations of these were tested. Among all these models, best was seen under combination of MODIS with LAI products with a deviation of <3.5%. Independent usage of each vegetation indices has not resulted in to good yield as the error was >13%. It has been concluded that combination of remote sensing derived vegetation indices and LAI when assimilated in crop models resulted in better prediction of yields.

Aboelghar *et al.* (2011) conducted an experiment to estimate the rice yield using SPOT and LAI. By using regression equations, measured yield is being related to satellite-derived LAI. Remote sensing generated LAI have been assessed against the field LAI to produce yield models. Relating LAI as a biophysical parameter to the yield, red and near-infra-red bands are the spectral variables used in this study either alone or in the form of vegetation indices. Among all the other models higher dominance has been observed in LAI and infrared models with 0.94 and 0.88 as the coefficient of determinants. From this, it has been concluded the integration of crop models with satellite imagery results in yield generation before harvest.

Gumma *et al.* (2022) stated that the use of advanced tools like remote sensing and crop models for rice yield estimation will result in to better outcomes when both these are integrated. By use of Sentinel -2 data, spectral matching techniques (SMTs) and crop information collected during surveys crop classification was done. Remotely sensed LAI was produced by use of Landsat 8 data based on SAVI equation. The model simulated

LAI values were compared with the sentinel -2 LAI values and it has been observed that there is good correlation exists between them with a coefficient of determination 0.7.

Pazhanivelan *et al. (*2022) selected Thanjavur, Tamilnadu as the study area where three rice cultivars (BPT 5204, CR 1009, and ADT 45) have been cultivated for research purposes. DSSAT has been used for spatial rice yield estimation where calibration and validation have been performed. Model-simulated LAI values have been compared with the RS LAI. Results show that the integration of remote sensing with the models and spectral indices-based regression analysis resulted in R^2 value of > 0.80, NRMSE of <10%, and results in agreement of >90%. Remote sensing data integration with the DSSAT model and spectral indices-based regression analysis are potential methodologies for spatially predicting rice crop yields.

Filippi *et al*. (2019) devised a method to forecast grain yield by employing machine learning using random forest models and intricate, multi-farm information. This study employed multiple large-scale agricultural operations in Western Australia as the subjects of investigation.The farms covered an area ranging from 11,000 to 17,000 hectares every year. The results indicate that the concordance correlation coefficient of Lin's model ranged from 0.89 to 0.92 when compared to the model yield predictions.

2.8 Validation of the estimated yield with statistics

Son *et al.* (2016) developed a method for assimilating remotely sensed data into a crop simulation model (DSSAT) to predict rice production in Taiwan. The data assimilation was processed using the particle swarm optimization (PSO) approach to include biophysical variables in the DSSAT model for estimating rice production. Estimated yield results were then compared with the government's statistics, the RMSE was 11.7% and the mean absolute error was 9.7%.

Setiyono *et al.* (2019) integrated SAR data into crop yield simulation and full validation of yield forecast and estimations in Tamil Nadu, India. Remote sensing data integration into a crop model captures rice crop responses to environmental variables across vast geographical coverage, which is otherwise unattainable. The system captures climatic information using a process-based crop simulation model and gives a mid-season yield projection for rice policy and planning. SAR-based yield estimations for the 2014 -15

season were compared with the government yield statistics varied from 3.12 to 3.87 t ha^{-1}, with 15% NRMSE and 552 kg ha^{-1} RMSE.

Gumma *et al.* (2022) assimilated remote sensing data into the DSSAT crop simulation model for yield estimation of different crops. CCE yields were validated with the government statistics from the Department of Agriculture and then the simulated yields were then compared with the CCE yields. A correlation of more than 0.70, Model Efficiency of 0.75, MAE of 307 and RMSE of 386 kg ha^{-1} was observed.

A brief review has been collected from the previous study and research. An overall summary for the above was mentioned reveals that higher accuracy and precision regarding crop growth monitoring can be obtained with the use of renote sensing technology. With the development of different crop simulation models effect of climate change, abiotic and biotic stress on crop yield can be assessed in very less stipulated time period and also these can be used to evaluate over long run. In mant stuies LAI has been considered as the key criterion for the crop yield estimation as it is directly corealted with the yield. LAI has been measured with the different portable instruments but there was limited research on comparing the ceptometer LAI with crop model generated LAI. From the above literature it can be clearly seen that there was scanty research on the yield estimatiin at the field level. Hence indepth study was considered for the above review and this study has been taken forward by employing the leaf area index (LAI) as the primary criterion for integrating remote sensing technology and crop simulation models.

Chapter III

MATERIAL AND METHODS

This chapter describes the paramters for selecting study area, DSSAT- Crop Simulation Model, remote sensing technologies and its application for grain yield estimation in rice. Details of materials and methods used in this study for the assimilation of crop models into remote sensing for rice yield estimation and the workflow for this study purpose have been mentioned below.

3.1 Overview of the study area

Telangana is under the southern plateau agro-climatic zone, which is characterized by a hot and dry environment. The state shares its northern and eastern borders with Maharashtra and Chhattisgarh, and its southern and southeastern borders with Andhra Pradesh, its western border with Karnataka, and its northern border with Rayalaseema. Srisailam and Nagarjuna Sagar projects are the two major hydroelectric projects

constructed on River Krishna and the Sriram Sagar project on river Godavari. The prominent perennial rivers in Telangana state are the Godavari in the north and the Krishna in the south, in addition to 16 other minor rivers. The Kaleshwaram Lift Irrigation Project (KLIP) is one of the world's largest multi-stage lift irrigation systems, developed in the Godavari river basin, transforming rainfed land into irrigated farmland.

Rice is the predominant crop in Telangana state, and agriculture is the state's primary economic driver. Rice, maize, cotton, sorghum, castor, peanuts, soybeans, and red gram are among the important crops. The development of dams and lift irrigation projects increased the availability of water, allowing farmers to opt for double cropping. Most of the land is now irrigated, as compared to previous years when agriculture relied on rainfall, resulting in crop failures.

Karimnagar district, which is in the northeastern part of the state has 16 mandals and has an area of 2128 km^2, a latitude of 18026'13" N, a longitude of 79007'27" E, and an elevation of 300m above mean sea level, has been chosen as a study area (Fig. 3.1). The climate of this area is dry, with hot summers and cold winters and the area receives most of the precipitation from southwest monsoons. The minimum temperature in kharif was from 20°C to 28°C, while in Rabi it was 18°C to 26°C and maximum temperatures of the area in kharif ranged from 31°C to 40°C, 28°C to 40°C during Rabi. The Dominant soils in the district are black and red sandy loam soils. The average annual rainfall of the district is 898.3 mm while the actual rainfall received during the crop-growing seasons June 2021 to March 2022 was 1360 mm (Fig. 3.2). Detailed weather data village wise has been mentioned under Appendix-I.

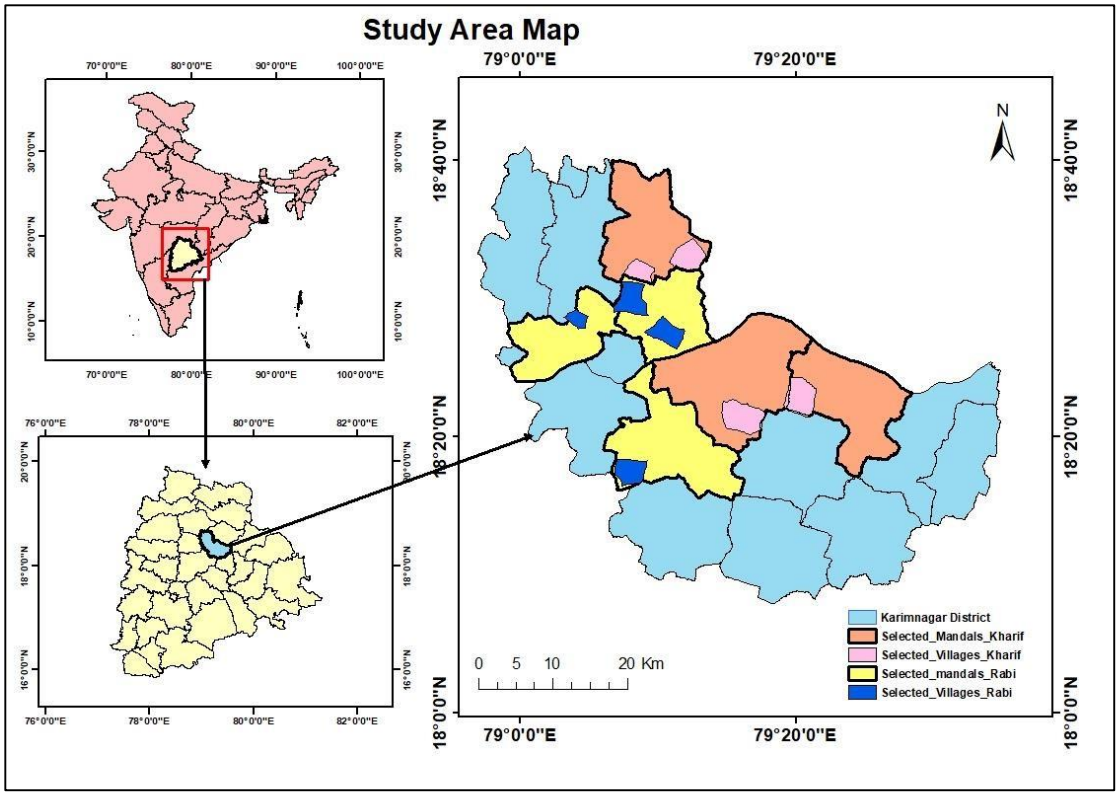

Fig. 3.1. Study area map with selected mandals and villages in Karimnagar district

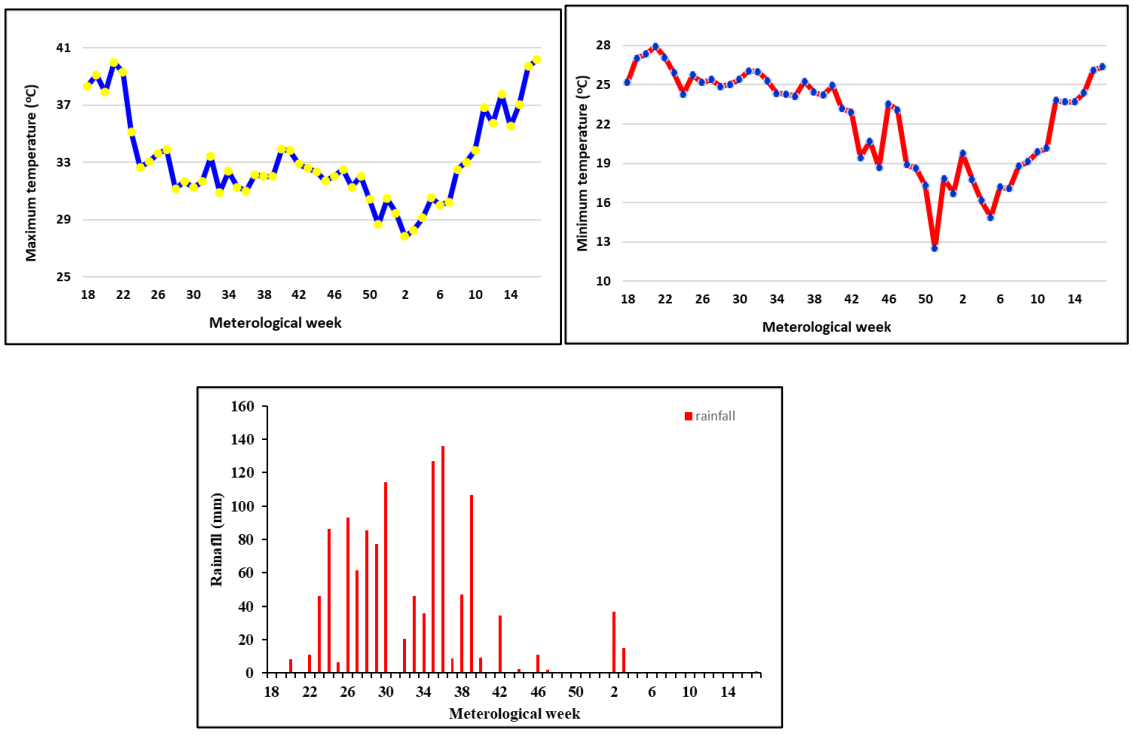

Fig. 3.2. Average monthly maximum, minimum temperatures, and precipitation during growing seasons

3.2 Optimization of CCE Locations

3.2.1 Selection of study area

The selection of the study area was done by taking into consideration of soil, rainfall, digital elevation points, crop type, irrigated or rainfed, and road connectivity which have importance for the effective in conduct of research.

3.2.1.1 Soil map:

Based on the data from the NBSSLUP soil map for the Karimnagar district was prepared from the state soil map. There were four different types of soil (clay, clay skeletal, loamy, and loamy skeletal) were found in the study area (Fig. 3.3). The clay and clay skeletal are major soils that have occupied < 80 %, whereas loamy and loam skeletal are minor soils occupying <20 % area. Soil nutrient status details have been collected from the soil health card which is available on the Department of Agriculture and Farmers of low, medium and high.

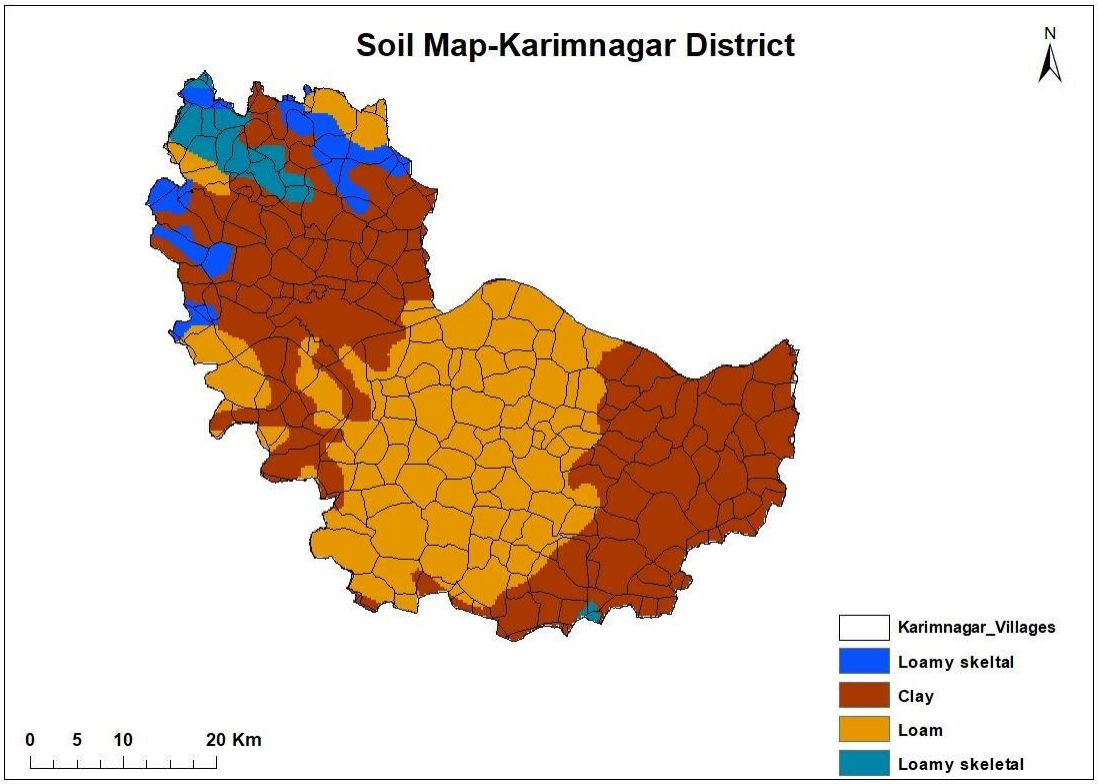

Fig. 3.3. Soil map for Karimnagar district

3.2.1.2 Rainfall map:

Rainfall is considered as one of the prime inputs for the agriculture sector. Rainfall details for the last 20 years have been collected from CHIRPS (Climate Hazards Group Infrared Precipitation with Station data). The average rainfall in this area was 890 mm which comes under the semi-arid condition where it receives most of the rainfall during the southwest monsoon period (Fig. 3.4). Based on rainfall received, the entire district was classified into four groups i.e., < 1003 mm, 1003-1028 mm, 1028-1061 and > 1061 mm. A major part of the district area is under 1003-1028 mm and a minor part of the area is under >1061 mm.

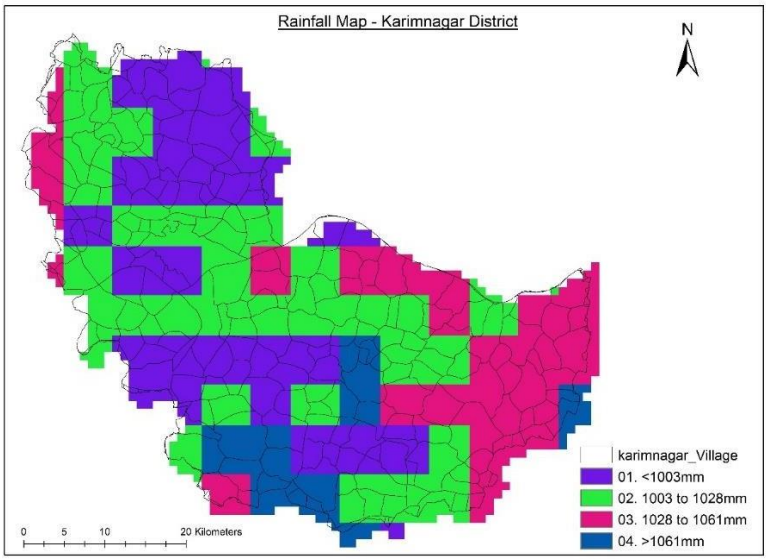

Fig. 3.4. Rainfall map for Karimnagar district

3.2.1.3 Digital Elevation Map:

Digital Elevation Model (DEM) is a digital representation of the elevation of the ground surface concerning any reference datum. Based on the DEM elevation suitable crops can be selected and cultivated. Based on the Digital Elevation Model study area has been classified into 3 classes i.e., < 252 m, 252-298 m and > 292 m (Fig. 3.5). The Major part of the study area falls under the elevation of > 292 m.

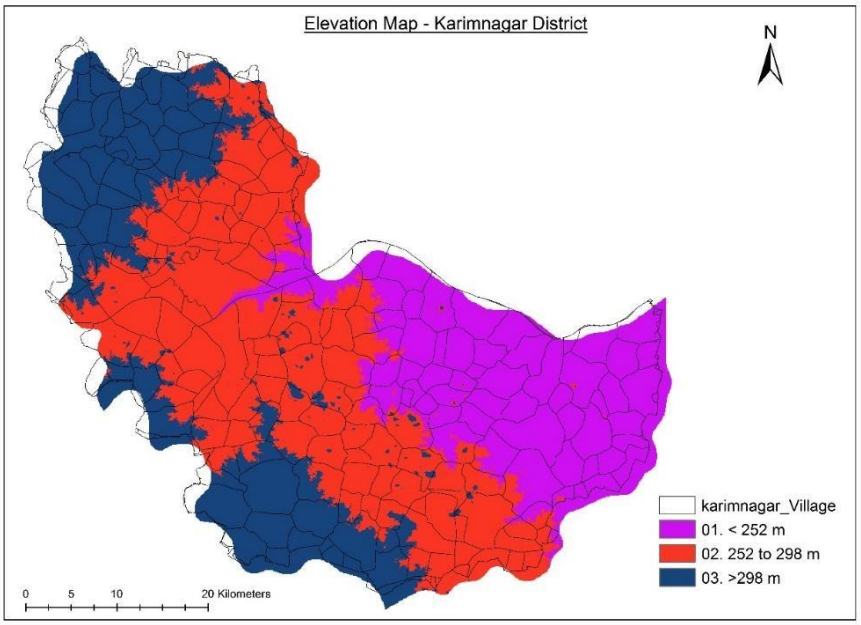

Fig. 3.5. Digital Elevation Map for Karimnagar district

3.2.1.4 Crop Type Map:

Crop classification and crop type maps plays a vital role in selecting the study area by forecasting crop yield, collection crop production statistics, facilitating crop rotation records, mapping soil productivity, identifying crop stress factors, and monitoring storm and drought damage. Crop classification and crop type map of the previous year (2020-21) were developed using sentinel 2 (10 m resolution) on the basis of NDVI values. Major crops identified were rice, maize, cotton and pulses (Fig. 3.6). The area under each class were mentioned below. Area of rice -rice was around 36 thousand ha, while rice -pulses occupy an area of 83 thousand ha, pulses/ maize-maize covers an area of 7 thousand ha. Rice fallow occupies and rea of 3 thousand ha and cotton fallow occupies and area of 23 thousand ha and pulses occupy an area of 2 thousan ha. Mixed crops covers an area of23 thousand ha and other LULC occupies an area of 36 thousand ha. There was a clear distinction observed between irrigated and rainfed land. For the study purpose, areas under single and double crop rice fields were selected irrespective of the irrigation. A major part of the rice grown area is under irrigated conditions due to the availability of canal water for irrigation.

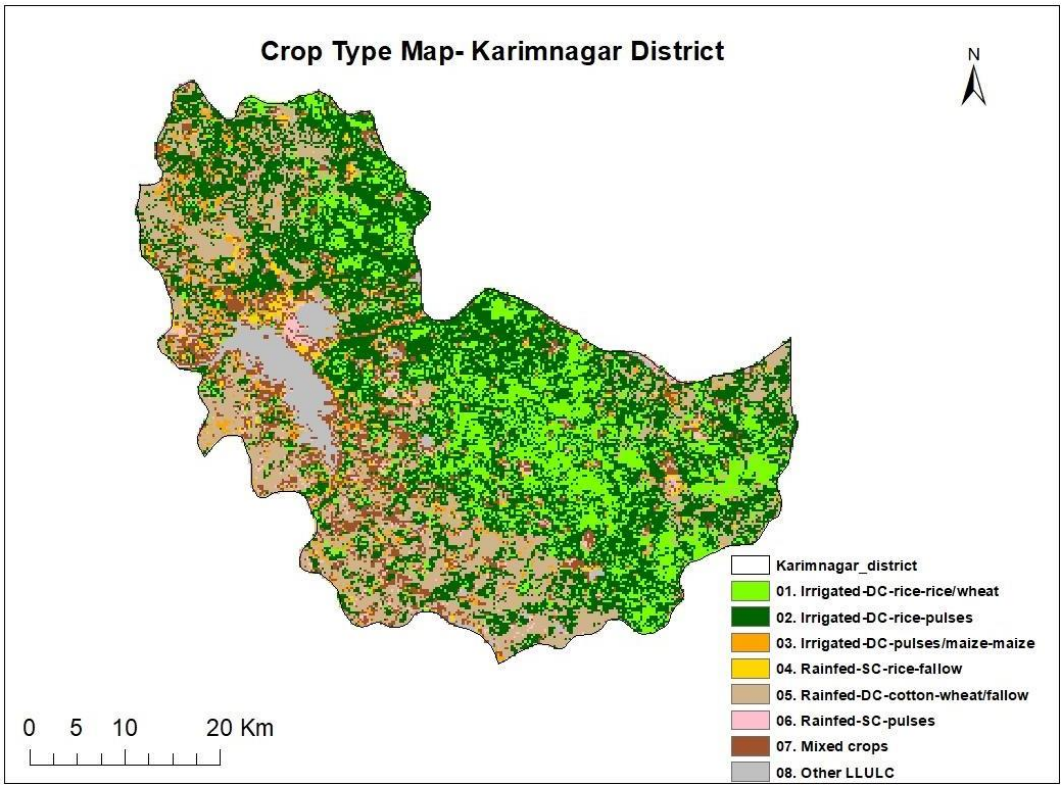

Fig. 3.6. Crop type map of Karimnagar district

3.2.2 Selection of villages

The villages having good road connectivity and nearness to Karimnagar city were considered in the selection of the villages. The selected villages had variations in rainfall, soil and elevation. A combination of the rainfall, soil and elevation has been assessed to identify the homogeneity in the sites of study. During kharif, four villages (Rukmapur, Vedurugattu, Elbaka and Gangipalle) and in rabi four villages (Renikunta, Malkapur, Durshed, and Nagnur) falling in different mandals having a large area under rice were selected (Fig. 3.7).

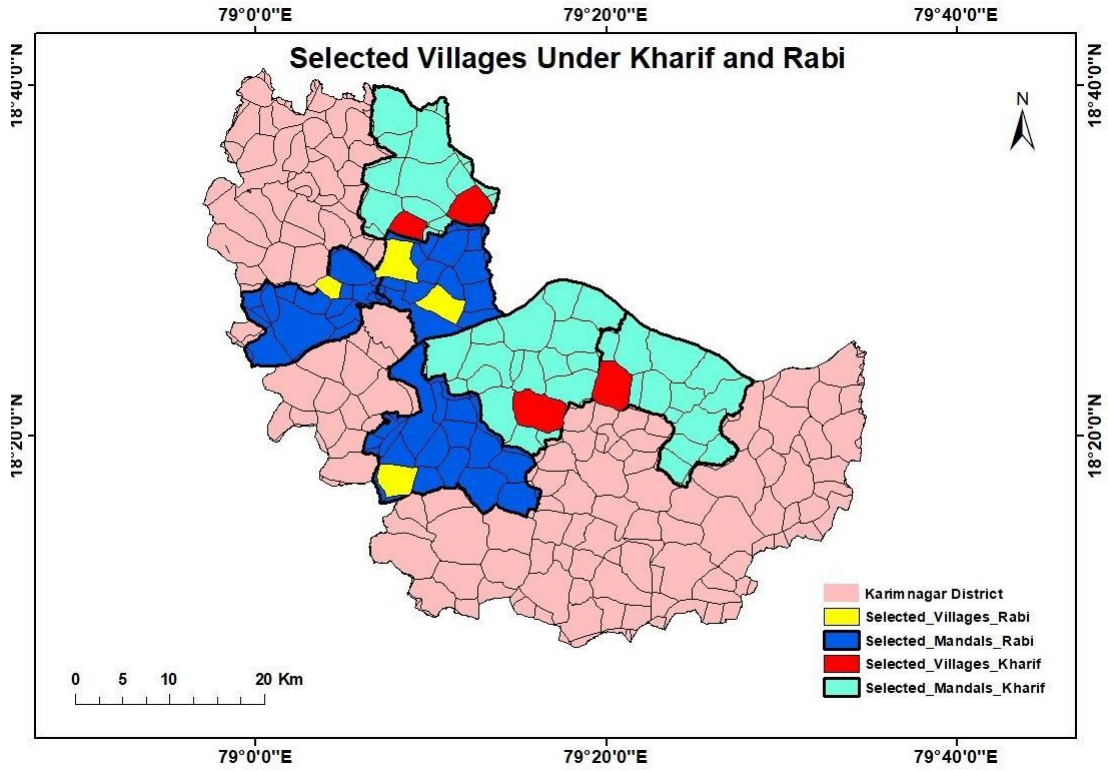

Fig. 3.7. Selected Villages for Kharif and Rabi

3.3 Ground Data Collection

Ground truth data refers to information acquired on-site and it facilitates the correlation of visual data with real objects and materials on the ground. The acquisition of ground truth data allows remote sensing data to be calibrated and aids in the interpretation and analysis of what is being sensed.

3.3.1 Field Visits

Field visits have been scheduled for every 15 days according to the satellite passing time and prevailing weather conditions in the district. With the help of the village agriculture extension officers' the fields in the villages were selected. A total of 220 ground truth points were collected during kharif and rabi which were used to perform supervised classification and for validation (Plate 1 and 2). In each field latitude and longitude points were acquired using GPS and LAI at different growth stages using LAI- Ceptometer. The major crops grown in this district in kharif were rice, whereas in rabi rice, maize and cotton in kharif extended to rabi season.

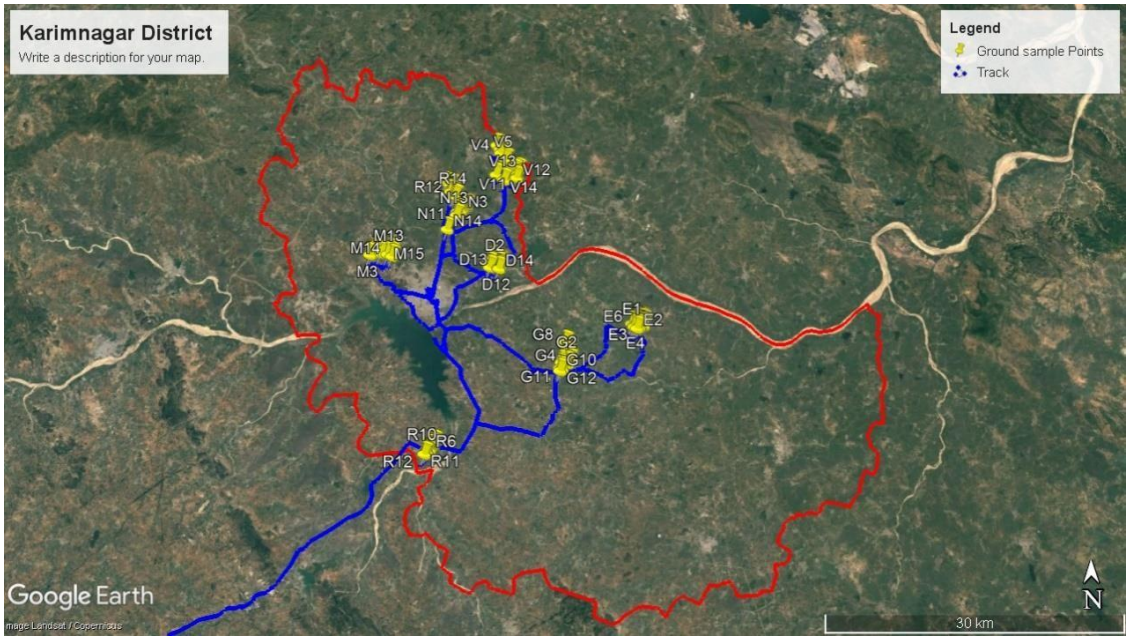

Plate 1. Ground data sample points collected during the visits

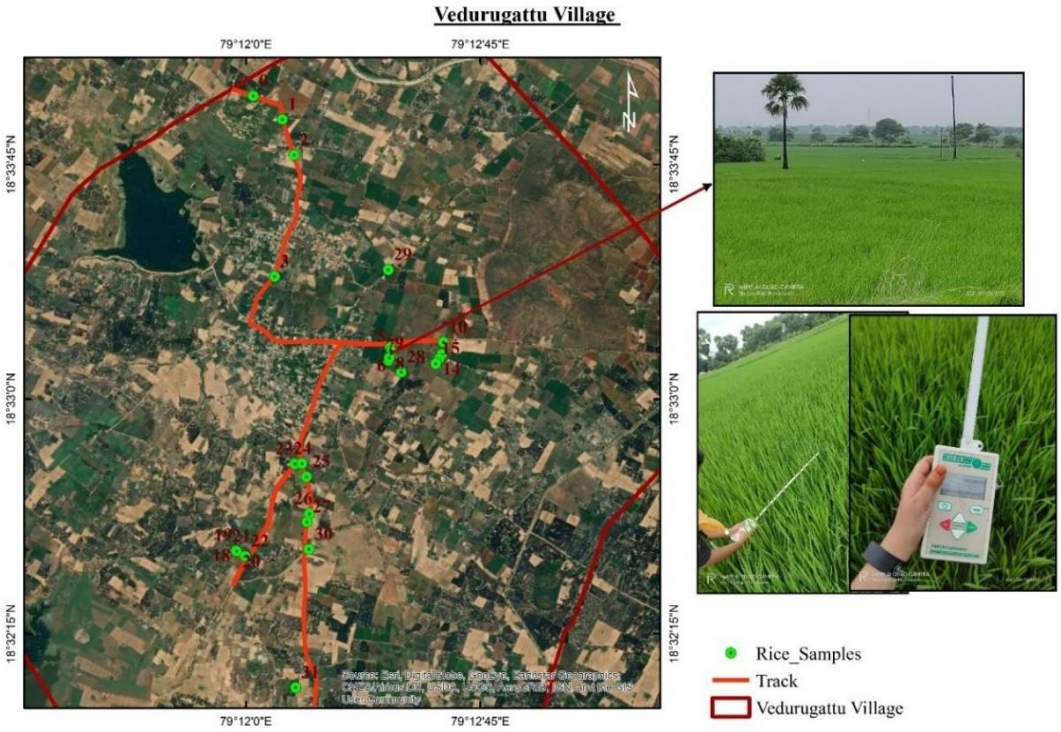

Plate 2. Ground truth data points collected in selected village

3.3.2. Farmers Interaction

During visits, the interaction with farmers was done (Plate 3) in all the selected villages. Fifteen fields were chosen and monitored regularly in each village at a distance of 200m from each field to avoid overlapping into a single pixel in the satellite image. A questionnaire was prepared and the data was acquired on detailed management practices like cultivar used, nursery sowing, transplanting, irrigation, and fertilizer application adopted by the farmers. A detailed questionnaire is given under Appendix II. Field ID's were given according to the village name for easy identification.

Plate 3. Interaction with farmers during field visits

Kharif:

In Kharif season Elbaka, Gangipalle, Rukmapur and Vedurugattu villages were selected for the study. Normal sowing time in Kharif for the selected villages was in July except in the case of Elbaka village, where early sowings were done in June. Fields having MTU1010 and BPT 5204 were selected as they represent medium and long duration varieties. Most of the farmers followed nitrogenous fertilizer recommendations ranging from 135 kg ha^{-1} to 225 kg ha^{-1}. Phosphorous application ranged from 60 kg ha^{-1} to 90 kg

ha^{-1} and potassium application was from 40 kg ha^{-1} to 60 kg ha^{-1}, which was more than the recommended dosage. A major source of irrigation is through canal and bore wells. Yields vary in different villages and the yields ranged from 3500-5800 kg ha^{-1} (Elbaka), 3500-5800 kg ha^{-1} (Gangipalle), 3500-5800 kg ha^{-1} (Rukmapur) and 3500-5800 kg ha^{-1} (Vedurugattu).

Rabi:

Durshed, Nagnur, Malkapur and Renikunta villages were selected for study as they were identified as the major rice growing areas in the rabi season. Nursery sowing time in these villages is from December 2nd fortnight to January end and transplanting is done with four to five-week-old seedlings in all the villages. The majority of the rice growing areas are under the MTU1010 variety. The source of irrigation is through canals and borewells. The farmers applied nitrogen fertilizer level of 135 kg ha^{-1} to 200 kg ha^{-1}. The paddy yields varied in different villages and ranged from 4800-7000 kg ha^{-1} in Durshed, 4500-7500 kg ha^{-1} in Nagnur, 5500-6800 kg ha^{-1} in Malkapur and 4500-6500 kg ha^{-1} in Renikunta.

3.3.3 Nitrogen Fertilizer Application

During the ground data visits while interacting with the farmers the amount of nitrogen fertilizer applied has been collected from individual farmers. The source of nitrogen fertilizer for the crop is urea. The range of nitrogen fertilizer in Elbaka village was 100 kg ha^{-1} to 180 kg ha^{-1}, in Rukmapur it was 140 kg ha^{-1} to 180 kg ha^{-1}, while in Vedurugattu it was 100 kg ha^{-1} to 180 kg ha^{-1} and in gangipalli it was 120 kg ha^{-1} to 180 kg ha^{-1}. An average in all villages was 145 kg ha^{-1} except in Rukmapur it was 160 kg ha^{-1}.

In rabi selected villages application of 120 kg ha^{-1} to 200 kg ha^{-1} in Durshed, 140 kg ha^{-1} to 180 kg ha^{-1} in Nagnur, 120 kg ha^{-1} to 180 kg ha^{-1} in Malkapur and 140 kg ha^{-1} to 200 kg ha^{-1} in renikunta. The average was around 160 kg ha^{-1} in all the villages except Renikunta it was around 170 kg ha^{-1}.

3.3.4 Collection of Leaf Area Index (LAI)

The leaf area index is defined as the leaf area of photosynthetic tissue per unit of ground area which is a dimensionless variable. Leaves exchange energy, carbon, and water with

the atmosphere thus acting as an active interface (Cutini *et al.* 1998). LAI is a bio-physical parameter that is directly related to the yield and it was considered a vital input parameter in many models for diagnosing the crop, grain, and biomass yield estimation.

LAI was collected at different crop stages - transplanting, tillering, grain filling, and maturity stages during the kharif and rabi seasons. Accupar LP 80 ceptometer was used for this study as it can measure above and below-canopy. In each field, LAI was acquired at three different points to reduce the bias. At each point, four readings were taken to minimize the effects of inadvertent leaf movement. Among these, mean data was considered as the input. The readings were collected when the level of Photosynthetically Active Radiation was > 400, as the instruments cannot respond to <400 nm. Before obtaining readings during each visit, the devices are calibrated precisely and the LP-80 contains a calibrated external PAR sensor, which measures PAR simultaneously above and below the canopy. For calibration purposes this sensor is used by the LP-80 to calibrate the AccuPAR probe, ensuring that the PAR response of the external sensor and the probe are identical. At the time of taking the readings, precautions were taken so that the row direction would not overlay with the sun direction by keeping the LAI Probe perpendicular to the row directions. Images during the LAI collection with the ceptometer has been mentioned below (Plate 4).

Plate 4. Collection of LAI in the field using LAI Ceptometer

3.3.5 AccuPAR LP- 80 Ceptometer

The AccuPAR model LP-80 designed by Decagon devices which is a menu-driven, battery-operated linear PAR ceptometer was used to measure light interception in plant canopies and to calculate Leaf Area Index (LAI) by non-destructive sampling (Plate 5). It consists of an integrated microprocessor-driven data logger and probe and the probe contains 80 independent sensors spaced one cm apart. The photosensors measure PAR (Photosynthetically Active Radiation) in the range of 400 to 700 nm waveband. The AccuPAR displays PAR in µmol $m^{-2}s^{-1}$. The AccuPAR can be operated in environments with temperatures from 0 to 50° C and in relative humidities of up to 100%. An added advantage of this instrument is that it saves time and labour, log data unattended for short periods, can record data up to 2000 samples which can be downloaded later with the help of the software LP-80.

The LP-80 uses the following equation to calculate LAI:

$$L = \frac{[(1 - \frac{1}{2K})\, f_b - 1]\ln\tau}{A(1 - 0.47 f_b)} \qquad \textbf{Eq. (3.1)}$$

Where, K = extinction coefficient

f_b = beam fraction (ratio between diffuse and beam radiation)

A = leaf absorptivity

τ = ratio of transmitted and incident PAR

Plate 5. Accupar Lp-80/LAI Ceptometer

3.3.6 Global Positioning System (GPS) tracker

Global Positioning System tracker was used during field visits for navigating and tracking the path (Plate 6). It also determines the exact location with latitude and longitude values of the location at time of the data collection. This helps in the precise collection of data. With this waterbody, built-up, plantations, rice crops and other crops have been pointed which are used during supervised classification. Using this tracker in each field three points are pointed for future use.

Plate 6. GPS Tracker

3.4. Mapping rice areas

3.4.1 Supervised Classification

Classifying the study area districts in both Kharif and rabi seasons was done by supervised classification with the use of ERDAS software. Supervised classification is most frequently employed for quantitative analysis of remote sensing image data (Richards, 2022). A set of training data sets that were collected during ground data collection was used. In supervised classification, the analyst selects and digitizes polygons (training areas) and places these polygons in an AOI (Area of Interest) layer from which to create the signature files, rather than using an automated routine to define the most separable classes. Knowledge of the data, and of the classes desired is required before classification. While doing the classification rice, other crops, built-up, waterbody, orchards and other LULC were identified. Maximum likelihood classification was opted where pixels are classified based on the probability-based rule. This equation calculates the statistical probability of a pixel belonging to a specific signature.

3.4.2 Accuracy Assessment

LULC mapping requires accuracy assessment which is a crucial step in the processing of remote sensing data because classification complexity enhances error probability (Congalton, 1991). It compares the classified image to ground truth data or some other data source deemed to be accurate. User's accuracy, producer's accuracy, kappa's coefficient and error matrix have to be computed for determining the relevancy of the resultant data. Users' accuracy refers to the likelihood that a pixel classified as belonging to a specific category corresponds to that category on the ground. Therefore, it measures the reliability of the map (Banko 1998). The producer's accuracy is determined by the classification accuracy of the reference pixels. It contains the error of omission, which refers to the portion of observed ground features that are not classified on the map. The Kappa Coefficient is obtained from a statistical method that evaluates the classification's accuracy. The formulas for user and producer accuracy were given below under eq. 3.2 and 3.3.

$$\text{Producer's Accuracy} = \frac{\text{Number of correctly classified pixels of a particular class}}{\text{Number of reference pixels of the same class}} X\ 100$$

(Eq. 3.2)

$$\text{User's Accuracy} = \frac{\text{Number of correctly classified pixels of a particular class}}{\text{Number of classified pixels in the class}} X\ 100 \qquad \textbf{(Eq. 3.3)}$$

3.4.3 ERDAS Software

ERDAS Imagine is *a simple raster-based software package designed specifically to extract information from imagery*. This was created for beginners but is also capable of performing a wide range of activities, from fundamental classification to advanced customization. ERDAS IMAGINE is an all-inclusive geospatial-imaging tool for GIS experts that offers remote sensing, photogrammetry, LiDAR analysis, basic vector analysis, and satellite image processing. In addition, it provides advanced features including graphical data modelling, advanced image classification, point cloud classification, and enhanced hyperspectral capabilities. In this research, ERDAS was used to perform the supervised classification for both seasons and to calculate the accuracy assessment of the classified map.

3.5 Yield Estimation

3.5.1 DSSAT

The University of Florida's developed Decision Support System for Agro-technology Transfer (DSSAT), which is a software application program, simulates 42 crops, including CERES-Barley, CERES-Maize, CERES-Rice, CERES-Sorghum, CERES-Sunflower, and CERES-Wheat etc., This software comprises databank management programs for soil, weather, crop management, experimental data, utilities, and application programs mentioned in plate 7. (Hoogenboom *et al.* 2013 and Jones *et al.* 2003).

3.5.2 DSSAT – Data sets

DSSAT crop models require weather, soil and crop management practices. DSSAT interface has been shown under Plate 7.

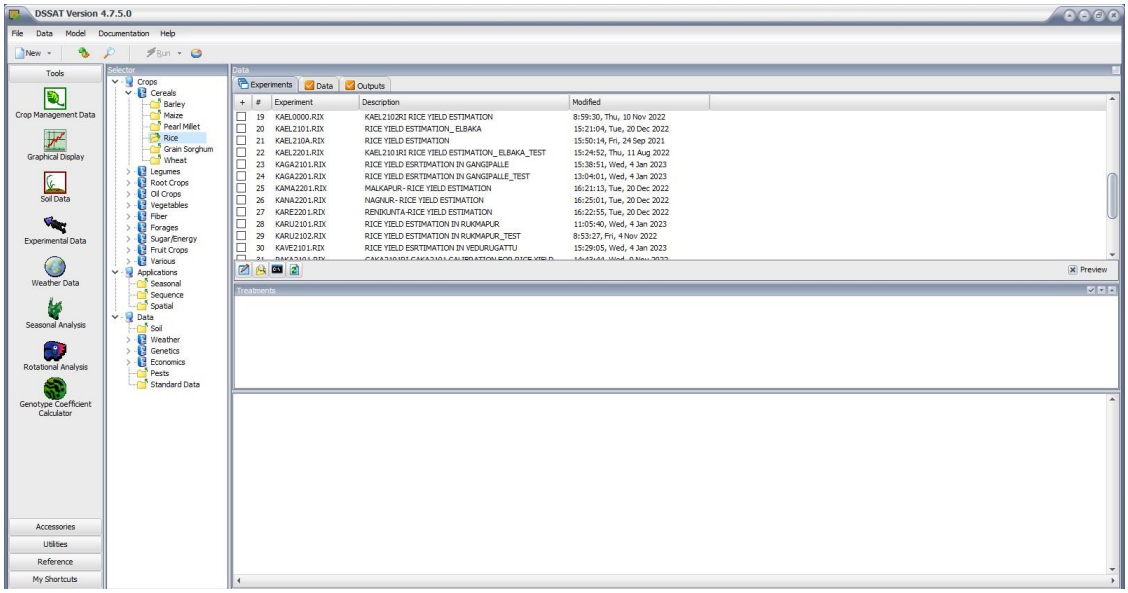

Plate 7. DSSAT User Interface

a. Site data

Latitude, longitude and altitude of the selected points are required for creating crop management file.

b. Weather data

Weather inputs such as daily maximum and minimum temperatures, rainfall, and solar radiation were considered as the minimum data set for the DSSAT model to simulate (Plate 8). Dew point temperature, wind speed, photosynthetically active radiation, minimum relative humidity, and vapor pressure are all optional daily inputs. For this study, maximum and minimum temperatures and rainfall were collected separately over the course of two seasons i.e., from May 2021 to May 2022 from automated weather stations located near the selected villages in the Karimnagar district. Solar radiation was computed through the Hargreaves equation using maximum and minimum temperatures. After the data was obtained, the weather file was prepared with the help of the weatherman tool present in the DSSAT. After entering the data file, it was saved with WTH extension with formatted text (space delimited) i.e., CSV.

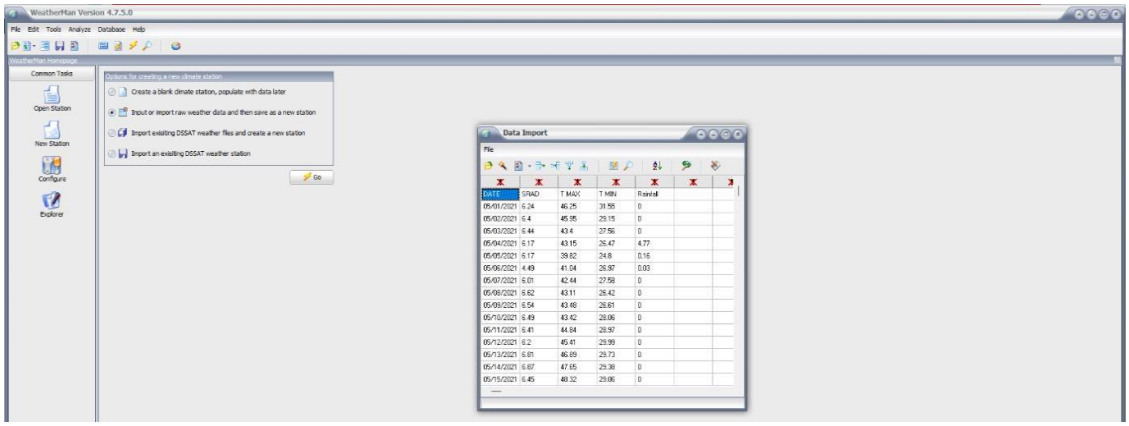

Plate 8. Weather file creation in DSSAT

c. Soil data

DSSAT requires certain soil parameters for its simulation. Measured soil properties like soil texture (sand, silt, and clay percent), pH, EC, cation exchange capacity, nitrogen content, organic carbon percent, and bulk density were used as inputs, collected from ISRIC 2.0, which has a spatial resolution of 250 m (Plate 9). The soil component window is presented in Plate 8. Runoff curve number (RCN) and drainage coefficient (SWCON) were adjusted as per default values to simulate negligible runoff considering the study area has flat topography, good soil structure and moderately drained soils. With the use of Google Earth points field-wise data were collected for each field in depth wise i.e., 0-200 cm. Soil files were saved with SOL extension. Using the general soil database, additional characteristics such as drained upper limit, lower limit, and saturation limits were determined based on the soil texture pedo-transfer characteristics which are provided in the DSSAT models.

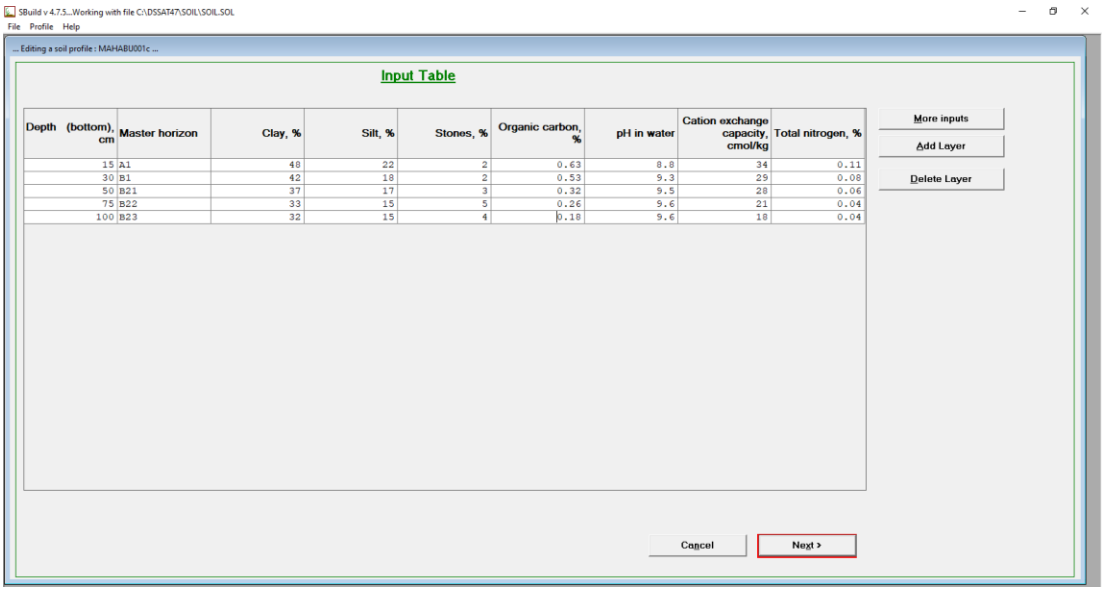

Plate 9. Soil profile data creation in DSSAT

d. Crop data

Crop data like the crop variety and phenological and genotypic coefficients required for running and calibrating the model are mentioned below.

P_1 - Time period (expressed as growing degree-days [GDD] in ^oC above a base temperature of 9oC) from seedling emergence during which the rice plant is not responsive to changes in photoperiod.

P_2O - Longest day length (in hours) at which the development occurs at a maximum rate.

P_2R - Extent to which phasic development leading to panicle initiation is delayed for each hour increase in photoperiod above P_2O.

P_5- Time period in GDD ^oC-d) from the beginning of grain filling (3 to 4 days after flowering) to physiological maturity with a base temperature of 9^oC.

G_1 - Potential spikelet number coefficient as estimated from the number of spikelets per g of main culm dry weight (less leaf blades and sheaths plus spikes) at anthesis.

G_2 - Single grain weight (g) under ideal growing conditions, i.e. non-limiting light, water, nutrients, and absence of pests and diseases.

G_3 - Tillering coefficient relative to IR64 cultivar under ideal conditions

e. Crop management

A questionnaire was developed to collect crop management practices like cultivar, date of transplanting, no of hills/plant, depth of sowing, fertilizer dosage, quantity and duration of irrigation from the farmers (Annexure --). Most popular cultivars like MTU1010 (120 days), BPT5204 (150 days) were selected. The package of practices followed by the farmers was incorporated to the model.

3.5.3 Calibration of the model

In the DSSAT model, cultivar-specific genetic coefficients have been calibrated the using GLUE (Generalized Likelihood Uncertainty Estimation) coefficient estimator, which is available from the latest version of DSSAT 4.5 (Plate 10). GLUE uses Monte Carlo sampling from prior distributions of the coefficients and a Gaussian likelihood function to determine the best coefficients based on the data that are used in the estimation process. Here parameters (Phenological and growth parameters) option was selected and 10000 runs were chosen. After completion of selected runs program randomly generates parameters that are being estimated (either phenology or growth) from the prior distribution of parameter values and runs the model for each. Anthesis day after planting, physiological maturity day after planting, and yield were the three parameters fed to the model for creating A-file. Calibrated values that were generated were used for validation in the rabi season. If the statistical analysis falls under an acceptable range then the calibrated genotypic coefficients are accepted.

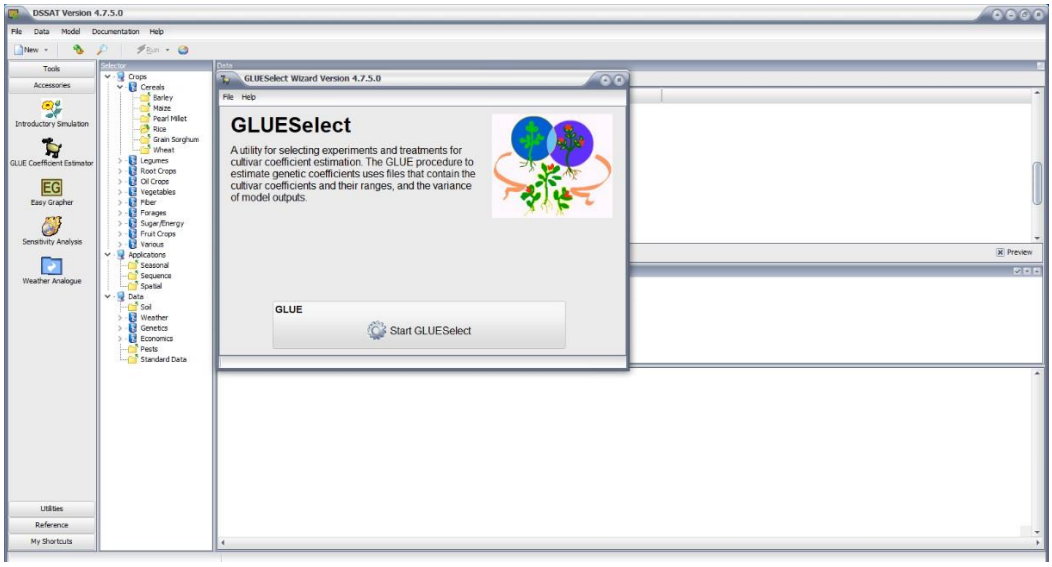

Plate 10. Calibration of the model using GLUE

3.5.4 Evaluating model using statistical measures

The model's performance was assessed using the coefficient of determination (R^2), absolute and normalized root mean square error (RMSE), and the Wilmot d index (Willmott *et al.* 1985), as well as modeling efficiency (ME). The RMSE and d-index values determine the model's ability to predict experimental data. A low RMSE and a d-value near one imply that the experimental data and model output are in good agreement. The normalized RMSE (%) represents the difference between the simulated and observed values. Based on the corresponding normalized RMSE (NRMSE) values of 10%, 10 - 20%, 20 -30%, and >30%, the model simulations in this research were classified as excellent, decent, fair, and poor (Loague and Green, 1991). Modelling efficiency ranges from minus infinity to 1.0. A negative ME indicates that the mean value of the experimental data is a better predictor than the model, whereas a positive ME indicates that the model and observations match perfectly. The model performance measurements equations are as follows

$$RMSE = [n - 1 \sum_{i=1}^{n} (\mathrm{Pi} - \mathrm{Oi})^2]^{0.5} \quad \textbf{Eq. (3.4)}$$

where P_i and O_i are the predicted and observed values, n is the number of observations

$$\text{D Index} = 1 - \left[\frac{\sum_{i=1}^{n} (P_i -)_i^2}{\sum_{i=1}^{n} [|P_i'| + |O_i'|]^2}\right] \quad \textbf{Eq. (3.5)}$$

Where n is the number of observations, P_i is the predicted observation, O_i is the measured observation, $P_i = P_i - M$, and $O_i = O_i - M$ (M is the mean of the observed variable) (Garnier *et al.* 2001).

$$\text{ME} = \left[\frac{[\sum_{=1}^{n} (\mathrm{O} - O) - \sum_{i=1}^{n} (P_i -)_i^2]}{\sum_{i=1}^{n} [O_i - O]^2}\right] \quad \textbf{Eq. (3.6)}$$

Where P_i, O_i are the predicted and observed values, n is the number of observations, and $\bar{O}$ is the mean of the observed variable.

3.6 Derivation of Remote sensing products

With the use of the Google Earth Engine code editor filter date was applied by the ground visit dates which were scheduled as per the satellite passing dates. An interval of 15 days

was taken for collecting satellite images for generating the satellite images i.e., kharif season June 1st fortnight to November 2nd fortnight and during rabi December 1st fortnight to April 1st fortnight. The dates were used to collect the satellite images for LULC generation during Kharif season were Remote sensing products like VV, VH, and VH/VV were derived from sentinel 1 and whereas from sentinel 2 Red (Band 4), NIR (Band 8), and NDVI were derived. These derived products were then compared with the field LAI to identify the correlation. Among these products, based on their correlation to the field LAI, NDVI was used for deriving the spatial LAI map by integrating with the DSSAT output.

3.6.1 Satellites used

Using (Google Earth Engine) GEE as a platform, satellite images were used for the study purpose.

Sentinel-1

Sentinel-1 is a Synthetic Aperture Radar (SAR) mission that provides continuous all-weather, day-and-night images in C-band (center frequency: 5.405 GHz) in four imaging modes with different spatial resolutions and coverages. Sentinel-1A was launched by the European Copernicus program on 3rd April 2014 and sentinel B on 25th April 2015. The eventual two satellite constellations can deliver a six-day repeat cycle at the equator. This is the first of the five missions that the ESA is developing for the Copernicus initiative. Sentinel-1 data are useful for mapping non-rice crops in the absence of optical data identification since they are all-weather capability, have a high spatial resolution (up to 10 m), and are publicly accessible (Jain *et al.* 2019; Milesi and Kukunuri, 2022 and Gumma *et al.*, 2024). Sentinel- 1(SAR) data can be acquired by default in Interferometric Wide swath (IW) mode with dual-polarization.

Sentinel-2

Sentinel-2 is a Copernicus Program Earth observation mission that captures optical images at high spatial resolution (10 m to 60 m) over land and coastal areas, which ensures capture with a high revisit frequency of 5 days. Currently, the mission consists of two satellites, Sentinel-2A and Sentinel-2B; a third satellite, Sentinel-2C, is undergoing testing in preparation for its launch in 2024. Monthly maximum NDVI with cloud

screening for the months of June to November 2021 and December 2021 to April 2022 were collected using data from sentinel-2 bands 4 (red wavelength) and 8 (NIR wavelength), both at a spatial resolution of 10m. Using the monthly Sentinel-2 NDVI data, the cropland mask generated from the additional data was refined in the study district.

Table 3.1: Details of sentinel 1 and sentinel 2

	Sentinel 1	**Sentinel-2**
Spectral range	3.75-7.5cm	0.47-0.6 μm
Resolution	5 m X 20 m	10, 20, 60 m
Orbital altitude	693 km	786 km
Sensor complement	C-SAR	MSI
wavelength	1cm to 1mm	1 micron
Bands	VV, VH	Red (Band 4) and NIR (Band 8)

3.6.2 NDVI:

NDVI measures the difference between red (which vegetation absorbs) and near-infrared light (which vegetation significantly reflects). NDVI reflects the greenness of a pixel, which plays a significant role in the distinction of cropland from others. NDVI values between 0.2 and 0.4 signify the area with sparse vegetation, 0.4 to 0.6 indicates moderate vegetation, and above 0.6 indicates a high density of greenness. The range of NDVI ranges from -1 to +1, and values closer to +1 indicate high greenness. NDVI can be computed by Eq 3.7

$$NDVI = (NIR - Red) / (NIR + Red) \quad \textbf{Eq. (3.7)}$$

3.6.3 Arc Map 10.7.1

In addition to mapmaking and map-based analysis, ESRI®ArcMap is the program for creating and modifying geographic and tabular data, as well as mapmaking. ArcMap's single-user interface permits the editing of shapefiles, coverages, and geodatabases. ArcMap has sophisticated CAD-based editing capabilities that enable the rapid and efficient creation of features while maintaining the spatial integrity of GIS data. Common map elements comprise the data frame comprising map layers for a defined extent in addition to a scale bar, north arrow, title, descriptive text, a symbol legend, etc.

In this research, the integration of remote sensing data with the DSSAT crop model which was used for the spatial distribution of yield and LAI was carried out using Arc Map.

3.6.4 Google Earth Engine

Google Earth Engine (GEE) is a robust web platform for large-scale cloud-based remote sensing data processing. It compiles the world's satellite imagery, trillions of scientific measurements dating back nearly four decades and makes it accessible online with techniques for scientists, research groups, and nations to mine this massive repository of data to detect changes, map trends, and quantify differences on the Earth's surface. Applications include identifying deforestation, identifying land cover, measuring forest biomass and carbon, and mapping roadless regions of the planet. The GEE computing engine offers JavaScript and Python APIs, allowing developers to design parallel algorithms easily. GEE contains USGS-processed Landsat 4, 5, 7, and 8 data, several MODIS products, including global composites, and Sentinel-1, 2, and 3-satellite imagery. The Code Editor (code.earthengine.google.com) is a web-based IDE for writing and implementing scripts. Components of GEE were depicted in Plate 11.

In this study, the Google Earth engine was used to download the satellite images during the respective period for performing supervised classification for both the kharif and rabi seasons. GEE was also used in deriving remote sensing products like NDVI which has been mentioned in detail under Appendix –III and Appendix- IV to integrate with the crop model.

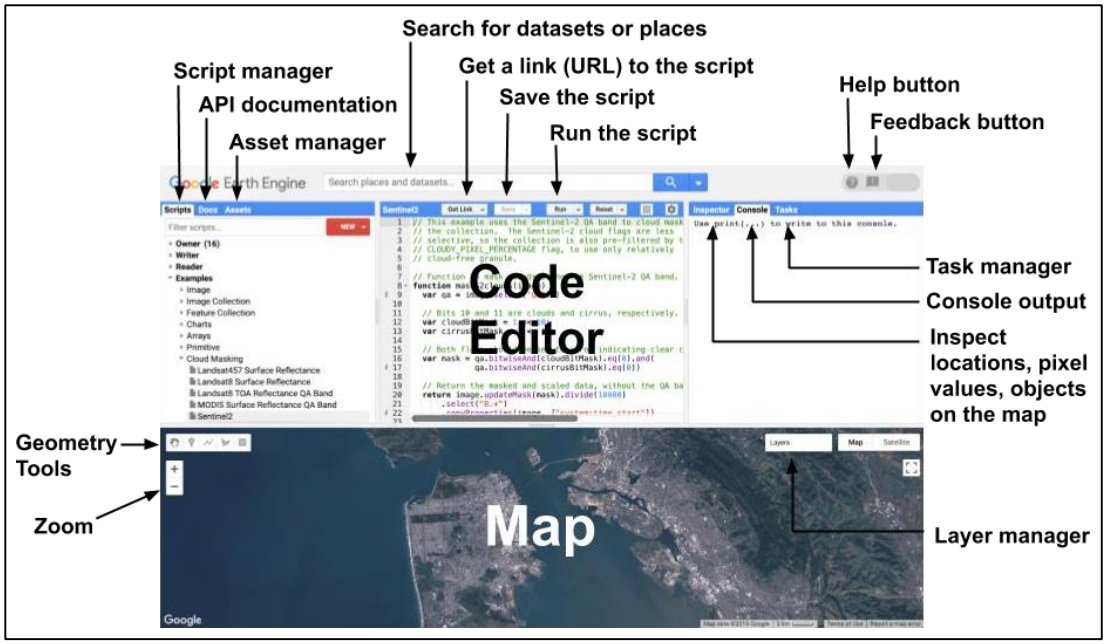

Plate 11. Components of Google Earth Engine

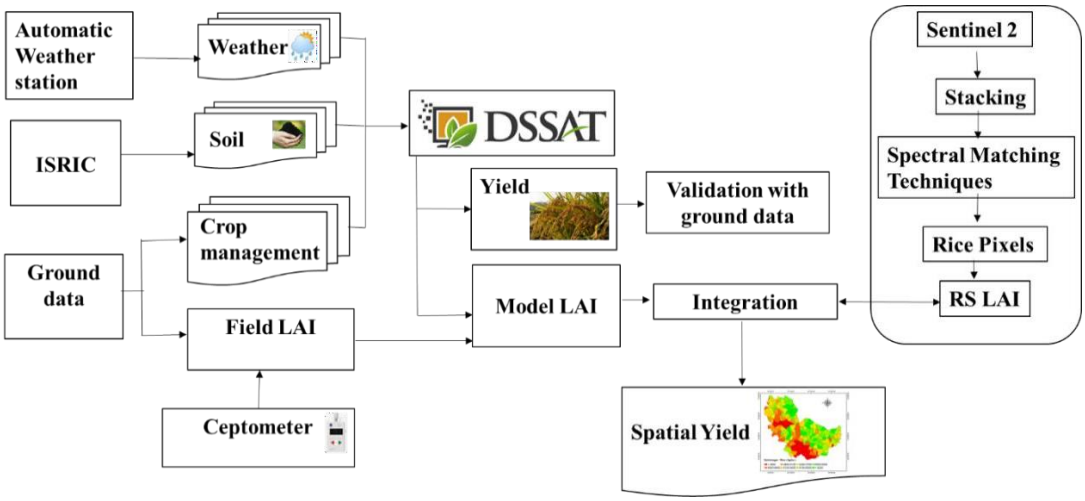

Fig.3.8 Schematic diagram for calculating the spatial rice yield estimation using RS data integrating with the simulation model

3.7 Integration of remote sensing data with crop model data to estimate optimized rice yields

The other vegetation and ambiguous areas were hidden by applying the rice mask from the crop map created using the supervised classification. By setting the NDVI threshold above 0.4, the noise in the identified rice mask was minimized and utilized in the subsequent step of determining the geographical distribution of yield. Figure 3.8 illustrates the methods employed to incorporate Remote Sensing products into the model for spatial yield distribution over the entire district.

3.7.1 Comparison of field LAI to model LAI:

To evaluate the model efficiency in estimating LAI, model LAI has been compared with the field LAI. Once a good relation and linear relation have been obtained integrating model LAI with NDVI derived from remote sensing has been done.

3.7.2 Comparison of NDVI to model simulated LAI:

LAI from the DSSAT model has been compared with the NDVI derived from remote sensing on the basis of corelation between them.

3.7.3 Generation of spatial rice LAI map:

On the basis of the linear regression generated among the model LAI and NDVI , a spatial LAI map was generated for the Karimnagar district .

3.7.4 Generation of spatial rice Yield map:

Spatial rice yield map was generated on the basis of the relation between the model simulated LAI and yield. The linear equation generated from the correlation was applied to the spatial LAI map to generate a spatial rice yield map.

3.8 Validation of the estimated yield

The estimated yield obtained from running the DSSAT model was compared with the district-level government yield statistics for the respective seasons to know the accuracy of the model.

Chapter IV

RESULTS

This chapter describes the experimental findings of the research conducted on "Assimilation of Remote Sensing Data into Crop Simulation Models for Rice Yield Estimation in Karimnagar District," during Kharif 2021 and rabi seasons of 2021-22. The outcomes of this research were presented in the form of tables, graphs, and photographs. This chapter seeks to examine and explain the main observations and conclusions of the current study.

4.1 Optimization of CCE Locations

4.1.1 Selection of Study Area

As mentioned earlier (chapter 3) crop-cutting experiment locations were optimized in the Karimnagar district based on the factors like soil maps, rainfall maps, crop type map and elevation points. Taking these factors in to consideration villages were selected which were Elbaka, Gangipalli, Vedurugattu and Rukmapur in kharif season and Durshed, Nagnur, Renikunta and Malkapur in rabi season. In all the selected villages soil types, rainfall were different.

4.1.2 Crop Cutting Experiments

In the selected villages during both season's crop-cutting experiments were conducted in the selected farmers' fields in an area of 5m*5m area which was plotted in the selected fields where the plants were cut and the grain was separated from the panicles (Fig. 4.3). The grain weight was taken and its moisture content was measured and the grain weight was adjusted to 14%. This weight was considered as the observed grain yield.

Plate 12: Crop cutting experiments performed in the selected villages

4.1.2.1 Kharif season

The data of the crop-cutting experiments showed a depicts grain yield variations. During the kharif season the grain yield ranged from 4000 to 5900 kg ha^{-1}. And the average kharif yield among all the villages studied was 5321 kg ha^{-1}.

In Elbaka village, the lowest grain yield was observed in EL6 i.e., 4300 kg ha^{-1} while the highest was recorded in EL2 site (5800 kg ha^{-1}). The difference between the highest and lowest grain yields was around 1500 kg ha^{-1}. The average grain yield observed was 5333 kg ha^{-1} (Table 4.9). In Vedurugattu village, the observed yields ranged from 5200 kg ha^{-1} to 5900 kg ha^{-1} with a deviation of 700 kg ha^{-1}. The highest was observed under the VE6 field ID while the lowest was noticed under VE2. On an average, the grain yield of this village was 5512 kg ha^{-1} (Table 4.10).

In Rukmapur village, the highest grain yield recorded was 5750 kg ha^{-1} in site RU9 and the lowest the lowest was observed in site RU5 (4800 kg ha^{-1}) with a grain yield deviation of 950 kg ha^{-1}. The average grain yield of this village was 5261 kg ha^{-1} (Table 4.11). The highest grain yield of 5700 kg ha^{-1} in Gangipalli was recorded at the GA8 site while the lowest grain yield was noticed at the GA2 site (4400 kg ha^{-1}) with a deviation in grain yield of 1300 kg ha^{-1}. On average, the grain yield of Gangipalli was 5178 kg ha^{-1} (Table 4.12).

4.1.2.2 Rabi season

As like in Kharif season, in the rabi season also the crop cutting experiments were performed in study villages - Durshed, Nagnur, Malkapur and Renikunta. Among all the villages, the observed grain yields were varying from 4000 kg ha^{-1} to 7400 kg ha^{-1}. On an average, rabi grain yield among all the villages was 6436 kg ha^{-1}. Individual village wise grain yields are mentioned in Tables 4.13 to 4.16.

In Durshed village, the highest grain yield of 7000 kg ha^{-1} was observed at the DU1 site, while the lowest was noticed at the DU6 site with a grain yield of 5600 kg ha^{-1}. A deviation of 1400 kg ha^{-1} was observed between higher and lower grain yield. An average grain yield of 6160 kg ha^{-1} was recorded in Durshed village (Table 4.13).

In Nagnur village, the highest grain yield was noticed at the NA9 site (7200 kg ha^{-1}) and the lowest grain yield was observed at the NA7 site (4000 kg ha^{-1}) with a deviation of 3200 kg ha^{-1}. The difference in grain yield between the highest and lowest was large due to a pest attack at the NA7 site. On average, 6327 kg ha^{-1} grain yield was recorded in this village (Table 4.14).

The average yield of Malkapur village was 6500 kg ha^{-1} (Table 4.15) with the lowest grain yield of 5900 kg ha^{-1} at the MA12 site while the highest grain yield was recorded at the MA1 site (6900 kg ha^{-1}). There was a deviation of 1000 kg ha^{-1} between the highest and lowest grain yield.

In Renikunta village, the highest grain yield was noticed at the RE12 site (7100 kg ha^{-1}) while the lowest grain yield was recorded at the RE3 site (6400 kg ha^{-1}) with an average grain yield of 6758 kg ha^{-1} (Table 4.16). There was a deviation in grain yield of 700 kg ha^{-1} between higher and lower grain yield recorded in the village.

From the above results it can be noted that yields vary in each village and village to village due to the adoption of different packages of practices like different times of sowing and transplanting time and levels of fertilizer application and irrigation.

4.2 LAI Estimation using LAI ceptometer

Using Accupar LP-80 ceptometer Leaf Area Index readings in the respective selected fields in the villages were collected during the ground data collection. Visits were planned so that all the growth stages were covered and a complete LAI trend could be obtained.

4.2.1 LAI of the rice crop during the Kharif season

During the Kharif season, Rukmapur, Vedurugattu, Elbaka and Gangipalli villages were selected for the study. Medium duration cultivar MTU1010 was grown in the major area and BPT-5204 a long duration variety to some extent. During the visits, time (i.e., September 6th, September 15th, October 1st, and October 21st) crops are under tillering, heading, flowering and maturity stages. In medium duration cultivar, the LAI readings ranged between 3.2 to 5.0 during the flowering stage (60-70 Days after transplanting, DAT), 4.01 to 4.5 at the grain formation stage, and 2.5 to 3.3 during the maturity stage. In long-duration cultivar BPT -5204, the LAI ranged between 4.8 to 5.2 during the heading stage and 3.0 to 3.9 during the maturity stage. It has been observed that after the peak vegetative phase, LAI declines because of the drying of the leaves (Chandrashekar *et al.* 2001). Maximum LAI recorded through the ceptometer for individual villages were presented in tables 4.1 and 4.2. Maximum LAI recorded was ranging from 3.5 to 4.8 under different villages.

Table 4.1 Maximum LAI recorded through ceptometer and DSSAT model in Elbaka (EL) and Vedurugattu (VE) village

Field ID	Ceptometer Max LAI	Model Max LAI	Field ID	Ceptometer Max LAI	Model Max LAI
EL1	4.8	4.9	VE1	4.7	4.3
EL2	4.8	4.7	VE2	5	5.1
EL3	4.4	4.3	VE3	4.6	4.7
EL4	4.5	4.6	VE4	4.4	4.1
EL5	4.5	4.6	VE5	4.6	4.3
EL6	3.6	3.9	VE6	4.1	4.3
EL7	4.4	4.2	VE7	4.3	4.1
EL8	4.1	4.0	VE8	4.4	4.3
EL9	4.5	4.3	VE9	4.7	5.0
EL10	4.8	4.6	VE10	4.7	4.9
EL11	4.4	4.0	VE11	4.6	4.2
EL12	4.5	4.2	VE12	4.6	4.6

Table 4.2 Maximum LAI recorded through ceptometer and DSSAT model in Rukmapur (RU) and Gangipalli (GA) village

Field ID	Ceptometer Max LAI	Model Max LAI	Field ID	Ceptometer Max LAI	Model Max LAI
RU1	4.1	3.9	GA1	4.4	4.2
RU2	4.0	3.5	GA2	3.5	3.0
RU3	4.1	3.8	GA3	3.8	3.8
RU4	4.0	3.7	GA4	3.9	4.1
RU5	4.0	4.0	GA5	3.6	3.4
RU6	4.6	4.5	GA6	4.7	4.5
RU7	4.1	3.8	GA7	4.0	4.0
RU8	3.9	4.0	GA8	4.7	4.1
RU9	4.8	4.7	GA9	4.0	4.1
RU10	4.2	4.0	GA10	3.8	3.9
RU11	4.2	4.4	GA11	3.7	3.8
RU12	4.8	4.5	GA12	4.7	4.6
RU13	4.8	5.0	GA13	3.8	3.8
RU14	4.6	4.8	GA14	4.7	4.6
RU15	4.5	4.7			

4.2.2 LAI of the rice crop during Rabi season

During the Rabi season four villages - Renikunta, Malkapur, Durshed and Nagnur were selected for sample collections. During this season, only medium duration variety MTU 1010 was grown popularly. Visits were made on January 27th, February 17th, March 8th, and April 8th which coincided with crop growth stages of transplanting, maximum tillering, grain filling, and maturity stages. The LAI readings during the maximum tillering stage ranged from 4.6 to 6.1, at the flowering stage, it ranged from 4.1 to 5.6 and

near to maturity stage it was 2.2 to 3.5. The maximum LAI recorded with the ceptometer and the LAI simulated with the model was 3.4 to 6.1 in different villages (Table 4.3 and 4.4).

Table 4.3 Maximum LAI recorded through ceptometer and DSSAT model in Durshed (DU) and Malkapur (MA) village

Field ID	Ceptometer Max LAI	Model Max LAI	Field ID	Ceptometer Max LAI	Model Max LAI
DU1	5.8	6.4	MA1	5.9	5.9
DU2	5.6	5.8	MA2	5.6	5.6
DU3	5.5	5.8	MA3	5.6	5.6
DU4	4.6	5.4	MA4	5	5
DU5	4.7	5.5	MA5	5.6	5.6
DU6	4.6	5	MA6	5.7	5.7
DU7	5	5.7	MA7	5.4	5.4
DU8	5	5.6	MA8	5.3	5.3
DU9	5	5.5	MA9	5.5	5.5
DU10	4.7	5.4	MA10	5.6	5.6
DU11	5.5	5.8	MA11	5.5	5.5
DU12	5	5.8	MA12	5	5
DU13	5.1	5.7	MA13	5.7	5.7
DU14	5	5.5			
DU15	5.1	5.8			

Table 4.4 Maximum LAI recorded through ceptometer and DSSAT model in Renikunta (RE) and Nagnur (NA) village

Field ID	Ceptometer Max LAI	Model Max LAI	Field ID	Ceptometer Max LAI	Model Max LAI
RE1	5.9	6.2	NA1	5.9	6.2
RE2	6	6.2	NA 2	5.7	2.7
RE3	6	6.2	NA 3	5.6	6.2
RE4	5.8	6	NA 4	3.4	3.1
RE5	5.8	6.2	NA 5	5.5	6.3
RE6	6.1	6.4	NA 6	5.6	6.3
RE7	5.5	6	NA 7	3.2	2.6
RE8	5.5	6.1	NA 8	5.7	6.3
RE9	5.9	5.9	NA 9	6.2	6.5
RE10	5.8	6.4	NA10	5.8	6.1
RE11	5.5	5.9	NA11	5.8	6.2
RE12	5.5	6			

4.3 Mapping of Rice Growing Areas

Supervised classification has been performed using ERDAS Imagine and ARC GIS for classifying the satellite data as used by different scientists (Patil *et al.* 2012, Abiy and Suryabhagavan 2016 and Rwanga and Ndambuki 2017).

4.3.1 Supervised classification

The supervised classified map of Karimnagar district during the kharif season was depicted in fig. 4.1. The area of the different class categories in both the seasons obtained from supervised classification were given in table 4.5. From the classified map in the kharif season, the largest area was occupied by rice with 143 thousand ha and other LULC occupied 43 thousand ha. Water bodies and built-up occupy an area of 1 thousand ha

each, while other crops and orchards occupy an area of 5588 ha and 2154 ha respectively. An overall accuracy of 93.04 % was observed with a kappa coefficient of 0.89. During the rabi season, rice occupied an area of 114166 ha, while other

covers an area of 54047 ha. Other crops in the rabi season include maize and pulses which are grown in an area of 28418 ha. Waterbody and built-up areas each occupy 95 thousand and 86 thousand ha respectively.

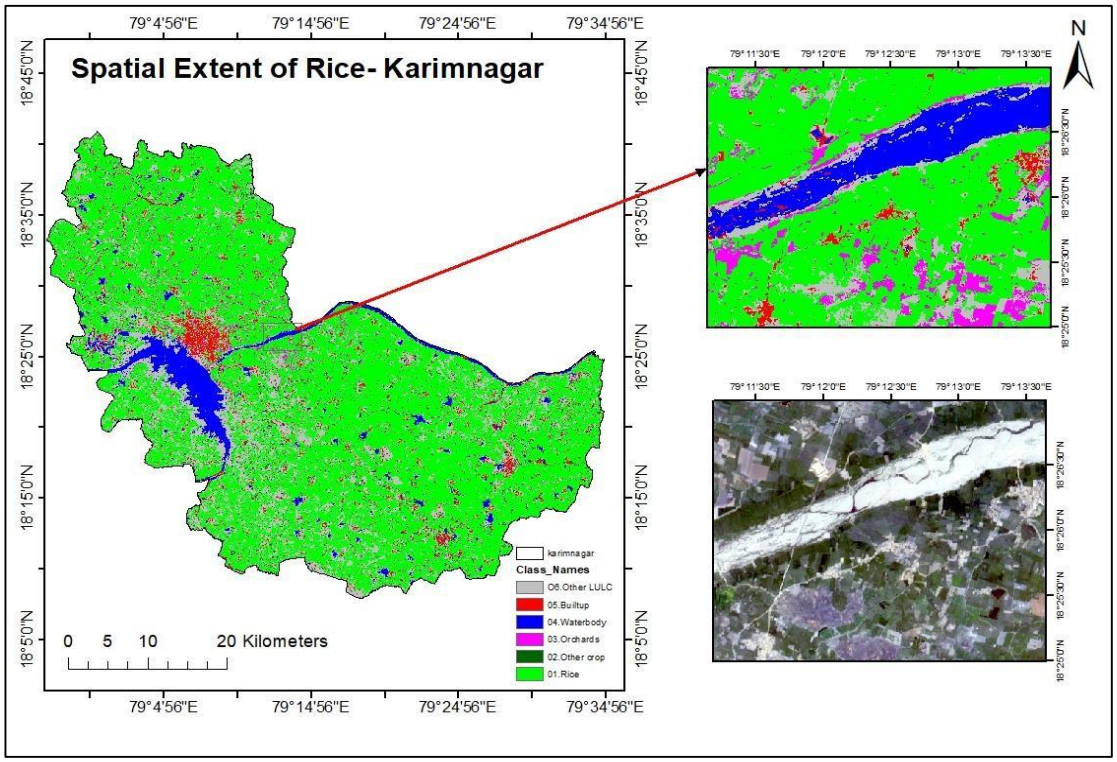

Fig. 4.1 Mapping of rice area in Karimnagar District during Kharif 2021

The total rice area in Karimnagar district during kharif in the classified map was 143 thousand ha which was compared with the area given by government statistics of Telangana was 147 thousand ha (https://agri.telangana.gov.in/). In the rabi season the cultivated rice area resulted from the classified map was 114 thousand ha while the rice area given by Telangana government statistics was 130 thousand ha.

Table 4.5 Area of the respected classes from the classified map during Kharif season

Class Name	Kharif Area (ha)	Rabi Area (ha)
Rice	146602	114166
Other Crop	5588	28418
Orchards	2154	3049
Waterbody	10566	9582
Builtup	10041	8689
Other LULC	43000	54047

Supervised classification for rabi is mentioned below under Fig.4.2. The supervised classification map shows that the light green color denotes rice-growing areas, whereas the dark green color indicates other crops such as cotton and maize.

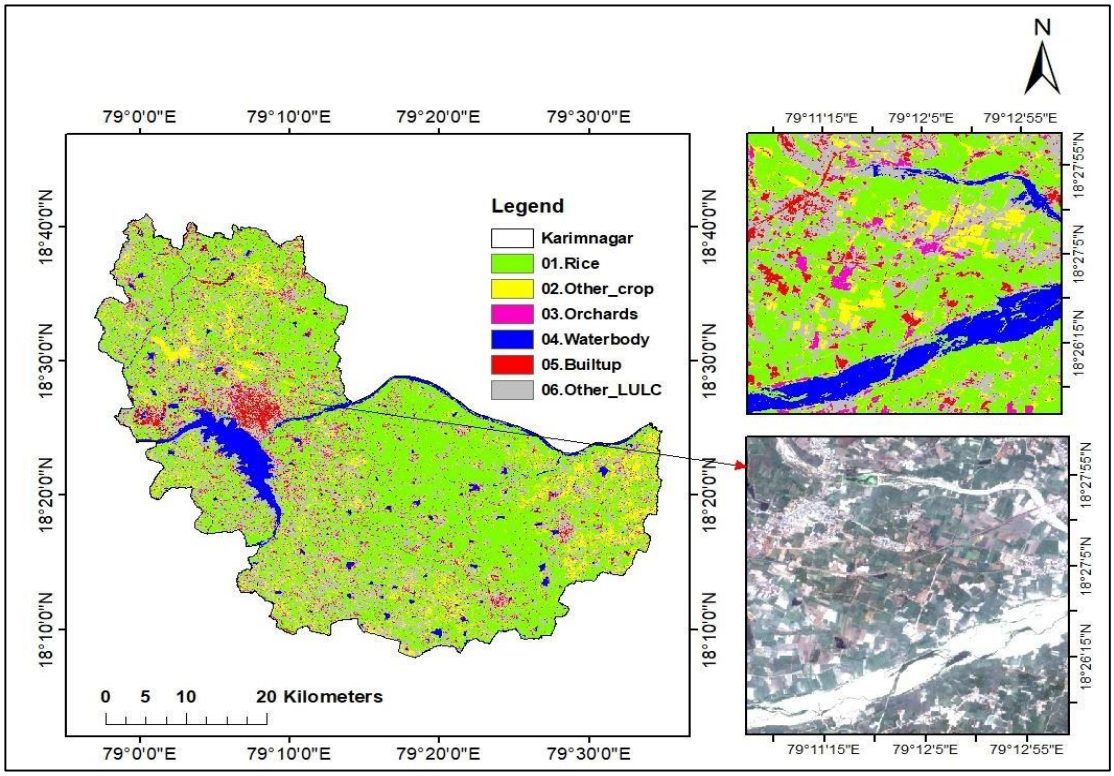

Fig. 4.2 Mapping of the rice area in Karimnagar District during Rabi 2021

The dark blue color represents the body of water, while the red color represents the built-up. Pink color represents orchards. The grey color in the categorized map depicts places having various LULC classes such as forest area wasteland, and scrubland, among others.

4.3.2 Accuracy assessment

Accuracy assessment was performed for both the season's supervised classification images to know the level of accuracy and identify the errors. It involves the comparison of a place on the classified map against the Google Earth map or reference data for the same site. Agreement of classification with the ground data was measured by means of overall accuracy and kappa statistics. A total of 220 ground data points were collected during kharif season and in that 156 points were used for training and 64 points were used for validation during kharif season, while in rabi season a total of 200 ground data points were collected and out of that 131 samples were used for training and 69 were used for validation durng rabi season. From the classified map, during Kharif season it can be seen that good accuracy has been obtained in terms of users and producers with a kappa coefficient of 0.89. An overall accuracy of 94.23% (Table 4.6) has been obtained.

Table 4.6 Confusion Matrix showing classification accuracy of Karimnagar district during Kharif 2021

Classified	Rice	Other crops	Orchards	Water body	Built up	Other LULC	Totals	Users accuracy (%)
Rice	95	0	0	0	1	2	98	96.94
Other crops	0	6	1	0	0	0	7	85.71
Orchards	0	1	7	0	0	0	8	87.5
Waterbody	0	0	0	11	0	0	11	100
Built up	0	0	0	0	18	0	18	100
Other LULC	3	0	0	0	1	10	14	71.43
Totals	98	7	8	11	20	12	156	
Producers accuracy (%)	96.94	85.71	87.5	100	90	83.33		
Overall accuracy (OA)				94.23%				
Kappa coefficient				0.899				

For the rabi season, classified map accuracy assessment was performed using the same methodology as that of Kharif and it was observed that overall accuracy of 88.5% and a kappa coefficient of 0.85 has been obtained for the supervised classification map using the ERDAS imagine (Table 4.7).

Table 4.7. Confusion Matrix showing classification accuracy of Karimnagar district during Rabi 2021-22

Classified	Rice	Other crops	Orchards	Water body	Built up	Other LULC	Totals	Users accuracy (%)
Rice	49	2	0	0	0	0	51	96.08
Other crops	1	16	0	0	0	0	17	94.12
Orchards	1	4	15	0	0	0	20	75
Waterbody	0	0	0	14	0	1	15	93.33
Built up	1	0	0	0	12	2	15	80
Other LULC	2	0	0	0	1	10	13	76.92
Totals	54	22	15	14	13	13	131	
Producer's accuracy (%)	90.74	72.73	100	100	92.31	76.92		
Overall accuracy (OA)				88.5%				
Kappa coefficient				0.85				

4.4 Yield Estimation

4.4.1 Calibration of the model

Model calibration or parameterization is the adjustment of parameters to the local conditions so that simulated values compare well with the observed ones (Timsina and Humphreys, 2006). Calculating the genetic coefficient of cultivars is the first step in the conventional use of the CERES models. The DSSAT model has been calibrated with GLUE (Generalized Likelihood Uncertainty Estimation). Model calibration has been done using the kharif season data which was collected during the ground data. Data used

for calibration includes the sowing date, anthesis day, grain yield, straw yield and maximum LAI. After running the model with the specific number of runs (i.e., 10000) for the selected cultivar i.e., MTU1010 model generated cultivar coefficients. As they are in the acceptable range of statistical analysis the calibrated coefficients were considered for further usage. In this research the model generated calibrated values for the MTU 1010 cultivar were used (Table 4.8).

Table 4.8 Calibrated values for the MTU1010 cultivar

Genetic Parameters	Description	Coefficients for MTU 1010
G1	Time period (expressed as growing degree days [GDD] in ◦C above a base temperature of 9 ◦C) from seedling emergence during which the rice plant is not responsive to changes in photoperiod. This period is also referred to as the basic vegetative phase of the plant	440
P_2O	Critical photoperiod or the longest day length (in hours) at which the development occurs at a maximum rate. At values higher than P20 developmental rate is slowed, hence there is a delay due to longer day lengths	165
P_2R	The extent to which phasic development leading to panicle initiation is delayed (expressed as GDD in ◦C) for each hour increase in photoperiod above P20	350
P5	The time period in GDD (◦C) from the beginning of grain filling (3–4 days after flowering) to physiological maturity with a base temperature of 9 ◦C	12
G1	Potential spikelet number coefficient as estimated from the number of spikelets per g of main culm dry weight (less lead blades and sheaths plus spikes) at anthesis. A typical value is 55	60
G2	Single grain weight (g) under ideal growing conditions, i.e. non-limiting light, water, nutrients, and absence of pests and diseases	.0240

G3	Tillering coefficient (scalar value) relative to IR64 cultivar under ideal conditions. A higher tillering cultivar would have a coefficient greater than 1.0	1.0
G4	Temperature tolerance coefficient. Usually 1.0 for varieties grown in normal environments. G4 for japonica type rice growing in a warmer environment would be 1.0 or greater. Likewise, the G4 value for indica type rice in very cool environments or seasons would be less than 1.0	1.0

4.4.2 Simulation of rice grain yield and comparison with the observed yields

DSSAT crop simulation model was used for rice yield estimation in both kharif and rabi seasons. Different weather files, soil files and X-build files were created for the chosen villages as the selected farmers followed varied packages of practices like sowing and transplanting date and quantity of fertilizers applied. After running the model, the deviation between simulated and observed grain yields was worked out by comparing it with the observed yields that were recorded from the crop-cutting experiments.

4.4.2.1 Kharif rice grain yields

In Kharif season, the simulated yields with the deviation from observed rice grain yields of the selected villages - Elbaka, Gangipalli, Vedurugattu and Rukmapur are given in Tables 4.9, 4.10, 4.11 and 4.12. On an average the simulated grain yield in kharif was 5339 kg ha^{-1}.

In Elbaka village, highest grain yield (5982 kg ha^{-1}) was noticed at the EL1 site, while the lowest grain yield was observed at EL6 site (4218 kg ha^{-1}) with a deviation in grain yield of 1764 kg ha^{-1} (Table 4.9.) On comparison of observed and simulated grain yields, there was deviation of 8.5 kg ha^{-1} to 434 kg ha^{-1} with an average of observed grain yield of 5348 kg ha^{-1} and simulated grain yield of 5397 kg ha^{-1}.

Table 4.9 Observed and simulated rice grain yields in Elbaka village

Field ID	Observed Yields, kg ha^{-1}	Simulated Yields, kg ha^{-1}	Deviation in yield, kg ha^{-1}
EL1	5700	5982	282
EL2	5800	5804	4
EL3	5400	5325	-75
EL4	5600	5492	-108
EL5	5600	5500	-100
EL6	4300	4218	-82
EL7	5100	5339	239
EL8	4700	5000	300
EL9	5400	5459	59
EL10	5400	5866	466
EL11	5400	5307	-93
EL12	5600	5483	-117

Highest grain yield (6018 kg ha^{-1}) was observed at VE9 site inVedurugattu village, while the lowest was noticed at VE7 site with yield of 5046 kg ha^{-1} (Table 4.10). Among all the fields, a deviation in grain yield ranged between 35 kg ha^{-1} to 268 kg ha^{-1} with a mean of observed and simulated grain yield of 5525 kg ha^{-1} and 5512 kg ha^{-1}.

Table 4.10 Observed and simulated rice grain yields of Vedurugattu village

Field ID	Observed Yields, kg ha^{-1}	Simulated Yields, kg ha^{-1}	Deviation in grain yield, kg ha^{-1}
VE1	5600	5436	164
VE2	5950	6001	-51
VE3	5500	5763	-263
VE4	5300	5160	140
VE5	5500	5426	74
VE6	5250	5427	-177
VE7	5300	5046	254
VE8	5400	5365	35
VE9	5750	6018	-268
VE10	5700	5813	-113
VE11	5400	5204	196
VE12	5500	5644	-144

A deviation between the observed and simulated grain yield ranged between 54 kg ha^{-1} and 286 kg ha^{-1}. It can be observed from the results that in Rukmapur village highest grain

yield of 6221 kg ha^{-1} was noticed at RU13 site, while the lowest was recorded at RU7 site with a grain yield of 4784 kg ha^{-1}. On an average, the observed and simulated grain yield in Rukmapur village was 5261 kg ha^{-1} and 5264 kg ha^{-1} respectively (Table 4.11).

Table 4.11 Observed and simulated rice grain yields of Rukmapur village

Field ID	Observed Yields, kg ha^{-1}	Simulated Yields, kg ha^{-1}	Deviation in grain yield, kg ha^{-1}
RU1	5100	4993	107
RU2	4900	4580	320
RU3	5100	4814	286
RU4	4900	4616	284
RU5	4800	5000	-200
RU6	5500	5537	-37
RU7	5000	4784	216
RU8	5000	5187	-187
RU9	5750	5674	76
RU10	5125	5179	-54
RU11	5250	5495	-245
RU12	5750	5524	226
RU13	5750	6221	-471
RU14	5500	5737	-237
RU15	5500	5631	-131

In Gangipalli village, the highest grain yield was noticed at GA14 site with a grain yield of 5668 kg ha^{-1}, while the lowest was observed at GA2 site with a grain yield of 4141 kg ha^{-1} (Table 4.12). In this village, a deviation in observed and estimated grain yield ranged between 18 kg ha^{-1} and 266 kg ha^{-1}. On an average, the simulated grain yield was 5174 kg ha^{-1}, while the observed grain yield was 5168 kg ha^{-1}.

Table 4.12 Observed and simulated rice grain yields of Gangipalli village

Field ID	Observed Yields, kg ha^{-1}	Simulated Yields, kg ha^{-1}	Deviation in grain yield, kg ha^{-1}
GA1	5400	5330	-70
GA2	4400	4141	-259
GA3	4900	4986	86
GA4	5100	5284	184
GA5	4800	4597	-203
GA6	5600	5549	-51
GA7	5200	5184	-16

GA8	5700	5359	-341
GA9	5200	5361	161
GA10	5100	5190	90
GA11	4700	4964	264
GA12	5700	5668	-32
GA13	5100	5081	-19
GA14	5600	5668	68

4.4.2.2 Rabi Rice Grain Yields

In rabi season, four villages - Durshed, Nagnur, Renikunta and Malkapur were selected for the study and the yields were simulated by using the model. The observed grain yields obtained from the crop cutting experiments were compared with the model simulated grain yields to find the deviation between them and to know the model accuracy in estimating the grain yield under varying management conditions. On an average the simulated grain yields in rabi was 6858 kg ha^{-1}.

In Durshed village, the highest grain yield of 7479 kg ha^{-1} was noticed at DU1 site, while the lowest of 6000 kg ha^{-1} was obtained at DU6 site with a deviation in grain yield of 1479 kg ha^{-1} (Table 4.13). The deviation between observed and simulated yields ranged between 300 kg $ha^{-1}$and 600 kg ha^{-1} with an average observed yield of 6160 kg ha^{-1} and simulated grain yield of 6630 kg ha^{-1}.

Table 4.13 Observed and simulated rice grain yields of Durshed village

Field ID	Observed Yields, kg ha^{-1}	Simulated Yields, kg ha^{-1}	Deviation in grain yield, kg ha^{-1}
DU1	7000	7479	479
DU2	6500	6863	363
DU3	6400	6800	400
DU4	5700	6200	500
DU5	5800	6400	600
DU6	5600	6000	400
DU7	6000	6600	600
DU8	6000	6600	600
DU9	6100	6500	400
DU10	5800	6300	500
DU11	6500	6800	300
DU12	6300	6833	533
DU13	6300	6680	380
DU14	6100	6500	400

DU15	6300	6900	600

In Nagnur village, the highest grain yield was noticed at NA9 site with grain yield of 8177 kg ha^{-1}, while the lowest was observed at NA7 site with grain yield of 3271 kg ha^{-1} (Table 4.14). Deviation in observed grain yield ranged from 459 kg ha^{-1} to 977 kg ha^{-1} among the fields. The average simulated grain yield was 6740 kg ha^{-1}, while the average observed grain yield was 6327 kg ha^{-1}.

Table 4.14 Observed and simulated rice grain yields of Nagnur village

Field ID	Observed Yields, kg ha^{-1}	Simulated Yields, kg ha^{-1}	Deviation in grain yield, kg ha^{-1}
NA1	6900	7437	537
NA 2	6700	7281	581
NA 3	6600	7307	707
NA 4	4500	4041	-459
NA 5	6600	7388	788
NA 6	6700	7319	619
NA 7	4000	3271	-729
NA 8	6800	7319	519
NA 9	7200	8177	977
NA10	6800	7281	481
NA11	6800	7319	519

In Malkapur village, the highest grain yield observed was 7100 kg ha^{-1} at MA13 site, while the lowest grain yield was noticed at MA12 site (6100 kg ha^{-1}). Among all the fields, a deviation of 183 kg ha^{-1} to 418 kg ha^{-1} was recorded among the observed grain yields with a mean of observed and simulated grain yield of 6500 kg ha^{-1} and 6717 kg ha^{-1} respectively (Table 4.15).

Table. 4.15 Observed and simulated rice grain yields in Malkapur

Field ID	Observed Yields, kg ha^{-1}	Simulated Yields, kg ha^{-1}	Deviation in grain yield, kg ha^{-1}
MA1	6900	6500	-400
MA2	6500	6317	-183
MA3	6500	6831	331
MA4	6500	6800	300
MA5	6700	7081	381
MA6	6700	6932	232

MA7	6300	6600	300
MA8	6200	6544	344
MA9	6500	6918	418
MA10	6500	6800	300
MA11	6500	6800	300
MA12	5900	6100	200
MA13	6800	7100	300

In Renikunta village, the highest grain yield of 7438 kg ha^{-1} was noticed at RE2 site, while the lowest was recorded at RE12 site (7107 kg ha^{-1}). Deviation between the observed and simulated grain yield ranged between 334 kg ha^{-1} to 781 kg ha^{-1}. The average observed and simulated grain yields in the village were 6758 kg ha^{-1} and 7345 kg ha^{-1} respectively (Table 4.16).

Table 4.16 Observed and simulated rice grain yields in Renikunta

Field ID	Observed Yields, kg ha^{-1}	Simulated Yields, kg ha^{-1}	Deviation in grain yield, kg ha^{-1}
RE1	6900	7316	416
RE2	7000	7438	438
RE3	7100	7434	334
RE4	6800	7294	494
RE5	6800	7395	595
RE6	7000	7617	617
RE7	6500	7281	781
RE8	6500	7269	769
RE9	6800	7294	494
RE10	6800	7516	716
RE11	6500	7182	682
RE12	6400	7107	707

4.4.3 Evaluation of the DSSAT model

4.4.3.1 Kharif

Observed yields across the selected villages in Karimnagar ranged from 4100 kg ha^{-1} to 5800 kg ha^{-1}, whereas the simulated yields ranged from 4300 kg ha^{-1} to 6000 kg ha^{-1} in the four villages studied.

A comparison of observed yields with model simulated yields showed a linear relationship. The regression's coefficient of determination R^2 of 0.80 has been resulted between observed and simulated yields which reveals that there is a minor deviation between the observed and simulated yields (Fig 4.6). Result shows that the model has accurately estimated rice grain yields under varying management conditions.

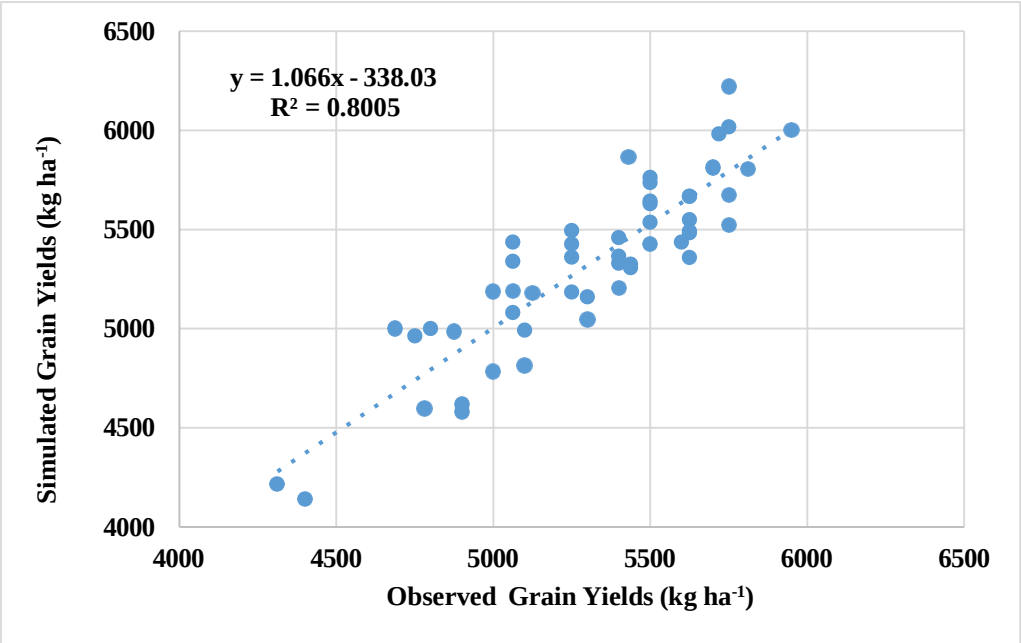

Fig.4.3 Correlation between the observed versus simulated grain yield (kg ha^{-1}) in Kharif season

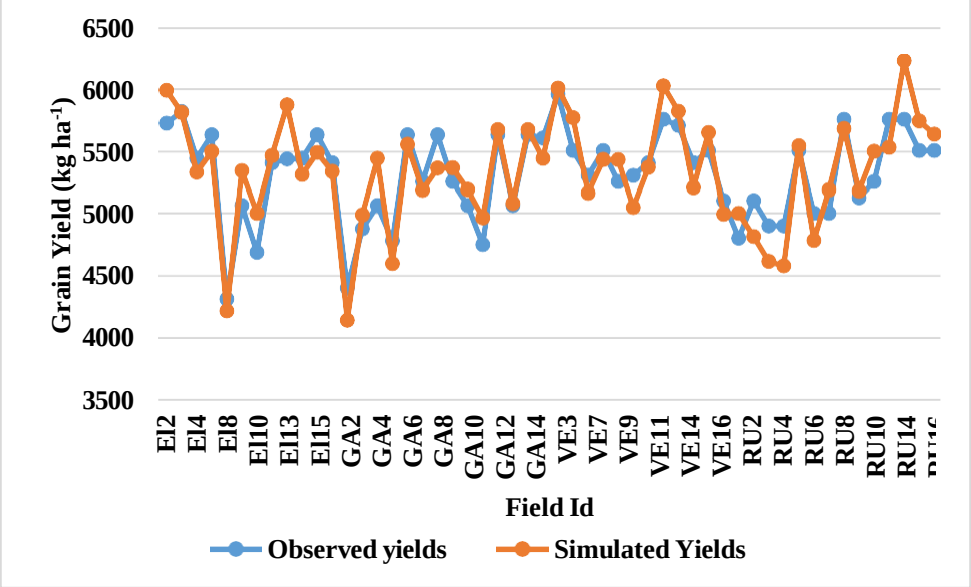

Fig. 4.4 Comparison of observed versus simulated grain yield (kg ha^{-1}) in Kharif season

The comparison made between observed and simulated grain yields showed that there is a minor deviation in the grain yields in few fields (Fig 4.7). The reduction in yields in some fields is be due to effect of pests and diseases and delay in nursery sowing period leading to the variation in temperature during the peak development stage that could affect the grain yield of rice crop.

The statistical analysis performed with the simulated results to find out whether the model has predicted yields under acceptable range showed that the correlation obtained was greater than 0.70, root mean square error (RMSE) was within the range 238 to 400 and D- Index of more than 0.70 (Table 4.17). An overall status of the statistical analysis reveals that model has simulated rice grain yields under the acceptable range hence, it is proven that the model can be used for grain yield estimation under varying package of practices.

Table 4.17 Statistical analysis of the grain yield for selected Kharif villages

Village Name	R^2	RMSE	D-Index
Elbaka	0.80	374	0.86
Gangipalle	0.87	238	0.93
Rukmapur	0.76	400	0.73
Vedurugattu	0.72	270	0.88

4.4.3.2 Rabi

The observed grain yields among the four selected villages of Karimnagar district during Rabi ranged from 4500 kg ha^{-1} to 7400 kg ha^{-1} while, the simulated grain yields ranged between 4000 kg ha^{-1} to 8100 kg ha^{-1} (Table 4.13 to 4.16).

It can be seen that a R^2 value of 0.89 was found with very few outliers. With the same data, a line graph has also been constructed (Fig.4.9) which indicates more or less observed and simulated grain yields follows the same trend.

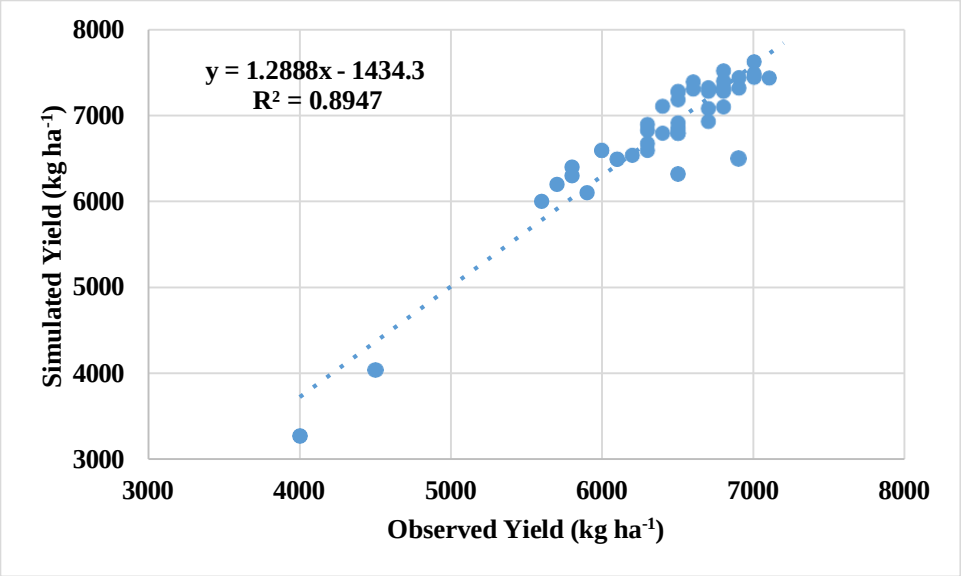

Fig 4.5 Correlation between the observed versus simulated grain yield (kg ha^{-1}) in Rabi season

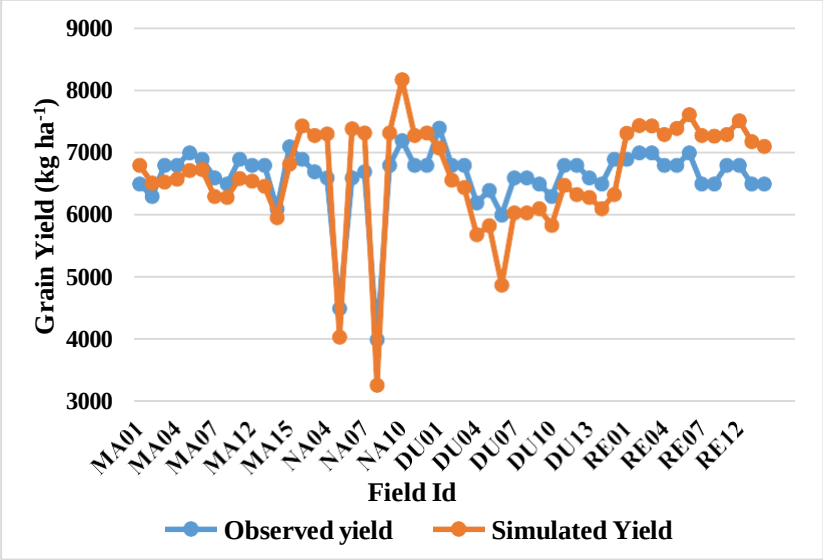

Fig.4.6 Comparison of observed versus simulated grain yield (kg ha^{-1}) in Rabi season

The statistical analysis of the grain yield of rabi season correlation (R^2) was above 0.85 among different sites of four villages, while the RMSE was in the range of 241 to 880 and D- Index was above 0.70 that indicates that model has predicted grain yields under acceptable range. From this it can be concluded that the model can be used further for yield estimation under varying package of practices and different climatic conditions.

Table 4.18 Statistical analysis of the grain yield for selected Rabi villages

Village Name	R2	RMSE	D-Index
Durshed	0.85	241	0.77
Nagnur	0.88	519	0.73
Malkapur	0.88	544	0.76
Renikunta	0.88	880	0.83

4.4.4 Comparison of measured LAI and model simulated LAI

The LAI recorded with the ceptometer during different growth stages was used to compare with the DSSAT model simulated LAI to know the similarity between them. The maximum LAI noted among different stages of crop growth and the maximum LAI simulated by the model were selected and were compared between them (Fig 4.10). The LAI values ranged between 3.5 and 5.0. It was observed that a correlation of 0.77 was achieved in case of kharif (Fig. 4.10). Few outliers were removed which were due to some constraints noticed with the model and ceptometer.

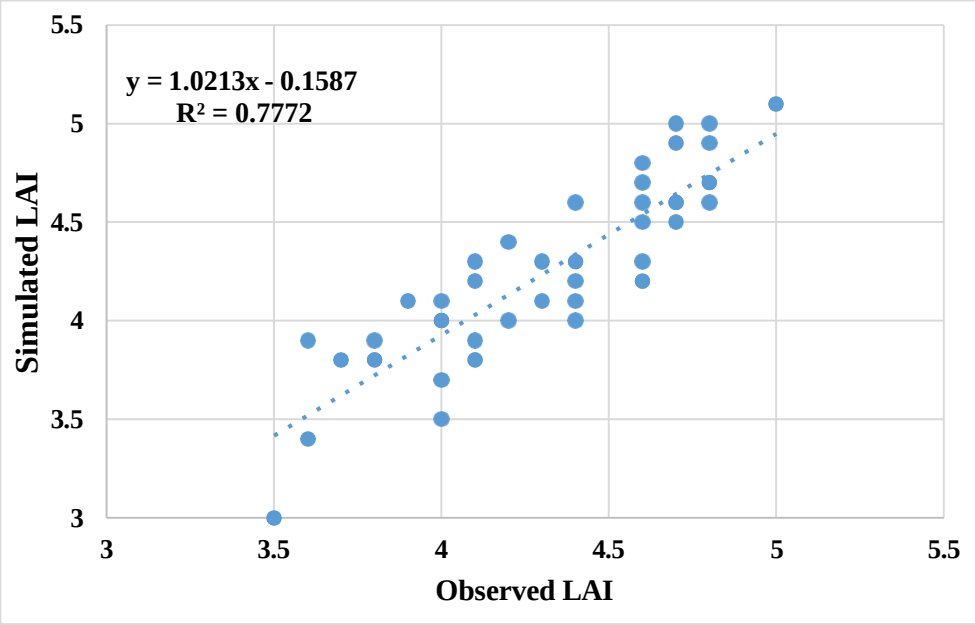

Fig. 4.7 Comparison of Observed maximum LAI and model simulated maximum LAI in Kharif season

Similar to kharif season, during rabi season also a R^2 value of 0.80 was noticed with LAI values ranging from 5.0 to 6.2 (Fig. 4.11). A linear correlation was observed which implies that good similarity between ceptometer and model simulated LAI.

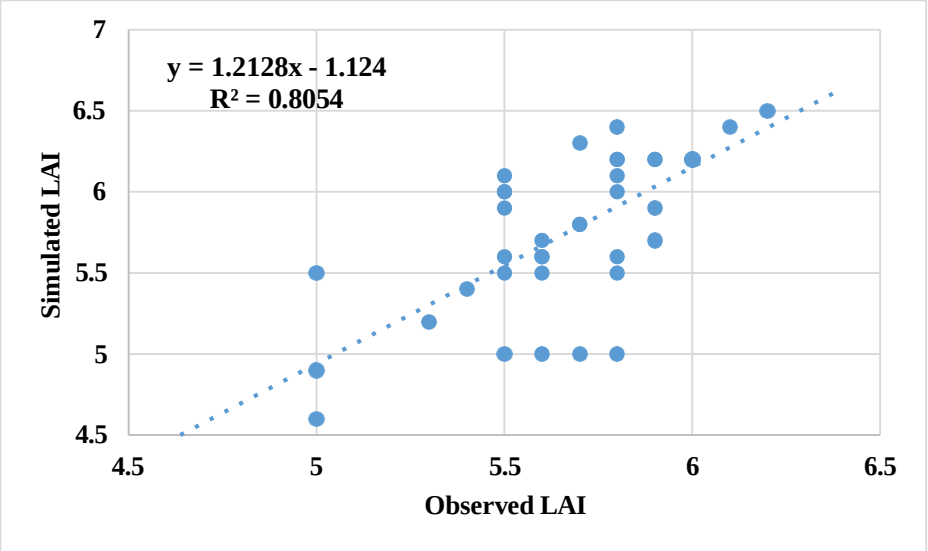

Fig. 4.8 Comparison of Observed maximum LAI and model simulated maximum LAI in Rabi season

4.4.5 Relation of yield and LAI

Yield attributes like number of panicles per m^2, number of grains per panicle and seed weight contributes to the yield of the plant. Among all the above-mentioned yield attributes, grain yield shows a good correlation with the LAI. This has been supported by many researchers that LAI has a good positive correlation with the yield. In both the seasons, relation between grain yield and maximum LAI has been established.

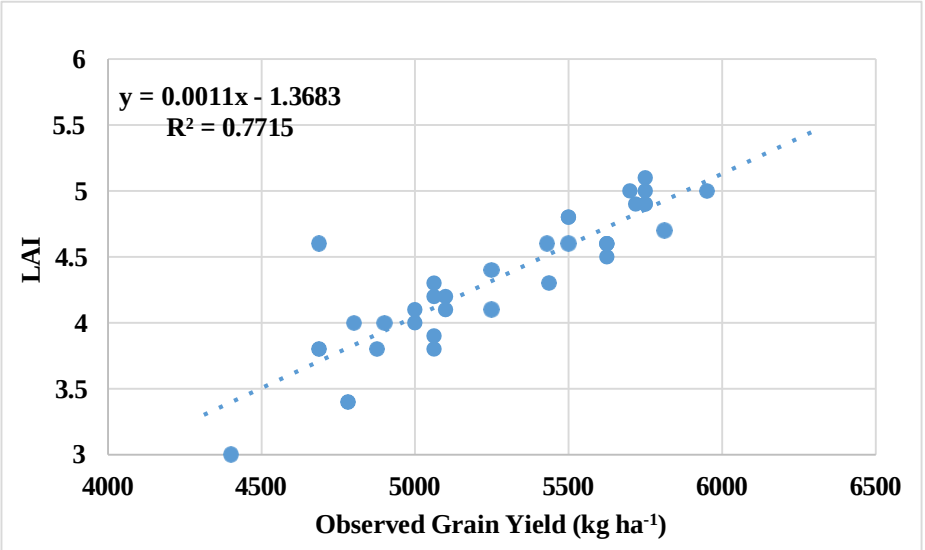

Fig. 4.9 Relation between observed grain yield and LAI in Kharif season

In rabi season, a relation between observed yield and LAI has been noted with a R^2 value of 0.78 (Fig. 4.13). This reveals that with increase in LAI, yield increases up to a certain extent.

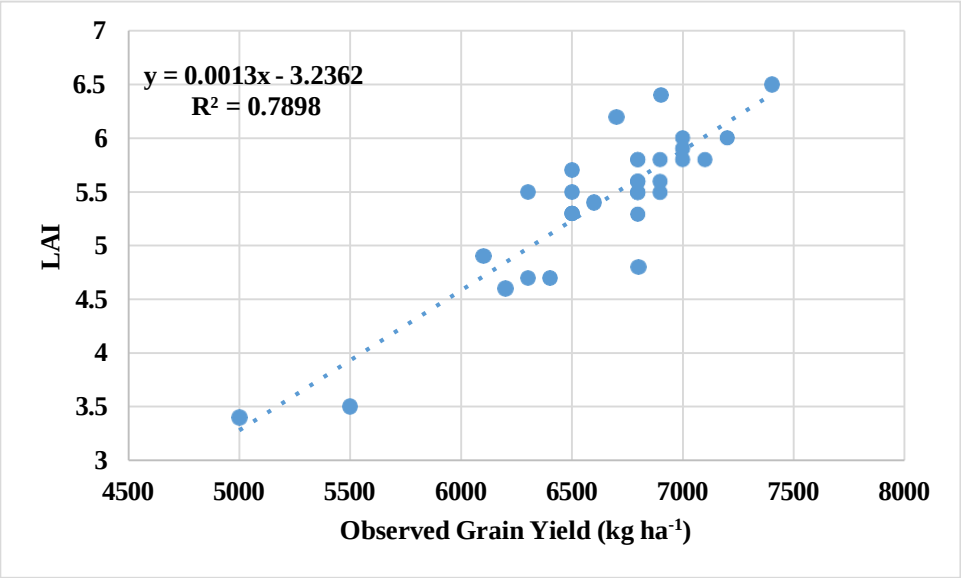

Fig. 4.10 Relation between observed yield and LAI in Rabi season

4.4.6 Correlation between Model yield and LAI

It has been observed that the LAI has a positive correlation with the yield. Once the spatial LAI map has been generated, relation between the model simulated yield and the simulated LAI has been worked out.

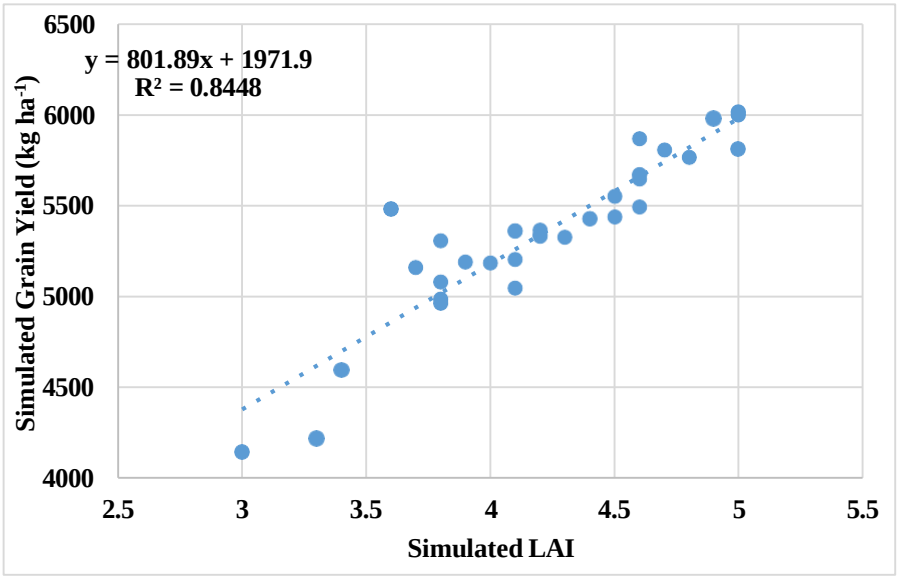

Fig.4.11 Comparison of simulated grain yield and LAI in Kharif season

An R^2 value of 0.84 was observed between the model yield and LAI in Kharif season (Fig. 4.14).

Similar to the Kharif season, the relationship between simulated LAI and simulated grain yield was performed for the Rabi season and it has been observed that a R^2 value of 0.85 was noticed between model simulated yield and LAI (Fig.4.15).

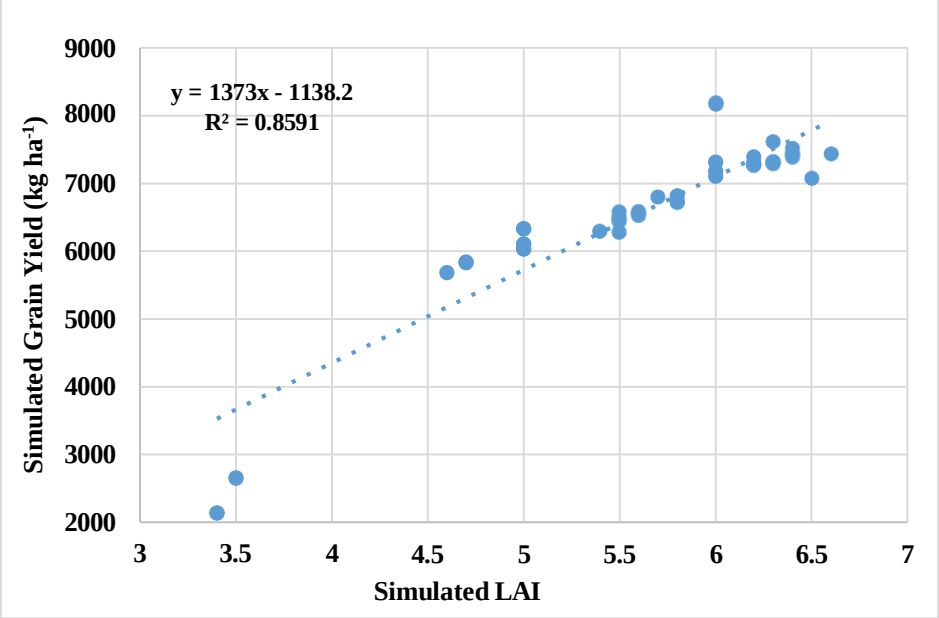

Fig.4.12 Comparison of simulated yield and LAI in Rabi

The relation between model yield and model LAI obtained during both the seasons shows a good relation between them, where yield can be used as a main criterion for generating grain yield through the LAI as a key element.

4.5 Relation between yield and quantity of fertilizer applied

Supply of nutrients is the prime factor which determines the crop growth. The production of photosynthates and their translocation to sink depends upon mineral nutrition. Nitrogen is an integral part of chlorophyll and precursor for many enzymes and amino acids and plays vital role in plant metabolism. During the ground truth data collection, the quantity of fertilizer applied by the farmers of each site was recorded. The correlation studies were made between observed grain yield with that of amount of nitrogen applied at each site was done to know the relation between them. It can be seen that a linear correlation was observed between grain yield and nitrogen applied (Fig. 4.4 and 4.5) with R^2 value of 0.82 and 0.83 during kharif and rabi seasons respectively.

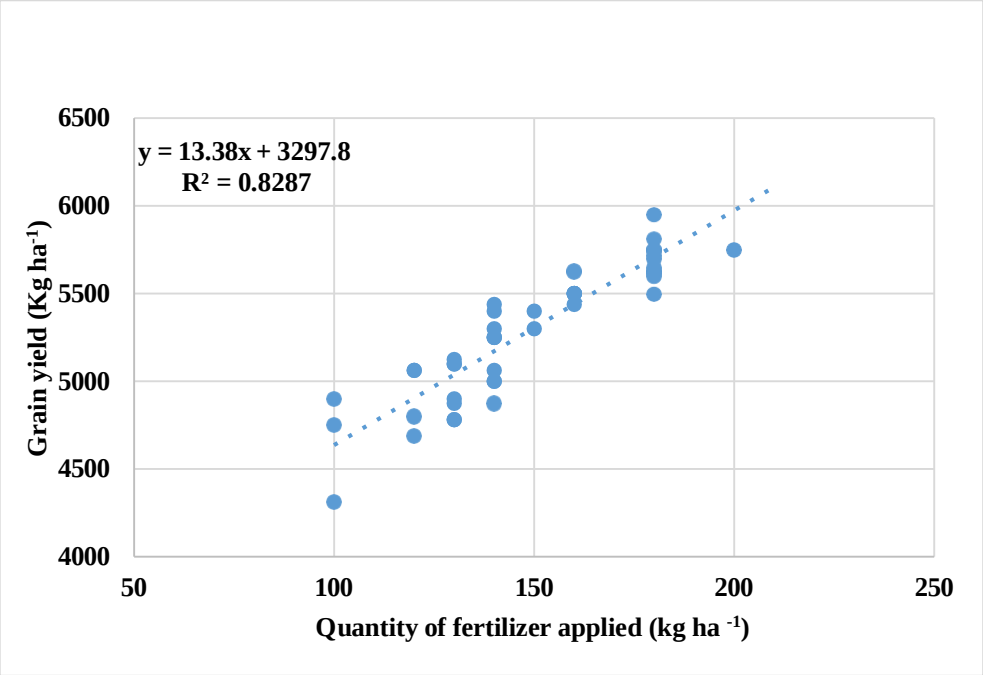

Fig. 4.13 Relation between grain yield and quantity of nitrogen applied in Kharif season

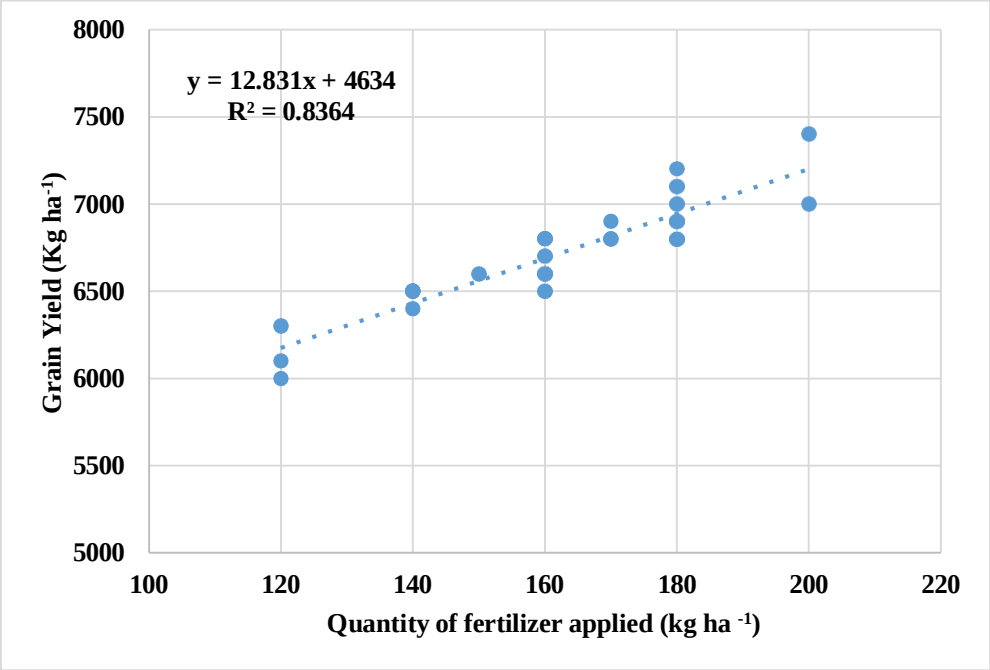

Fig. 4.14 Relation between grain yield and quantity of nitrogen applied in Rabi season

4.6 Derivation and Integration of crop simulation model with Remote sensing products

4.6.1 Integration of model LAI with the remote sensing product- NDVI

Various remote sensing products from sentinel 1 & 2 like NDVI, VV, VH, band 4 and band 8 can be used to relate with leaf area Index to develop a correlation. Many studies have proven that NDVI is one among the various parameters which has shown a good correlation with the Leaf Area Index. A correlation of 0.82 in kharif was observed between NDVI and LAI (Fig. 4.16). NDVI defines the difference between the visible and near infra-red reflectance of plant cover. NDVI values varies from -1 to 1. The results obtained from present study between NDVI and LAI shows a good agreement among them.

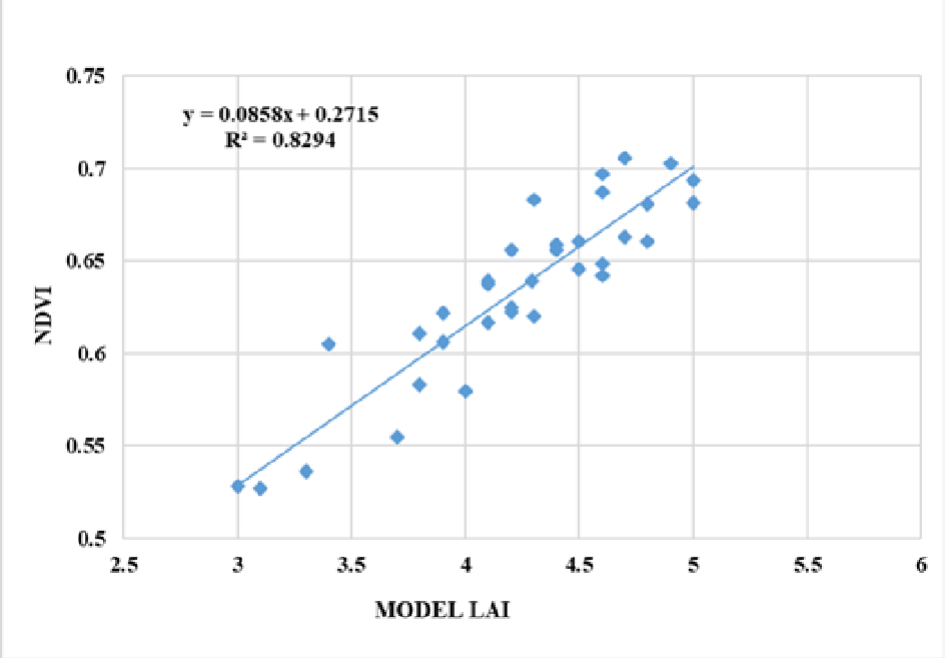

Fig. 4.15 Correlation between the NDVI and model LAI in Kharif season

For the rabi season also, among all the products NDVI showed a correlation of 0.81 with LAI (Fig.4.17). From the results of both kharif and rabi season, it can be clearly noted that NDVI is one among the important parameter which can be used to integrate with LAI for further yield estimation.

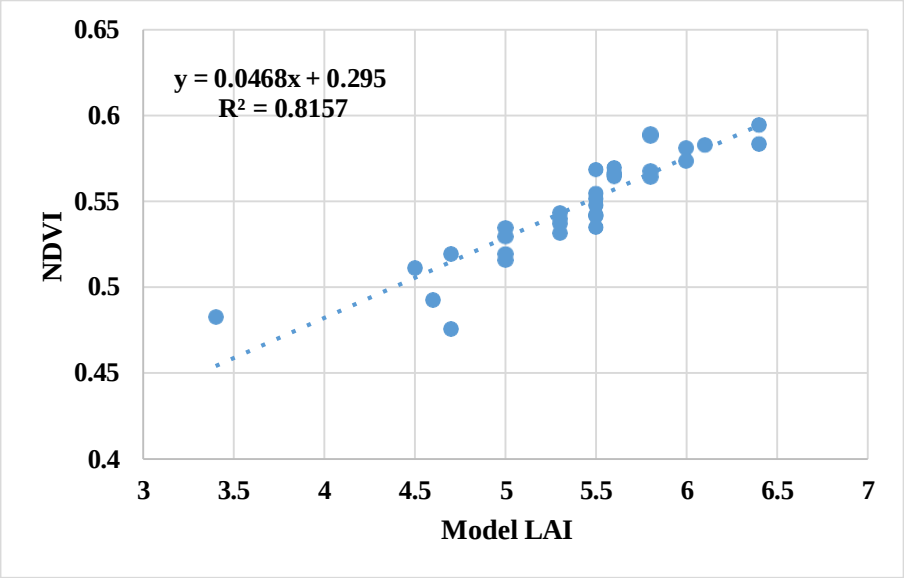

Fig.4.16 Correlation between the NDVI and model LAI during Rabi season

4.6.2 Generation of spatial LAI map

As NDVI showed a good correlation with the LAI, this has been used as a parameter to generate spatial LAI map for the Karimnagar district for both kharif and rabi season (Fig. 4.18 and Fig. 4.19). For this, the NDVI image was masked with the rice mask that was obtained while performing supervised classification. NDVI threshold of more than 0.4 was noticed which implies that the rice cultivated area was used to eliminate the noise in the masked image. Using the linear equation (Eq.4.1) generated from the correlation between the NDVI and model LAI, remote sensing LAI was generated.

The equation used for generating spatial LAI of kharif season is as follows.

$$LAI = 0.0858 \times NDVI + 0.2715 \qquad \text{Eq. (4.1)}$$

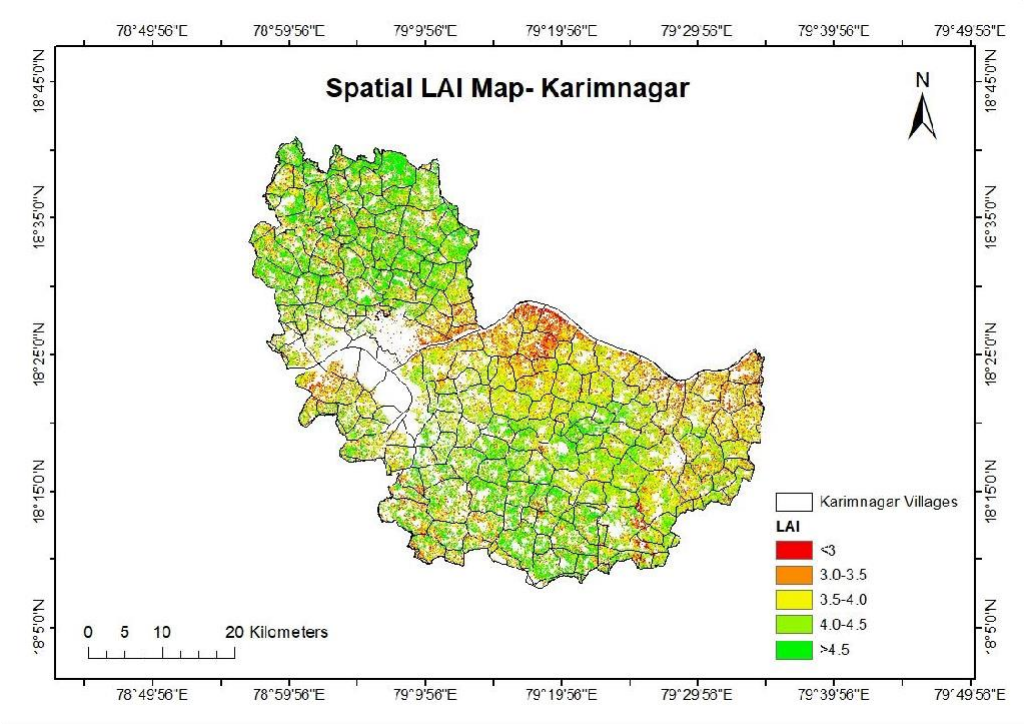

Fig.4.17 Spatial LAI map of Karimnagar in Kharif season

The equation used for generating spatial LAI of rabi season is as follows.

$$LAI = 0.0468 \times NDVI + 0.295 \quad \text{Eq. (4.2)}$$

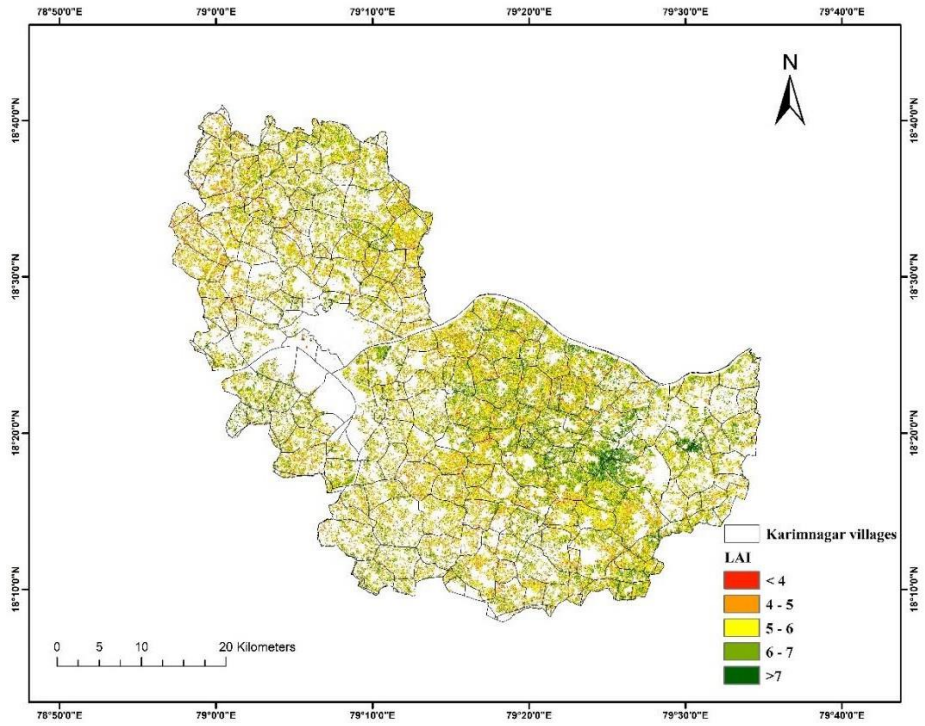

Fig.4.18 Spatial LAI map of Karimnagar in Rabi season

4.6.3 Generation of spatial yield map

To generate the spatial yield map for both kharif and rabi seasons, the linear equation obtained between the model LAI and model yield and spatial LAI map was used. As discussed earlier a R^2value of 0.84 (Fig.4.14) and 0.85 (Fig.4.15) for kharif and rabi seasons respectively was observed between model LAI and yield hence the equation obtained through this relation was used to generate spatial yield map.

The equation (4.3) used to generate the spatial yield map of Karimnagar in kharif is as follows

Yield = 801 × LAI – 1971 **Eq. (4.3)**

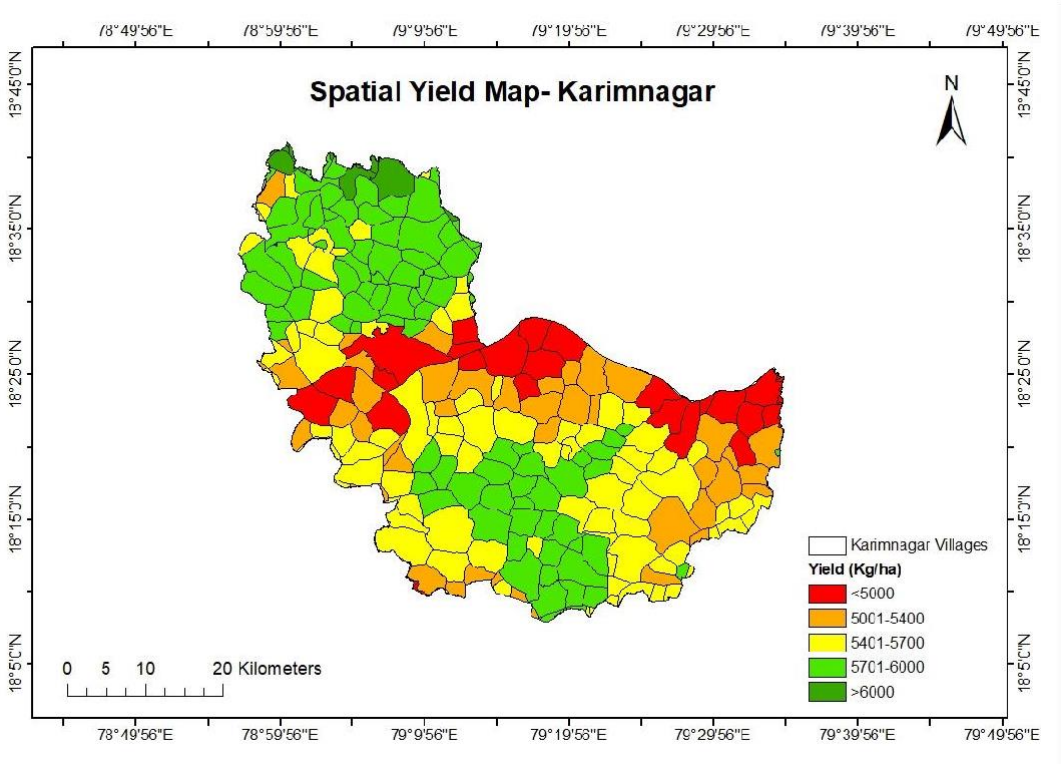

Fig. 4.19 Spatial yield map of Karimnagar in Kharif season

From the spatial yield map (Fig. 4.20), it can be seen that most of the areas falls under the yield range of 5700 to 6000 kg ha^{-1}. Lowest of less than 5000 kg ha^{-1} was observed under the lower Maneru dam area where construction was there.

The equation (4.4) used to generate spatial yield map of Karimnagar district in rabi season is mentioned below

Yield = 1373× LAI – 1138.2 **Eq. (4.4)**

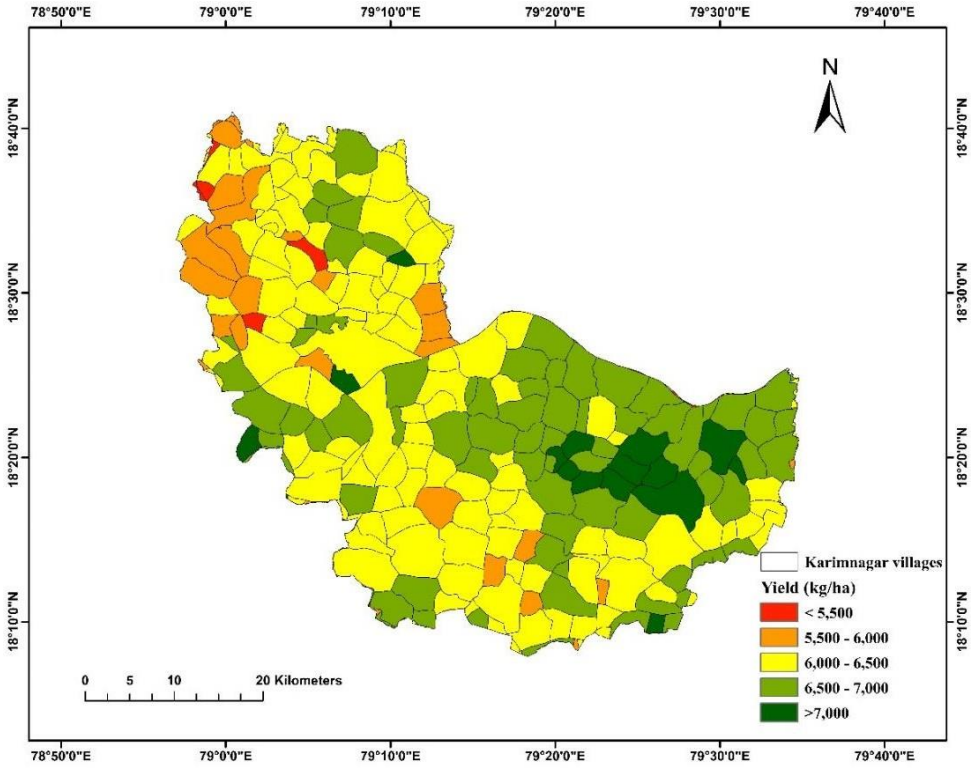

Fig. 4.20 Spatial yield map of Karimnagar in Rabi season

From the yield maps of rabi (Fig. 4.21), it can be noticed that rabi yields are higher than the kharif yields. In rabi, most of the district is under the yield range of 6500 to 7000 kg ha^{-1} which implies a good quantity of grain yield in the district. Lower grain yields were observed in the Lower Maneru Dam area.

4.7 Validation of spatial generated yield

The spatially distributed model yield was used to validate with the government statistics to know the efficiency of the remote sensing in estimating the rice yields through the above-mentioned procedure. The model mean yield in kharif season for the Karimnagar district was 5300 kg ha^{-1}. The same was seen in rabi season, where the model mean yield in rabi season was 6459 kg ha^{-1}.

From the above mentioned detailed results, it can be noted that LP- 80 accupar ceptometer can be effectively used to measure the LAI, while the DSSAT model can be used for

assessing rice yields and LAI under varied management conditions. NDVI shows a good correlation with the LAI thus keeping it as a prime component from remote sensing for spatial yield estimation. It can be concluded that integrating the remote sensing satellite data with crop models by considering LAI as the principal component can effectively predict crop yields, which can benefit policy- and decision-makers in implementing insurance schemes.

Chapter V

DISCUSSION

In this chapter, the reasons for the findings mentioned in the results chapter are discussed. Outcomes of the current research and the major causes for such results were briefly mentioned along with the similar studies performed by other researchers which supports the outcomes of the present study.

5.1 Optimization of CCE Locations

5.1.1 Selection of Study Area

As mentioned earlier in results chapter 4.1 section villages were sopted for the further study purpose based on soil, rainfall, elevation and crop type map. It can be seen from the fig. 3.3 that most of the district falls under clay soil and loamy soil. Most of the selected villages in both seasons falls under clay soils except Elbaka, Gangipalli and Renikunta. While with respect to rainfall there was no much deviation in the rainfall on the whole district as seen under Fig.3.4. In case of elevation all the opted villages in both seasons falls under an elevation range of 252-298m, while Elbaka and Gangipalli were under less than 252 m elevation level. In case of crop type map most part of the selected villages are under rice crop with irrigated conditions.

By taking into consideration all the above points four villages in each season i.e., kharif and rabi were selected for further collecting the readings for LAI and CCE's.

5.1.2 Crop Cutting Experiments

Crop cutting experiments were performed in the selected fields in both the seasons. Grain yields were collected, recorded and expressed as t ha^{-1} at 14% moisture.

5.1.2.1 Kharif Season

In kharif season on an average the observed grain yield was 5324 kg ha^{-1}, the lowest grain yield was 4000 kg ha^{-1} and highest grain yield was 5900 kg ha^{-1}. From the outcomes mentioned in results chapter it can be observed that among all the selected villages, the higher grain yield of 5900 kg ha^{-1} was recorded in Vedurugattu village and also the range

of grain yields were higher in the same village followed by Rukmapur village and other vilages.

The reason for achieving higher yields in Vedurugattu village might be due to sowing of nursery in July first fortnight and timely transplanting. All the rice fields in the village followed the same sowing time and transplanting in time leading to coincidence of sufficient amount of rainfall during the tillering stage and required sunshine hours at reproductive stage leading to higher grain yield.

The grain yield data presented in Table 4.9 to 4.12 shows that in some of the fields in all the villages the grain yields were low (less than 4500 kg ha^{-1}) against an average grain yield of 5324 kg ha^{-1} with a deviation of 824 kg ha^{-1}. One of the main reasons for lower grain yield is delay in sowing beyond august leading to exposure of crop to low temperatures during the reproductive stage which result in high sterility and reduction in grain yield (Naik et al. 2015).

On comparing the deviation between the highest and lowest yields, the deviation less (700 kg $ha^{-1)}$ in Vedurugattu village due to following of proper sowing time, while the higher deviation 1500 kg ha^{-1} was noticed in Elbaka village which might be due to attack of pests and delay inn sowing time. From the results, it can be noted that in Elbaka village at EL6 site recorded the lowest grain yield (4313 kg ha^{-1}). The lower yield at this site was due to delay in nursery sowing and transplanting and water logging at booting stage (reproductive stage). For getting higher yields, an optimum time of sowing (before July first fortnight) has to be maintained. Sowing beyond this date at every 15 days interval up to 18th august results gradual decrease in grain yield (Naik *et al.* 2015, Sindhu *et al.* 2022). Sowing date also has a direct impact on the rate of establishment of rice seedling (Tashiro *et al.* 1991). Further, different rice varieties respond in different way to varied sowing dates (Akhter *et al.* 2016 and Rai and Kushwaha, 2008). Hence, the lower yields in few fields in all the villages might be due to the delay in sowing, attack of pests and diseases, and water logging at reproductive stage.

5.1.2.2 Rabi season

At many sites the grain yields were higher in the four villages (6200 kg ha^{-1}). However, due to lower yields at few sites the average yield of rabi season came down to 5279 kg ha^{-1}. It might be due to pest attack and differential crop management practices including

nursery sowing and transplanting. During rabi, the highest grain yield (7400 kg ha^{-1}) was observed in Durshed village, while the lowest of 4000 kg ha^{-1} was noticed in Nagnur village (Table 4.13 to 4.16).

The highest average grain yield was recorded in Renikunta and Malkapur villages followed by the rest selected villages. There was a deviation of 300 kg ha^{-1} between the highest and lowest average grain yields. These higher yields are due to the following of optimum sowing time, which plays a major role in ensuring proper growth and yield. In most of the villages, rabi season crop was sown during December second fortnight which resulted in an increase in grain yield. Sowing during the optimum time ensures proper sunshine hours and temperatures throughout the growth period.

Among all the villages, the lowest grain yield was recorded at NA4 and NA7 sites in Nagnur village due to the late sowing (January first fortnight) leading to delay in late transplanting and coinciding high temperatures during grain filling stage thus resulting in lower grain yields.

The comparison of rabi and kharif grain yields of Karimnagar district shows that the rabi grain yields were higher than kharif grain yields which might be due to the crop receiving of adequate sunshine hours and low pest incidence. Several studies show that in rabi season pest and disease incidence is low as compared to kharif season (Jena *et al.* 2018) due to prolonged rainfall and high humid conditions in kharif season compared to rabi season.

5.2 LAI Estimation using LAI ceptometer

5.2.1 Ceptometer readings during Kharif season

In Elbaka village, the maximum LAI readings with Accupar LP-80 ceptometer were ranged between 3.6 and 4.8. The lowest of LAI 3.6 was due to the effect of late sowing rice nursery in July second fortnight. Maximum LAI value of 4.1 to 5 was recorded in Vedurugattu village, which is a good LAI value and this might be due to the proper growth of the crop which happened because of nursery sowing in July first fortnight and adoption of proper management practices. In Rukmapur village, the maximum LAI ranged between 3.9 and 4.8, while in Gangipalli, it was 3.5 to 4.7. Sowing time plays a major role in plant growth and development and it ensures vegetative growth takes place when there is an optimum temperatures and sunshine hours (Patel *et al.* 2019). The optimum

sowing time make certain that when the minimum night temperatures are warmest and the grain filling occurs when milder autumn temperatures are more likely. Further, there are reports that delay in planting during kharif from15 June to 15 July decreased leaf area index values by 10% (Rai and Kushwaha, 2008).

5.2.2 Ceptometer readings during Rabi season

During the rabi season, the LAI recorded with ceptometer ranged between 3.2 and 4.6 (Table 4.3 and 4.4). In Durshed village, it ranged between 4.6 and 5.8, in Malkapur it was from 5 to 5.9, in Renikunta it was from 5.5 to 6.1, while in Nagnur it was 5.6 to 6.2.

At different stages of crop growth, the maximum LAI was observed during the rabi season as compared to Kharif season. This might be due to the availability of more sunshine hours for photosynthesis and thereby increased growth and development. Yang et al. (2021) reported that due to high solar radiation more amount of biomass is accumulated leading to higher Leaf area.

The major constraint for use of the ceptometer for LAI is that it works only under the photosynthetically active radiation (PAR) above 400nm units thus declining its efficiency of measurement during cloudy weather conditions. There are reports that with 10% shift in PAR leads to a 4-20-fold rise in LAI, implying that LAI readings are more sensitive to incident PAR (Hyer and Goetz, 2004 and Pokavai and Fodor, 2019). From the LAI readings using the LP-80 ceptometer, it can be noted that the instrument over and underestimates the LAI values sometimes but it is difficult to find out because of developing research on these parameters. This instrument readings are more sensitive to the PAR and sunshine hours.

5.3 Mapping of Rice Growing Areas

The supervised classification of Karimnagar district was performed for identification of different classes from the satellite data in ERDAS imagine (Abiy and Suryabhagavan, 2016; Rwanga, S. and Ndambuki, 2017) and ARC GIS softwares.

5.3.1 Supervised Classification

From the classified map (Fig. 4.1 and 4.2), it is seen that in both the seasons rice is the dominating class among all the categories occupying an area of 143 thousand ha and 103 thousand ha in kharif and rabi season respectively. As per Telangana Govt. statistics, the

total area under rice cultivation in Karimnagar was 147 thousand ha and 105 thousand ha in kharif and rabi seasons respectively during 2020-2021 (Government of Telangana, 2021). There is a deviation of less than 3% between observed and Govt statistics of rice area in both the season which strongly reveals that the classified map using the ERDAS was quite good enough for further proceeding in the research. It can be seen that rabi rice growing area is low as compared to kharif rice area because of lesser water supply thereby few fields were occupied with other crop like cotton, maize, groundnut etc. These crops were grown as they require low water than rice hence, rice area decreased. On the other hand, in kharif due to sufficient amount of water and rainfall, rice was grown without any water deficit.

Through the Supervised classified map (Fig. 4.1 and 4.2), it can be noted that rice is one of the important crops grown in the district, because of the development of irrigation water from project - Lower Manair Dam which was constructed on Manair river a tributary of the Godavari. The supply water for irrigation with the construction of Lower Maneru Dam led to increase of cultivated area under rice in Karimnagar district.

The area of other crops in rabi was high as compared to kharif season (Table 4.5). This increase in area under other crops in rabi was due to growing of various crops unlike growing single crop rice in kharif season. There was a decline of 984 ha area of water body in rabi season as compared to the kharif season which might be due to low rainfall in rabi and increase in temperature leading to evaporation of water from water bodies such as ponds and rivers.

Based on the statistical reports, it is observed that there was a deviation of 2.7% and 3.7% between the classified map and the area mentioned by the government of Telangana. This concludes that the mapping of rice areas in Karimnagar district using the ERDAS was accurate enough to produce reliable results for performing supervised classification. Hence, these results were taken in to consideration for further research process.

5.3.2 Accuracy assessment

From both accuracy assessment reports it can be noted that the use of ERDAS and Arc GIS for performing supervised classification achieved an acceptable range of overall accuracy and kappa coefficient. The users and producers' accuracy for both the seasons in most of the classes were above 75%, kappa coefficients were above 0.85 indicating

better results (Table 4.6 and 4.7). Even though, there were lower accuracies in few classes which might be because of misclassifying i.e., mixing of classes mainly among the crop lands only. In kharif season accuracy levels might be interrupted due to unavailability of proper data because of cloud cover leading to lower accuracy in results. In both the seasons, rice has shown accuracy of more than 95% which is achieved due to its unique NDVI signature values. As compared to other classes, water body has contrast signatures so 100% accuracy has resulted in terms of user's and producer's levels, while built up area also had good acceptable range of accuracy due to its distinctive signature values. The lower accuracy of other LULC data might be due to almost similar signatures with rice, few classes of rice and other LULC which misclassified as other LULC and rice (Table 4.2 and 4.3). Lower accuracy resulted in few classes can be corrected by collecting a greater number of training samples and use of high-resolution data. However, use of sentinel 1 data effectively resulted in good accurate range of accuracy for generating Land Use Land Cover classification (Gumma *et al.,* 2024 and Gumma *et al*., 2023). Similarly, Makande and Oyalde *et al.* (2020) concluded that Sentinel 1 SAR result has been effectively used for producing an acceptable accurate land cover map of Lagos State with relevant advantages for areas with cloud cover. While Sekertekin *et al.* (2017) used Landsat, sentinel data with ERDAS for classifying LULC and found a kappa coefficient of above 0.70 and overall accuracy of more than 70 % and therefore, they concluded that sentinel gives better results. Similarly, with the same methodology for detecting the changes in land use and land cover using the ERDAS and sentinel data kappa coefficient of 0.80 and overall accuracy of 85 % has been obtained and revealed that use of sentinel data resulted in effective outcome of classification with acceptable range of accuracy levels. Vikeh and Patil (2016) used EDRAS for detecting the changes in land use and land cover using ERDAs and obtained an accuracy of 85%. Patil *et al. (*2012) performed supervised classification with maximum likelihood estimation (MLE) and maximum distance (MD) and found a high overall accuracy of 91%. Hence, it can be concluded that classification using ERDAS achieves higher accuracy and also using of sentinel data gives reliable results.

5.4 Yield estimations

5.4.1 Calibration of the model

As mentioned previously, DSSAT model has been calibrated using the GLUE (Generalized Likelihood Uncertainty Estimation). The finally obtained vegetative genetic

parameters like P_1, P_2O, P_2R, P_5 and reproductive cultivar G_1, G_2, G_3 and G_4 were mentioned under results chapter (Table 4.8). Genetic coefficients are sets of parameters that describe the genotype and environmental interactions. They summarize quantitatively how a particular cultivar responds to environmental factors. After performing statistical analysis, it has been observed that the model generated genetic parameters for MTU1010 calibrated using the GLUE were under acceptable range. This indicated that model has accurately calibrated the coefficients. However, the juvenile phase coefficient (P_1), photoperiodism coefficient (P_2R) and grain filling duration coefficient (P_5) of MTU1010 were 440-, 350- and 12-degree days (°C), respectively which were low as compared to other varieties like BPT 5204 as because of its shorter duration. The obtained genetic parameters were compared with the other researchers who have performed calibration for the same cultivar. The results for MTU1010 cultivar were near to the values obtained by Kadiyala *et al.* (2015) who has performed calibration for MTU1010 cultivar using DSSAT for Hyderabad, Telangana region where the statistical results like R^2 of 0.93, P_1, P_2R and P_5 were 407. 367 and 11.7 respectively were observed. Similarly, calibration for other rice varieties (basmati 370 and IR 2793-80-1) were performed and an R^2 of 0.78 and 0.76 has been resulted using the GLUE (Nyangau *et al.* 2014).

5.4.2 Simulation of Grain Yield and comparison with the observed yields

DSSAT model has been used for estimating the rice yield under varied management practices in both the seasons. The deviation between observed and simulated yields were noted and reasons for the same were discussed below.

The kharif average yield was 5324 kg ha^{-1}, while the model simulated average was 5339 kg ha^{-1} . The highest simulated grain yield among all the villages was 6221 kg ha^{-1} (RU13 site) in Rukmapur village while the lowest was of 4141 kg ha^{-1} in Gangipalli village (GA2 site). Among all the selected villages, in kharif the average simulated yield was highest in case of Vedurugattu village i.e., 5512 kg ha^{-1}, while the lowest (5168 kg ha^{-1}) was recorded in Gangipalli village. On comparison of observed and simulated yields in all the villages, there is deviation of 8.5 kg ha^{-1} to 471 kg ha^{-1} which is acceptable on basis of statistical analysis. Average yield from the DSSAT model in Karimnagar district during kharif was 5324 kg ha^{-1} as compared to the government statistics of 5014 kg ha^{-1} with a deviation of less than 10% (Bellamkonda *et al.* 2020).

In rabi season the observed average yield was 5279 kg ha^{-1} and the average model simulated yield was 5349 kg ha^{-1} . Among all the villages, the highest grain yield of 8177 kg ha^{-1} was recorded in Nagnur while the lowest of 3217 kg ha^{-1} was noted in the same village. The highest average simulated yield was recorded in Renikunta village i.e., 7345 kg ha^{-1} whereas, the lowest was noted in Durshed village (6125 kg ha^{-1}) with a deviation of 138 kg ha^{-1} to 1123 kg ha^{-1} among all the villages.

It has been observed that there are variations in the yields of the same village which might be due to adoption of different package of practices and under such situations, the CERES rice model can be used (Mirakhori *et al.* 2017). Among the management practices, the time of sowing nursery and transplanting and nitrogen level of application play great role. Delay in sowing beyond July 1st fortnight in kharif and lower level of fertilizer N application results in lesser grain yield.

The DSSAT model is found to be sensitive for the sowing windows. Sowing during july first fortnight resulted in better grain yield with lesser reduction while sowing during July second fortnight resulted in lower yields due to the temperature fluctuations. Similar results were reported that under late sown conditions beyond July 1st week leads to drastic reduction (Kadiyala *et al.* 2007) in the yield due to exposure of plants to low temperatures during the reproductive stage at Jagtial in Telangana state.

During kharif and rabi seasons in Vedurugattu and Renikunta villages, the highest grain yields were recorded because of sowing at optimum time. On comparing the observed and simulated grain yields, it was found that the simulated grain yield followed the trend of observed values. The DSSAT model also counts for individual day for grain development, hence an optimum sowing time is most important. From the results obtained, it can be concluded that DSSAT CERES rice model can be strongly recommended for using under varying package of practices as CERES rice for yield estimation had found good agreement with the observed values under different dates of sowing and fertilizer applications (Mirakhori *et al.* 2017 and Kaur and Kaur 2022).

5.4.3 Evaluation of the DSSAT model

The sensitivity of the model in assessing the crop yields across varied management practices has been evaluated and these results were then compared with the observed yields. It has been found that simulated yields in kharif ranged between 4300 kg ha^{-1} and

6000 kg ha^{-1}, while in rabi it was 3217 kg ha^{-1} and 8177 kg ha^{-1}. On the other hand, the observed yields ranged between 4000 kg ha^{-1} to 7000 kg ha^{-1} in rabi, while in kharif it was 4000 to 5900 kg ha^{-1} and the deviation among observed and simulated yields was minimum (Tables 4.9 to 4.12). Further, an R^2 value of 0.80 was observed in both the seasons with observed and model simulated yield ((Figures 4.6 and 4.8), which agrees that Ceres rice model is very effective enough in estimating the rice yields under varying management conditions.

In both the seasons, in most of the cases simulated yields were higher than the observed yields (Fig. 4.7 and 4.9) as the model do not consider the abiotic stress damage like that of water logging which was a major problem in kharif season. Other drawbacks of DSSAT model is that it will not consider the effect of nutrient deficiencies and application of minor nutrient like sulphur, iron etc., not responsive to major nutrient phosphorous and potassium and also the effects of pest and disease incidence (Abayechaw, 2021; Jones *et al.* 2003 and Kadiyala *et al.* 2015). Deka *et al.* (2016) reported that the model can be effectively used by policy and decision makers to plan agriculture based economic decisions at regional level.

Correlation of the grain yield was observed to be above 0.70 and D- index of above 0.70 in all the villages (Table 4.17 and 4.18), where above 0.6 indicates that the model and the field data are in good agreement. Statistical results in both the seasons reveals that values obtained were under acceptable range and thus the CERES- Rice model can be used further for predicting the rice yields. The results show the conformity with the findings of Sudarshan *et al.* 2013 (D-index 0.60, R^2 0.80), Deka *et al.* 2016 (R^2 0.85 and RMSE 401 kg ha^{-1}), Mirakhori *et al.* 2017 (R^2 0.85, NSE 0.89) and Ahmad *et al.* 2013 (R^2 0.97) under CERES rice model.

The findings of this study indicate that the DSSAT model has showcased high level of accuracy in predicting both yields and LAI across various management practices. Further, there is a potential in use of crop simulation models as a technology driven tool to identify the most effective management strategies for rice production.

5.4.4 Comparison of measured LAI and model simulated LAI

The maximum LAI recorded with the ceptometer and the DSSAT model simulated LAI was used to build a graph to know the similarity between them (Table 4.1 and Table 4.2).

There was a R^2 value of 0.77 and 0.80 was observed during kharif and rabi between them. These results reveal that Accupar LP-80 ceptometer is quite good enough in measuring LAI during different growth stages of the crop. De Jesus *et al. (*2001) reported R^2 value of 0.97 between the ceptometer and the conventional method. Similarly, Wilhelm *et al. (*2000) compared LAI with varied LAI meters i.e., LAI 2000, Accupar and sunscan and found a correlation of 0.94, 0.93, 0.79 with the field measured LAI respectively. Similar findings were recorded by Ali et al. (2021) which show a correlation of 0.94 between the estimated LAI using the SEBAl equation and measured LAI using the ceptometer. Mirakhori *et al.* 2017 used CERES rice to simulate LAI and found a correlation of above 0.70. Hence, from the results obtained in this study, it can be concluded that there was a good agreement in LAI between the ceptometer and DSSAT model (CERES rice) measured value. Further, these tools give reliable results of LAI for further carrying out research on yield estimations in rice.

5.4.5 Relation of yield and LAI

Many attributes of rice crop contribute to the grain yield of the crop. In case of rice, the number of tillers per m^2, LAI, number of panicles, grains per panicle and 1000 grain weight etc., contribute to the grain yield. Increase in LAI leads to increment in the grain yield to some extent. In case of kharif and rabi rice, corelation of 0.77 and 0.78 respectively (Fig. 4.12 and 4.13) was noticed between observed grain yield and LAI, while R^2 value of 0.84 and 0.85 (Fig. 4.14 and 4.15) was observed between the simulated yield and LAI which implies that LAI and grain yield were in good agreement. Many studies have shown that LAI maintains a good relation with the grain yield. Aboelghar *et al. (*2011) showed a correlation of 0.82 between the grain yield and LAI in rice. High yield scenarios exhibited highest LAI among the collected samples. An increase in LAI was found to be significantly associated with both the biological and grain yield, thereby leading to the increased yields. Results reported by Singdha *et al.* (2022) showed a correlation of 0.64 between maximum LAI simulated from the APSIM and NDVI generated from remote sensing. From this, it can be understood that the model has simulated effectively the grain yield as the grain yield and LAI values followed the same trend with that of observed values. Such an information leads to do further studies by considering LAI as the main component for rice yield estimation. Further, it was established that LAI at different stages of the crop affects number of grains per panicle

and 1000 grain weight contributing to the grain yield (Hashimoto *et al.*2023) and LAI can be used for monitoring and estimating the rice yield.

5.5 Relation between yield and quantity of fertilizer applied

One of the main prominent factors determining the crop yield was application of fertilizers at right quantity and optimal dose. Mineral nutrition plays a major role in production of photosynthates and their translocation to sink. Among all the fertilizers, nitrogen is of utmost mineral influencing the crop yield in rice, as it is an integral part of chlorophyll and precursor for many enzymes and plays a vital role in metabolism (Manzoor *et al.* 2006 and Islam *et al.* 2008). During both the seasons, a correlation of above 0.75 was observed between the amount of fertilizer applied and the grain yield (Table 4.5). The range of N fertilizer application in rice in selected villages was from 100 to 200 kg ha^{-1} in both the seasons which was more than the recommended dose of nitrogen. Nitrogen contributes to carbohydrate accumulation in culms and leaf sheaths during the pre-heading stage and in to the grain during the ripening stage of rice (Bahmanyar and Ranjbar, 2007). Optimal amount of fertilizer application leads to increment in yield attributing characters which inturn effects on crop yield (Mrudhula and suneetha 2020).There was a linear correlation existed between the grain yield and nitrogen applied. This notifies that application of fertilizer mainly nitrogen leads to increase in grain yield. Most of the farmers in the selected villages were applying nitrogen fertilizer in the range of 140 kg ha^{-1} to 160 kg ha^{-1} and realizing highere yields (Fig. 4.4. and fig. 4.5). There are reports that application of 160 kg ha^{-1} resulted in better yield than 120 kg ha^{-1} and 200 kg ha^{-1} (Ramulu *et al.*2020, Ghansham *et al.*2015 and Pramanik *et al.*2013). Though the recommended level of fertilizer N is 100 to 120 kg ha^{-1} but the rice crop is responding to higher levels of N application. This suggests that the recommendation of fertilizer for rice crop needs revision.

5.6 Derivation and Integration of crop simulation model with Remote sensing products

5.6.1 Integration of model LAI with the remote sensing products

Among all the yield attributes, LAI showed a good correlation hence this is taken further for finding the relation with the NDVI (section 5.7). The remote sensing products from sentinel 1 and 2 NDVI showed a correlation with the LAI. R^2 value of 0.82 and 0.81 were

noticed in kharif and rabi season (Fig. 4.16 and 4.17). A linear correlation implies a good fit between NDVI and LAI and this was supported by Ali *et al. (*2021) who observed R^2 value of 0.94 and 0.95 between NDVI and LAI respectively with measured and simulated values. Further, few studies investigated the relation among the remotely sensed factor (NDVI) and field measured parameters (LAI and grain yield) and found a linear correlation between them (Zheng *et al.* 2015; Goswami *et al.* 2015; Bhargav 2021 and Xiao *et al.* 2002). Zhou *et al.* (2017) estimated rice grain yield based on the LAI value and concluded that LAI was a reliable indicator for estimating yield. However, relying solely on LAI may not generate accurate estimation of yield as most notable results for yield estimation have been done by combining LAI with vegetation indices and thus integrating in to the crop models. The solitary usage of individual vegetation indices results in to an error of more than > 15% (Fang et al. 2011). Hence, combination of remote sensing derived vegetation indices i.e., NDVI and LAI when assimilated in to crop models result reliable prediction of yields with higher levels of accuracy.

In the present study, there was a good correlation observed between NDVI and LAI but it can be improved. Collection LAI data during kharif season or cloudy period is difficult thus affecting the NDVI values. From the results of both kharif and rabi season, it is observed that NDVI is one among the important parameters which can be used to integrate with LAI for estimating the spatial rice yield (Gumma *et al.* 2022).

5.6.2 Generation of spatial LAI map

The process used for generating the spatial LAI map was using the relation between LAI and NDVI (Section 4.11). In Russia, Ali *et al.* (2021) generated spatial LIA map using the relation between NDVI and LAI. During kharif (Fig. 4.18) the rice is being cultivated in the entire district, however, in few parts of Karimnagar, Gannervaram and Thimmapur area the LAI was not available due to the presence of the Lower Manair Dam and urban area. LAI of less than 3.5 was noticed in majority area in upper part of the Manakondur mandal villages and to some extent Veenavanka and Jammikunta mandals. LAI above 4 were recordedin Choppadandi, Ramadugu, Sankarapatnam and few parts of Thimmapur and Saidapur mandals because the rice yields under these mandals were higher as compared to others. The reason behind this was early sowing has been practiced in few villages which exposes the crop to high temperatures during the reproductive stage.

In rabi season, the LAI was low as compared to kharif as the rice cultivated area decreased to that of kharif season (rice replaced by other crops) (Fig. 4.19). From the map it can be seen that compared to the western part of the district (Gangadhara, Ramadugu, Choppadandi and Kothapally mandals), eastern parts of the district (Shankarapatnam, Veenavanka and Jammikunta mandals) accounts for higher rice areas in rabi season.

5.6.3 Generation of spatial yield map

The relation between the LAI and yield was used to generate the spatial yield map (Section 4.12). The relation between the LAI and grain yield was used by different researchers to generate the spatial rice yield of different parts of the Orissa, Andhra Pradesh and Nalgonda district of Telanagana (Gumma *et al.,* 2022, Gumma *et a*l., 2024and Snigdha *et al.* 2022). Several studies proved that satellite-derived products have been utilized in crop area and spatial crop yield estimation. In kharif rice, the grain yields of above 5700 kg ha^{-1} (Fig. 4.20) were observed under eastern part of the district (Choppadandi, Ramadugu and Gangadhara mandals) and few parts of the south (part of Thimmapur and Saidapur mandals). In rabi season, the grain yield of more than 6500 kg ha^{-1} (Fig.4.21) was noticed under the eastern part of the district (Jammikunta and Sankarapatnam mandals). In most parts of the district, the grain yield observed between 6000 to 6500 kg ha^{-1} which is a good yield.

The major reason for cultivating rice in both the seasons and achieving good yields were due to the availability of water through the irrigation project Lower Maneru Dam and also due to the presence of bore wells in the area.

5.7 Validation of spatial generated yield

Spatially generated yield has been validated against the government statistics and a deviation of less than 6 % was noticed in kharif and rabi seasons respectively. The average kharif yields of Karimnagar in 2021 was 5014 kg ha^{-1} reported by government statistics, while the model mean yield from spatial yield map was 5300 kg ha^{-1} . In rabi the predicted model mean yield was 6459 kg ha^{-1}, while from the government statistics the average yield of rabi in Karimnagar district was 6300 kg ha^{-1}. This shows that the integrating the remote sensing satellite data with the crop simulation models can effectively predict the crop yield under varying management conditions.

Chapter VI

SUMMARY AND CONCLUSIONS

A precise and timely crop yield estimates at regional, national and international levels is essential for making policy to overcome food security worldwide and helping farmers for crop insurance through insurance premium pricing by the companies. An investigation on "Assimilating of remote sensing Leaf Area Index into crop simulation models for rice yield estimation" was carried out during kharif 2020 and rabi 2021-22 to find out crop yield estimation based on the DSSAT model and compare the simulated LAI from remote sensing satellite data and DSSAT model. There are lack of studies on comparing the ceptometer LAI to any crop model simulated LAI and also yields estimation at local level though they were done at a broad level like state or district. Further, remote sensing and crop growth models are two discrete tools that can unravel various field and regional agronomic issues. In this study an assessment was made estimate rice grain yield at the village level, with the LAI estimated through remote sensing as its core component.

In Karimnagar district, four villages each in kharif and rabi were selected for further study based on soil, rainfall, crop type, and elevation points encompassing a wide range of potential combinations. The LAI was collected manually by using the accupar LP-80 ceptometer during different stages of the crop in both the seasons indicated that in medium duration cultivar, the LAI ranged between 4.6 to 6.1 at maximum tillering stage and 3.2 to 5.6 at flowering stage and 4.01 to 4.5 at grain formation stage and 2.2 to 3.5 at near to maturity stage in both seasons. The higher LAI values frequency was more during the rabi season as compared to kharif. Supervised classification performed for both the seasons using ERDAS and Arc GIS that rice is the major crop in the district during both the seasons. Accuracy showed that overall accuracy of 94.23% and 88.5% was recorded, while kappa coefficient of 0.89 and 0.85 was resulted in kharif and rabi season respectively which meant that mapping of rice areas in Karimnagar district using the ERDAS was accurate enough by producing reliable results.

In selected villages, the observed grain yield of rice obtained through crop cutting experiments in kharif ranged between 4000 to 5900 kg ha^{-1} while in rabi it ranged between 4500 kg ha^{-1} to 7200 kg ha^{-1}. On an average, kharif and rabi rice grain yields were 5324 kg ha^{-1} and 6436 kg ha^{-1}respectively in selected villages.

The average simulated rice grain yield in kharif and rabi were 5339 kg ha^{-1} and 6858 kg ha^{-1} respectively with DSSAT model which considered sentinel-2 satellite for estimation of LAI. The R^2 values of above 0.72 in kharif and above 0.85 in rabi, D index of 0.70 in both the seasons in all the villages showed the model is accurate for predicting yields. Deviation has been noted between observed and simulated values where the predicted values are higher than the observed values.

The correlation between observed rice grain yield with the quantity of nitrogen applied showed a R^2 value of 0.82 and 0.83 indicating that rice grain yield is dependent on the quantity of nitrogen applied.

A linear regression coefficient was observed between measured maximum LAI with ceptometer and the model simulated maximum LAI with R^2 value of 0.77 and 0.80. LAI and grain yield showed a linear correlation with R^2 value of 0.77 and 0.78 in kharif and rabi respectively with observed data (yield and LAI), while for the simulated values it was 0.84 and 0.85 respectively.

Integration of remote sensing with crop model data was based on the relation obtained between the NDVI and model LAI which showed a R^2 value of 0.82 and 0.81 in kharif and rabi season respectively. As good agreement was observed between them it has been confirmed that NDVI is one among the important parameter which can be used to integrate with LAI for grain yield estimation. Using the NDVI generated from the GEE, spatial LAI map was generated by the linear equation generated from the correlation between the NDVI and model LAI. The linear equation obtained between the model LAI and model yield was used to generated the spatial yield map on basis of spatial LAI map. From the spatial yield map, it can be concluded that most of the areas fall under the rice grain yield range of 5700 to 6000 kg ha^{-1} in kharif, while in rabi in the range of 6500 to 7000 kg $ha^{-1.}$

The spatially distributed model yield validated with the government agency grain yield statistics showed that the model mean yield in kharif season for the Karimnagar district was 5300 kg ha^{-1} which is near to Govt grain yield estimates (5014 kg ha^{-1}). During rabi season also, the model estimated mean rice grain yield (6458 kg ha^{-1}) was close to that of the average yield estimated by Govt (6600 kg ha^{-1}) showing that the deviation is acceptable.

Conclusions

- This study demonstrated the potential of integrating remote sensing products with the crop model by considering LAI as the principal component to estimate the rice yields at village level.
- Mapped spatial distribution of rice growing areas showed an accuracy of above 90%, in both seasons comparable to the government statistics.
- Input parameters in the DSSAT model were collected during the field visits, and R^2 value of above 0.80, was observed during kharif and rabi between observed and simulated yields, indicating that the model reliably produced results reflective of the field data.
- Ceptometer and model simulated LAI showed R^2 values of 0.77 and 0.80 in kharif and rabi seasons respectively indicating the model is efficient in generating the LAI.
- Yield and LAI were in good agreement with R^2 value of more than 0.75 hence the yield increases with an increase in LAI.
- Remote sensing product NDVI correlated with the LAI with R^2 value of more than 0.80 indicating that NDVI is best fit with the LAI.
- Spatial rice yield distribution in Karimnagar district was generated by assimilating remote sensing data into the crop simulation model which can be used in planning.

Future Line of Work

- Models should be properly calibrated to improve the accuracy and consistency of assimilating remote sensing data with crop models.
- There is a limitation in capacity of DSSAT model to address the impact of biotic stress caused by pests, diseases, and weeds. Hence, integrating dynamic pest and disease model is of utmost important.
- Along with LAI, other variables, including the fraction of absorbed photosynthetically active radiation and soil moisture, can be applied to increase the accuracy in assessing crop yields.
- As the chosen study area is limited to the district level and includes data from two seasons, the associated data is insufficient to draw definitive conclusions regarding climate change. Hence, the assessment has to be designed to evaluate the effects of climate change on crop yield, which can be extended under long-term scenarios.

- The crop yields accuracies can be enhanced by integrating machine learning (ML) algorithms and deep learning (DL) techniques.
- Fusion of SAR and Optical Imegery enhances crop identification, particularly during the Kharif season.

BIBILOGRAPHY

Abayechaw, D. (2021). Review on decision support system for agrotechnology transfer (DSSAT) model. *International Journal of Intelligent Information Systems*, *10*(6), 117-124.

Abiy Wogderes Zinna, A. W. Z., and Karuturi Venkata Suryabhagavan, K. V. S. (2016). Remote sensing and GIS based spectro-agrometeorological maize yield forecast model for South Tigray Zone, Ethiopia. *Journal of Geographic Information system*, 8(2): 282-292.

Aboelghar, M., Arafat, S., Yousef, M. A., El-Shirbeny, M., Naeem, S., Massoud, A., and Saleh, N. (2011). Using SPOT data and leaf area index for rice yield estimation in Egyptian Nile delta. *The Egyptian Journal of Remote Sensing and Space Science*, *14*(2), 81-89.

Aditya, K., Chandra, H., Basak, P., Kumari, V., and Das, S. (2020). District level crop yield estimation with reduced number of crop cutting experiments. *The Indian Journal of Agricultural Sciences*, *90*(6), 1185-1189.

Ahmad, S., Ahmad, A., Ali, H., Garcia y Garcia, A., Khan, M., Zia-Ul-Haq, M., and Hasanuzzaman, M. (2012). Application of the CSM-CERES-Rice model for evaluation of plant density and irrigation management of transplanted rice for an irrigated semiarid environment. *Irrigation Science, 31*. doi:10.1007/s00271-012-0324-6

Ahmad, S., Ahmad, A., Ali, H., Hussain, A., Garcia y Garcia, A., Khan, M. A., and Hoogenboom, G. (2013). Application of the CSM-CERES-Rice model for evaluation of plant density and irrigation management of transplanted rice for an irrigated semiarid environment. *Irrigation Science, 31*, 491-506.

Ahmad, T., Sahoo, P. M., Singh, M., and Biswas, A. (2021). Crop Cutting Experiment techniques for determination of yield rates of field crops. *DOL10, 13140*.

Ahmed, M. S., Marwa, G. M. and Gamal, A. El-Sanat. (2014) Evaluating AquaCrop model to improve crop water productivity on North Delta soils, Egypt. *Advances in Applied Science Research*, 5(5), 293–304.

Akhter, M., Mahmood, A., Raza, M. A., Haider, Z., Saleem, U., and Bibi, T. (2016). Effect of transplanting dates on cooking, milling and eating quality parameters of some fine and coarse grain rice lines. *Journal of Nutrition and Food Science*, *6*(552), 2.

Akinbile, C. (2013). Assessment of CERES-Rice model for rice production in Ibadan, Nigeria. *Agricultural Engineering International CGIR Journal*, *15*, 19-26.

Alejo, L. A. (2020). Assessing the impacts of climate change on aerobic rice production using the DSSAT-CERES-Rice model. *Journal of Water and Climate Change*, *12*(3), 696-708.

Ali, A. M., Savin, I., Poddubskiy, A., Abouelghar, M., Saleh, N., Abutaleb, K., and Dokukin, P. (2021). Integrated method for rice cultivation monitoring using Sentinel-2 data and Leaf Area Index. *The Egyptian Journal of Remote Sensing and Space Science*, *24*(3), 431-441.

Amarasingha, R.P.R.K., Suriyagoda, L.D.B., Marambe, B., Gaydon, D.S., Galagedara, L.W., Punyawardena, R., Silva, G.L.L.P., Nidumolu, U and Howden, M. (2015). Simulation of crop and water productivity for rice (Oryza sativa L.) using APSIM under diverse agro-climatic conditions and water management techniques in Sri Lanka. *Agricultural Water Management*. 160: 132-143.

Arias, M., Campo-Bescos, M. A., and Alvarez-Mozos, J. (2020). Crop classification based on temporal signatures of Sentinel-1 observations over Navarre province, Spain. *Remote Sensing*, *12*(2), 278.

Aschonitis, V., Papamichail, D., Lithourgidis, A., and Fano, E. (2014). Estimation of Leaf Area Index and Foliage Area Index of Rice Using an Indirect Gravimetric Method. *Communications in Soil Science and Plant Analysis, 45*. doi:10.1080/00103624.2014.907917

Bahmaniar, M. A., Ranjbar, G. A., and Ahmadian, S. H. (2007). Effects of N and K applications on agronomic characteristics of two Iranian and landrace rice (Oryza sativa L.) cultivars. *Pakistan Journal of Biological Sciences: PJBS*, *10*(6), 880-886.

Bahmanyar, M.A., Ranjbar, G.A. (2007). Response of rice cultivar to rates of nitrogen and potassium application in field and pot conditions. *Pakistan Journal of Biological Science*, 10(9): 1430-1437.

Balderama, O., Alejo, L., and Tongson, E. (2016). Calibration, validation and application of CERES-Maize model for climate change impact assessment in Abuan Watershed, Isabela, Philippines. *Climate, Disaster and Development Journal*, *2*(1), 11-20.

Banko, G. (1998). A review of assessing the accuracy of classifications of remotely sensed data and of methods including remote sensing data in forest inventory.

Basak, P. (2019) Agricultural Research Data Book; ICAR Research Data Repository for Knowledge Management: New Delhi, India.

Batchelor, W.D., Basso, B and Paz, J.O. (2002). Examples of strategies to analyze spatial and temporal yield variability using crop models. *European Journal of Agronomy*. 18(1-2): 141-158.

Behera, S. K., and Panda, R. K. (2009). Integrated management of irrigation water and fertilizers for wheat crop using field experiments and simulation modeling. *Agricultural water management*, *96*(11), 1532-1540.

Bellamkonda, J., Reddy, B. N. K., Rathod, S., Naik, B. B., Supriya, K., Nirmala, B., and Bhanusree, D. (2022). Application of the CERES-Rice Model for Rice Yield Gap Analysis. *International Journal of Environment and Climate Change*, 3471-3478.

Bellam, P. K., Gumma, M. K., Panjala, P., Mohammed, I., & Suzuki, A. (2023). Mapping shrimp pond dynamics: a spatiotemporal study using remote sensing data and machine learning. *AgriEngineering*, *5*(3), 1432-1447.

Bernardes, T., Moreira, M. A., Adami, M., Giarolla, A., and Rudorff, B. F. T. (2012). Monitoring biennial bearing effect on coffee yield using MODIS remote sensing imagery. *Remote Sensing*, *4*(9), 2492-2509.

Bhargav, M. (2021). Discrimination of rice ecosystem and yield estimation using temporal SAR (Synthetic Aperture radar) and optical RS (Remote Sensing) data in Jogulamba Gadwal district, Telangana. MSc Thesis. Professor Jayashankar Telangana State Agricultural University, Hyderabad, India.

Bouman, B.A.M. (1995). Crop modelling and remote sensing for yield prediction. *Netherlands Journal of Agricultural Science*, 43(2): 143-161.

Cai, Y., Guan, K., Peng, J., Wang, S., Seifert, C., Wardlow, B., and Li, Z. (2018). A high performance and in-season classification system of field-level crop types using time-series Landsat data and a machine learning approach. *Remote sensing of environment, 210*, 35-47.

Campos-Taberner, M., Garcia-Haro, F., Moreno, A., Gilabert, M. A., Sánchez-Ruiz, S., Martinez, B., & Camps-Valls, G. (2015). Mapping Leaf Area Index With a Smartphone and Gaussian Processes. *IEEE Geoscience and Remote Sensing Letters, 12*, 2501-2505.

Casa, R., Upreti, D., and Pelosi, F. (2019). Measurement and estimation of leaf area index (LAI) using commercial instruments and smartphone-based systems. *IOP Conference Series: Earth and Environmental Science, 275*, 012006.

Chamely, S.G., Islam, N., Hoshain, S., Rabbani, M.G., Kader, M.A. and Salam, M.A. (2015). Effect of variety and nitrogen rate on the yield performance of boro rice. *Progressive Agriculture,* 26(1):6-14.

Chandrasekhar, J., Rao, G. R., Reddy, B. R., and Reddy, K. B. (2001). Physiological analysis of growth and productivity in hybrid rice (Oryza sativa L.).

Choudhury, A and Jones, J. (2014). Crop yield prediction using time series models. Journal of Economics and Economic Education Research, 15(3): 53-67.

Clevers, J. G., Kooistra, L., and van den Brande, M. M. (2017). Using sentinel-2 data for retrieving LAI and leaf and canopy chloro phyll content of a potato crop. *Remote Sensing*, 9(5), 405.

Clevers, J.G.P.W., Biiker, C., Van Leeuwen,H.J.C., and Bouman, B.A.M (1994) A Framework for Monitoring Crop Growth by Combining Directional and Spectral Remote Sensing Information. Remote Sensing Environment, 50:161-170.

Congalton, R.G. (1991). A review of assessing the accuracy of classifications of remotely sensed data. *Remote Sensing of Environment*. 37(1): 35-46.

Cutini, A., Matteucci, G., and Mugnozza, G. S. (1998). Estimation of leaf area index with the Li-Cor LAI 2000 in deciduous forests. *Forest Ecology and Management*, *105*(1-3), 55-65.

De Jesus, W. C., do Vale, F. X. R., Coelho, R. R., and Costa, L. C. (2001). Comparison of two methods for estimating leaf area index on common bean. *Agronomy journal*, *93*(5), 989-991.

Deka, R., Hussain, R., Singh, K. K., Rao, V., Balasubramaniyam, R., and Baxla, A. K. (2016). Rice phenology and growth simulation using CERES-Rice model under the agro-climate of upper Brahmaputra valley of Assam. *Mausam*, *67*, 591-598.

Dong, T., Liu, J., Qian, B., Jing, Q., Croft, H., Chen, J., and Chen, P. (2016). Deriving maximum light use efficiency from crop growth model and satellite data to improve crop biomass estimation. *IEEE Journal of Selected topics in Applied Earth observations and Remote sensing*, *10*(1), 104-117.

Doraiswamy, P.C., Hatfield, J.L., Jackson, T.J., Akhmedov, B., Prueger, J and Stern, A. (2004) Crop condition and yield simulations using Landsat and MODIS. *Remote Sensing of Environment.* 92(4): 548-559.

Dorigo, W.A., Zurita-Milla, R., de Wit, A.J., Brazile, J., Singh, R and Schaepman, M.E. (2007). A review on reflective remote sensing and data assimilation techniques for enhanced agroecosystem modeling. *International Journal of Applied Earth Observation and Geoinformation*. 9(2): 165-193.

Dubey, S., Mandloi, D., Gavli, A., Latwal, A., Das, R., and Ray, S. (2019). Quality checking of crop cutting experiments using remote sensing data: a case study for rice crop in odisha. *ISPRS - International Archives of the Photogrammetry, Remote Sensing and Spatial Information Sciences, XLII-3/W6*, 461-466. doi:10.5194/isprs-archives-XLII-3-W6-461-2019

Dwivedi , M., Saxena, S., Neetu and S. S. Ray. (2019). Assessment of rice biomass production and yield using semi-physical approach and remotely sensed data .The *International Archives of the Photogrammetry, Remote Sensing and Spatial Information Sciences*, XLII-3/W6.

Enderle, D. I., and Weih Jr, R. C. (2005). Integrating supervised and unsupervised classification methods to develop a more accurate land cover classification. *Journal of the Arkansas Academy of Science*, *59*(1), 65-73.

Fan, L. Y., Gao, Y. Z., Brück, H. E. B. C., and Bernhofer, C. (2009). Investigating the relationship between NDVI and LAI in semi-arid grassland in Inner Mongolia using in-situ measurements. *Theoretical and applied climatology*, *95*, 151-156.

Fang, H., Liang, S and Hoogenboom, G. (2011). Integration of MODIS LAI and vegetation index products with the CSM–CERES–Maize model for corn yield estimation. *International Journal of Remote Sensing*. 32(4): 1039-1065.

Fang, H., Ye, Y., Weiwei, L., Wei, S., and Ma, L. (2018). Continuous estimation of canopy leaf area index (LAI) and clumping index over broadleaf crop fields: An investigation of the PASTIS-57 instrument and smartphone applications. *Agricultural and Forest Meteorology, 253*, 48-61. doi:10.1016/j.agrformet.2018.02.003

Filippi, P., Jones, E.J., Wimalathunge, N.S., Somarathna, P.D., Pozza, L.E., Ugbaje, S.U., Jephcott, T.G., Paterson, S.E., Whelan, B.M and Bishop, T.F. (2019). An approach to forecast grain crop yield using multi-layered, multi-farm data sets and machine learning. *Precision Agriculture*. 20(5): 1015-1029.

Francesconi, W., Srinivasan, R., Perez-Minana, E., Willcock, S. P., and Quintero, M. (2016). Using the Soil and Water Assessment Tool (SWAT) to model ecosystem services: A systematic review. *Journal of Hydrology*, *535*, 625-636.

Garnier, P., Néel, C., Mary, B., Lafolie, F. (2001). Evaluation of a nitrogen transport and transformation model in bare soil. *European Journal of Soil Science*. 52, 253–268.

Gebreselassie, Y., Mekonen, A. and Kassa, T., (2015). Field experimenta tion-based simulation of yield response of maize crop to deficit irriga tion using AquaCrop model, Arba Minch, Ethiopia. *African Journal of Agricultural Research,*10(4), 269–280.

Ghansham, P., Reddy, P. R. R., Srinivas, A., Reddy, S. N., and Madhavi, A. (2015). Nutrient uptake studies in machine transplanted rice (Oryza sativa L.) as influenced by nitrogen levels and split schedules. *Journal of Research PJTSAU*, *43*(4), 7-11.

Goswami, S., Gamon, J., Vargas, S., and Tweedie, C. (2015). *Relationships of NDVI, Biomass, and Leaf Area Index (LAI) for six key plant species in Barrow, Alaska* (No. e913v1). PeerJ PrePrints.

Government of Telangana. *Season and Crop Covergae Report Vanakalam—2021*; Report 2021; Government of Telangana: Hyderabad, India, 2021.

Gu, Y., Brown, J. F., Verdin, J. P., and Wardlow, B. (2007). A five-year analysis of MODIS NDVI and NDWI for grassland drought assessment over the central Great Plains of the United States. *Geophysical research letters*, *34*(6).

Gumma, M. K., Kadiyala, M., Panjala, P., Ray, S. S., Akuraju, V. R., Dubey, S., Whitbread, A. M. (2022). Assimilation of remote sensing data into crop growth model for yield estimation: A case study from India. *Journal of the Indian Society of Remote Sensing*, *50*(2), 257-270.

Gumma, M.K., Nelson, A., Thenkabail, P.S and Singh, A.N. (2011a). Mapping rice areas of South Asia using MODIS multitemporal data. *Journal of Applied Remote Sensing.* 5(1): 053547.

Gumma, M.K., Thenkabail, P.S., Hideto, F., Nelson, A., Dheeravath, V., Busia, D and Rala, A. (2011b). Mapping irrigated areas of Ghana using fusion of 30 m and 250 m resolution remote-sensing data. *Remote Sensing*. 3(4): 816-835.

Gumma, M.K., Thenkabail, P.S., Maunahan, A., Islam, S and Nelson, A. (2014). Mapping seasonal rice cropland extent and area in the high cropping intensity environment of Bangladesh using MODIS 500 m data for the year 2010. *ISPRS Journal of Photogrammetry and Remote Sensing*. 91: 98-113.

Gumma, M.K., Thenkabail, P.S., Teluguntla, P., Rao, M.N., Mohammed, I.A and Whitbread, A.M. (2016). Mapping rice-fallow cropland areas for short-season grain legumes intensification in South Asia using MODIS 250 m time-series data. *International Journal of Digital Earth*. 9(10): 981-1003.

Gumma, M.K., Thenkabail, P.S., Teluguntla, P.G., Oliphant, A., Xiong, J., Giri, C., Pyla, V., Dixit, S and Whitbread, A.M. (2020b). Agricultural cropland extent and areas of South Asia derived using Landsat satellite 30-m time-series big-data using random forest machine learning algorithms on the Google Earth Engine cloud. *GIScience and Remote Sensing*. 57(3): 302-322.

Gumma, M. K., Takashi, Y., Panjala, P., Deevi, K. C., Inthavong, V., Bellam, P. K., & Mohammed, I. (2023). Assessment of cropland changes due to new canals in Vientiane prefecture of Laos using earth observation data. *Smart Agricultural Technology*, *4*, 100149.

Gumma, M.K., Tummala, K., Dixit, S., Collivignarelli, F., Holecz, F., Kolli, R.N. and Whitbread, A.M. (2020a). Crop type identification and spatial mapping using Sentinel-2 satellite data with focus on field-level information. *Geocarto International*. 1-17.

Gumma, M. K., Panjala, P., & Teluguntla, P. (2024). Mapping heterogeneous land use/land cover and crop types in Senegal using sentinel-2 data and machine learning algorithms. *International Journal of Digital Earth*, *17*(1), 2378815.

Gumma, M. K., Panjala, P., & Teluguntla, P. (2024). Dryland cropping in different Land uses of Senegal using Sentinel-2 and hybrid ML method. *International Journal of Digital Earth*, *17* (1), 2378815.

Gumma, M. K., Panjala, P., Dubey, S. K., Ray, D. K., Murthy, C. S., Kadiyala, D. M., & Takashi, Y. (2024). Spatial Distribution of Cropping Systems in South Asia Using Time-Series Satellite Data Enriched with Ground Data. *Remote Sensing*, *16*(15), 2733.

Gumma, M. K., Nukala, R. M., Panjala, P., Bellam, P. K., Gajjala, S., Dubey, S. K., & Deevi, K. C. (2024). Optimizing Crop Yield Estimation through Geospatial Technology: A Comparative Analysis of a Semi-Physical Model, Crop Simulation, and Machine Learning Algorithms. *Agri Engineering*, *6*(1), 786-802.

Hashimoto, N., Saito, Y., Yamamoto, S., Ishibashi, T., Ito, R., Maki, M., and Homma, K. (2023). Relationship between Leaf Area Index and Yield Components in Farmers' Paddy Fields. *AgriEngineering*, *5*(4), 1754-1765.

Hasmadi, M., Pakhriazad, H., and Shahrin, M. (2009). Evaluating supervised and unsupervised techniques for land cover mapping using remote sensing data.

Geografia: Malaysian Journal of Society and Space, *5*(1), 1-10.

He, J., Dukes, M. D., Jones, J. W., Graham, W. D., and Judge, J. (2009). Applying GLUE for estimating CERES-Maize genetic and soil parameters for sweet corn production. *Transactions of the ASABE*, *52*(6), 1907-1921.

Hegarty-Craver, M., Polly, J., O'Neil, M., Ujeneza, N., Rineer, J., Beach, R.H., Lapidus, D. and Temple, D.S. (2020). Remote crop mapping at scale: Using satellite imagery and UAV-acquired data as ground truth. *Remote Sensing*, 12(12):1984.

Hoogenboom, G. (2013). Application of the CSM-CERES-Rice model for evaluation of plant density and irrigation management of transplanted rice for an irrigated semiarid environment. *Irrigation Science*, *31*, 491-506.

Hong, S.Y., Sudduth, K.A., Kitchen, N.R., Fraisse, C.W., Palm, H.L and Wiebold, W.J. (2004). Comparison of remote sensing and crop growth models for estimating within-field LAI variability. *Korean Journal of Remote Sensing*. 20(3): 175-188.

Hui, J., and Yao, L. (2018). A method to upscale the Leaf Area Index (LAI) using GF-1 data with the assistance of MODIS products in the Poyang Lake watershed. *Journal of the Indian Society of Remote Sensing*, 46, 551–560.

Hyer, E.J and Goetz, S.J. (2004). Comparison and sensitivity analysis of instruments and radiometric methods for LAI estimation: Assessments from a boreal forest site. *Agricultural and Forest Meteorology*. 122(3-4):157-174.

Ines, A.V., Das, N.N., Hansen, J.W and Njoku, E.G. (2013). Assimilation of remotely sensed soil moisture and vegetation with a crop simulation model for maize yield prediction. *Remote Sensing of Environment*. 138: 149-164.

Inglada, J., Arias, M., Tardy, B., Hagolle, O., Valero, S., Morin, D., Defourny, P. (2015). Assessment of an operational system for crop type map production using high temporal and spatial resolution satellite optical imagery. *Remote Sensing, 7*(9), 12356-12379.

Islam, M. M. A. F., Khan, M. A., Bari, A. F., Hosain, M. T., and Sabikunnaher, S. (2013). Effect of fertilizer and manure on the growth, yield and grain nutrient concentration of boro rice (Oryza sativa L.) under different water management practices. *Water Management*, 6(30, 44-51.

Jain, M., Rao, P., Srivastava, A. K., Poonia, S., Blesh, J., Azzari, G., and Lobell, D. B. (2019). The impact of agricultural interventions can be doubled by using satellite data. *Nature Sustainability*, *2*(10), 931-934.

Jena, M., Adak, T., Rath, P. C., Gowda, G. B., Patil, N. B., Prasanthi, G., and Mohapatra, S. D. (2018). Paradigm shift of insect pests in rice ecosystem and their management strategy. *ORYZA-An International Journal on Rice*, *55*(spl), 82-89.

Jonckheere, I., Fleck, S., Nackaerts, K., Muys, B., Coppin, P., Weiss, M., and Frederic, B. (2004). Review of methods for in situ leaf area index determination: Part I. Theories, sensors and hemispherical photography. *Agricultural and Forest Meteorology*, *121*, 19-35. doi:10.1016/j.agrformet.2003.08.027

Jones, J.W., Hoogenboom, G., Porter, C.H., Boote, K.J., Batchelor, W.D., Hunt, L.A., Wilkens, P.W., Singh, U., Gijsman, A.J., Ritchie, J.T., (2003). The DSSAT cropping system model. *European Journal of Agronomy*, 18, 235–265.

Kabir, M., Paul, D., Hossain, M., and Rahman, N. (2016). Estimating area and production of rice under different crop-cut methods in Bangladesh. *Bangladesh Rice Journal, 20*(1), 11-16.

Kadiyala, M. D. M., Jones, J. W., Mylavarapu, R. S., Li, Y. C., and Reddy, M. D. (2015). Identifying irrigation and nitrogen best management practices for aerobic rice–maize cropping system for semi-arid tropics using CERES-rice and maize models. *Agricultural Water Management, 149,* 23-32. Retrieved from https://www.sciencedirect.com/science/article/pii/S0378377414003394. doi:https://doi.org/10.1016/j.agwat.2014.10.019

Kaur, K., and Kaur, P. (2022). Simulation of yield of rice cultivars under variable agronomic management options using CERES-Rice and InfoCrop-rice models in irrigated plains of Punjab. *Agricultural Research Journal*, *59*(3).

Kenduiywo, B.K., Bargiel, D and Soergel, U. (20180. Crop-type mapping from a sequence of Sentinel-1 images. *International Journal of Remote Sensing*. 39(19): 6383 6404.

Kobayashi, N., Tani, H., Wang, X., and Sonobe, R. (2020). Crop classification using spectral indices derived from Sentinel-2A imagery. *Journal of Information and Telecommunication*, *4*(1), 67-90.

Kross, A., McNairn, H., Lapen, D., Sunohara, M., and Champagne, C. (2015). Assessment of RapidEye vegetation indices for estimation of leaf area index and biomass in corn and soybean crops. *International Journal of Applied Earth Observation and Geoinformation*, *34*, 235-248.

Kumar, P., Sarangi, A., Singh, D. K. and Parihar, S. S., (2014). Evaluation of AquaCrop model in predicting wheat yield and water productivity under irrigated saline regimes. *Irrigation and Drainage*, 63, 474–487; doi:https://doi.org/10.1002/ird.1841.

Li, H., Zhang, C., Zhang, S., and Atkinson, P. M. (2020). Crop classification from full-year fully-polarimetric L-band UAVSAR time-series using the Random Forest algorithm. *International Journal of Applied Earth Observation and Geoinformation*, *87*, 102032.

Li, M., Du, Y., Zhang, F., Fan, J., Ning, Y., Cheng, H and Xiao, C. (2020). Modification of CSM-CROPGRO-Cotton model for simulating cotton growth and yield under various deficit irrigation strategies. *Computers and Electronics in Agriculture*. 179: 105843.

Liu, H., Liu, H.., Lei, Q., Zhai, L., Wang, H., Zhang, J., Liu, X. (2017). Using the DSSAT model to simulate wheat yield and soil organic carbon under a wheat-maize cropping system in the North China Plain. *Journal of Integrative Agriculture, 16,* 2300-2307. doi:10.1016/S2095-3119(17)61678-2

Loague, K., Green, R.E., (1991). Statistical and graphical methods for evaluating solute transport models: overview and application. *Journal of Contaminant Hydrology*, 7, 51–73.

Lu, B., Kun, Y., Zhiming, W., Jing, W. and Jie, S., (2020). Adaptability evaluation of ORYZA (v3) for single-cropped rice under different establishment techniques in eastern China. *Agronomy Journal*, 112, 2741–2758.

Makinde, E. O., and Oyelade, E. O. (2020). Land cover mapping using Sentinel-1 SAR and Landsat 8 imageries of Lagos State for 2017. *Environmental Science and Pollution Research*, *27*(1), 66-74.

Manzoor, Z., Awan, T. H., Safdar, M. E., Ali, R. I., Ashraf, M. M., and Ahmad, M. (2006). Effect of nitrogen levels on yield and yield components of Basmati 2000. *Journal of Agricultural Research*, *44*(2), 115-120.

Masson-Delmotte, V., Zhai, P., Po¨rtner, H.-O., Roberts, D., Skea, J., Shukla, P., Pirani, A., Moufouma-Okia, W., Pe´an, C., Pidcock, R. (2018). Global warming of 1.5 OC: an IPCC special report on the impacts of global warming of 1.5 C above pre-industrial levels and related global greenhouse gas emission pathways, in the context of strengthening the global response to the threat of climate change,

sustainable development, and efforts to eradicate poverty. World Meteorological Organization Geneva, Switzerland.

Milesi, C and Kukunuri, M. (2022). Crop yield estimation at gram panchayat scale by integrating field, weather and satellite data with crop simulation models. *Journal of the Indian Society of Remote Sensing*. 50(2): 239-255.

Mirakhori, M., Mirshekari, B., Amiri, E., Paknejad, F., and Yarnia, M. (2017). Evaluation of CERES-Rice Model in Simulation of Rice Growth under Constraint Irrigation and Nitrogen Fertilizer Conditions. *Ambient Science, 03 and 04*. doi:10.21276/ambi.2016.03.sp2.ra03

Mosleh, M. K., Hassan, Q. K., and Chowdhury, E. H. (2015). Application of remote sensors in mapping rice area and forecasting its production: A review. *Sensors*, *15*(1), 769-791.

Mrudhula, K.A. and Suneetha, Y. (2020). Effect of nitrogen levels on growth, yield attributes and yield of rice variety BPT 2231-Akshaya. *The Pharma Innovation Journal*, 9(7):218-221.

Muslim, M., Romshoo, S.A and Rather, A.Q. (2015). Paddy crop yield estimation in Kashmir Himalayan rice bowl using remote sensing and simulation model. *Environmental Monitoring and Assessment*. 187(6): 1-12.

Naik, B. B., Reddy, D. R., Sreenivas, G., and Rani, P. L. (2015). Effect of sowing dates and varieties on growth, yield and economics of aerobic rice (Oryza sativa L.) during kharif season. *Journal of Research, PJTSAU*, 43(1):18-24.

Ngwira, A. R., Aune, J. B., and Thierfelder, C. (2014). DSSAT modelling of conservation agriculture maize response to climate change in Malawi. *Soil and Tillage Research*, *143*, 85-94.

Noureldin, N. A., Aboelghar, M. A., Saudy, H. S., and Ali, A. M. (2013). Rice yield forecasting models using satellite imagery in Egypt. *The Egyptian Journal of Remote Sensing and Space Science*, *16*(1), 125-131.

Nyangau, W., Mati, B., Kalamwa, K., Wanjogu, R., and Kiplagat, L. (2014). Estimating Rice Yield under Changing Weather Conditions in Kenya Using CERES Rice Model. *International Journal of Agronomy, 2014*, 1-12. doi:10.1155/2014/849496

Ozdogan, M., and Woodcock, C. E. (2006). Resolution dependent errors in remote sensing of cultivated areas. *Remote Sensing of Environment*, *103*(2), 203-217.

Panjala, P., Gumma, M.K and Teluguntla, P. 2022. Machine learning approaches and Sentinel-2 data in crop type mapping. In Data Science in Agriculture and Natural Resource Management (161-180). Springer, Singapore

Parker, G. G. (2020). Tamm review: Leaf Area Index (LAI) is both a determinant and a consequence of important processes in vegetation canopies. *Forest Ecology and Management*, *477*, 118496.

Patel, A. R., Patel, M. L., Patel, R. K., and Mote, B. M. (2019). Effect of different sowing date on phenology, growth and yield of rice-a review. 12-16

Patil, M. B., Desai, C. G., and Umrikar, B. N. (2012). Image classification tool for land use/land cover analysis: A comparative study of maximum likelihood and minimum distance method. *International Journal of Geology, Earth and Environmental Sciences*, *2*(3), 189-196.

Pazhanivelan, S., Geethalakshmi, V., Ramamoorthy, T., N.S, S., Kaliaperumal, R., Ramalingam, K., Quicho, E. (2022). Spatial Rice Yield Estimation Using Multiple Linear Regression Analysis, Semi-Physical Approach and Assimilating SAR Satellite Derived Products with DSSAT Crop Simulation Model. *Agronomy*, *12*, 2008. doi:10.3390/agronomy12092008.

Pitman, J. I. (2000). Absorption of photosynthetically active radiation, radiation use efficiency and spectral reflectance of bracken [Pteridium aquilinum (L.) Kuhn] canopies. *Annals of Botany*, 85, 101–111.

Pokovai, K and Fodor, N., (2019). Adjusting ceptometer data to improve leaf area index measurements. *Agronomy*. 9(12):866.

Pooja, Kumar, S., Gupta, K., Verma, S. and Singh, U.P. (2018). Effect of nitrogen scheduling on yield, nutrient content and uptake in boro rice lowland rice eco system. *Journal of Pharmacognosy and Phytochemistry*, 7(2):2145-2148.

Pramanik, K. and Bera, A. K. (2013). Effect of seedling age and nitrogen fertilizer on growth, chlorophyll content, yield and economics of hybrid rice. *International Journal of Agronomy and Plant Production*, 4(S): 3489-3499.

Priya, S., and Shibasaki, R. (2001). National spatial crop yield simulation using GIS-based crop production model. *Ecological Modelling*, *136*(2-3), 113-129.

Rai, H. K., and Kushwaha, H. S. (2008). Effect of planting dates and soil water regimes on growth and yield of upland rice. *Oryza-An International Journal on Rice*, *45*(2), 129-132.

Rajesh, K., Thatikunta, R., Naik, D. S., and Arunakumari, J. (2017). Effect of different nitrogen levels on morpho physiological and yield parameters in rice (Oryza sativa L.). *Inernational Journal of Current and Applied Science*, *6*(8), 2227-2240.

Raman, M.G., Kaliaperumal, R., Pazhanivelan, S and Kannan, B. (2019). Rice area estimation using parameterized classification of sentinel 1A SAR data. *The International Archives of Photogrammetry, Remote Sensing and Spatial Information Sciences.* 42: 141-147.

Ramulu, C., Reddy, P. R. R., and Narsaiah, E. (2020). Effect of nitrogen levels on yield and nutrient uptake of kharif rice (Oryza sativa L.) under different establishment methods. *Journal of Crop and Weed*, *16*(2), 106-112.

Ray, M., and Ray, M. (2018). Application of DSSAT Crop Simulation Model to Estimate Rice Yield in Keonjhar District of Odisha (India) under Changing Climatic Conditions. *International Journal of current Microbiology and Applied Sciences*, 7(4),659-667.

Richards, J. A. (2022). Supervised classification techniques. *Remote sensing digital image analysis*, 263-367.

Rogan, J., and Chen, D. (2004). Remote sensing technology for mapping and monitoring land-cover and land-use change. *Progress in planning*, *61*(4), 301-325.

Rwanga, S. S., and Ndambuki, J. M. (2017). Accuracy assessment of land use/land cover classification using remote sensing and GIS. *International Journal of Geosciences*, *8*(04), 611.

Saini, R., and Ghosh, S. K. (2018). Crop classification on single date sentinel-2 imagery using random forest and suppor vector machine. *The International Archives of the Photogrammetry, Remote Sensing and Spatial Information Sciences, 42*, 683-688.

Sakamoto, T., Yokozawa, M., Toritani, H., Shibayama, M., Ishitsuka, N., and Ohno, H. (2005). A crop phenology detection method using time-series MODIS data. *Remote sensing of environment*, *96*(3-4), 366-374.

Setiyono, T.D., Quicho, E.D., Holecz, F.H., Khan, N.I., Romuga, G., Maunahan, A., Garcia, C., Rala, A., Raviz, J., Collivignarelli, F and Gatti, L. (2019). Rice yield estimation using synthetic aperture radar (SAR) and the ORYZA crop growth model: development and application of the system in South and South-east Asian countries. *International Journal of Remote Sensing*. 40(21): 8093-8124.

Schut, A., Stephens, D., Stovold, R., Adams, M., and Craig, R. (2009). Improved wheat yield and production forecasting with a moisture stress index, AVHRR and MODIS data. *Crop and Pasture Science,* 60, 60–70.

Sekertekin, A., Marangoz, A. M., and Akcin, H. (2017). Pixel-based classification analysis of land use land cover using Sentinel-2 and Landsat-8 data. *The International Archives of the Photogrammetry, Remote Sensing and Spatial Information Sciences*, *42*, 91-93.

Shanmugapriya, P., Rathika, S., Ramesh, T and Janaki, P. (2019). Applications of remote sensing in agriculture-A Review. *International Journal of Current Microbiology and Applied Sciences*. 8(1): 2270-2283.

Sindhu, L., M. Devender Reddy and A. Sivasankar. (2022). Effect of different transplanting dates and age of seedlings on the performance of rice variety RNR 15048 in Odisha. *Crop Research*, 57 (3): 97-103

Singh, A. K., Tripathy, R. and Chopra, U. K. (2008). Evaluation of CERES-wheat and CropSyst models for water–nitrogen interac tions in wheat crop. Agricultural Water Management, 95, 776–786.

Snigdha, G. (2022). Rice yield estimation using remote sensing and crop simulation model in Nalgonda district, Telangana (Masters dissertation, Professor Jayashankar Telangana State Agricultural University).

Son, N.-T., Chen, C.-F., Chen, C.-R., and Minh, V.-Q. (2018). Assessment of Sentinel-1A data for rice crop classification using random forests and support vector machines. *Geocarto International, 33*(6), 587-601.

Son, N.T., Chen, C.F., Chen, C.R., Chang, L.Y and Chiang, S.H. (2016). Rice yield estimation through assimilating satellite data into a crop simumlation model. *International Archives of the Photogrammetry, Remote Sensing and Spatial Information Sciences*. 8.

Son, N.T., Chen, C.F., Chen, C.R., Guo, H.Y., Cheng, Y.S., Chen, S.L., Lin, H.S and Chen, S.H. (2020). Machine learning approaches for rice crop yield predictions using time-series satellite data in Taiwan. *International Journal of Remote Sensing*. 41(20): 7868-7888.

Sone, C., Saito, K., and Futakuchi, K. (2009). Comparison of Three Methods for Estimating Leaf Area Index of Upland Rice Cultivars. *Crop Science - CROP SCI, 49*. doi:10.2135/cropsci2008.09.0520

Sonobe, R., Yamaya, Y., Tani, H., Wang, X., Kobayashi, N., and Mochizuki, K.-i. (2018). Crop classification from Sentinel-2-derived vegetation indices using ensemble learning. *Journal of Applied Remote Sensing, 12*(2), 026019-026019.

Stark, S. C., Leitold, V., Wu, J. L., Hunter, M. O., de Castilho, C. V., Costa, F. R., and Saleska, S. R. (2012). Amazon forest carbon dynamics predicted by profiles of canopy leaf area and light environment. *Ecology letters*, *15*(12), 1406-1414.

Steduto, P., Hsiao, T., Raes, C. D. and Fereres, E., (2009). AquaCrop – the FAO crop model to simulate yield response to water: I. Con cepts and underlying principles. *Agronomy Journal*, 2009, 101, 426–437.

Stroppiana, D., Boschetti, M., Confalonieri, R., Bocchi, S., and Brivio, P. A. (2006). Evaluation of LAI-2000 for leaf area index monitoring in paddy rice. *Field Crops Research*, *99*(2-3), 167-170.

Sudharsan, D., Adinarayana, J., Reddy, D. R., Sreenivas, G., Ninomiya, S., Hirafuji, M., and Merchant, S. N. (2013). Evaluation of weather-based rice yield models in India. *International Journal of Biometeorology*, *57*, 107-123.

Tashiro, T. W. I. F., and Wardlaw, I. F. (1991). The effect of high temperature on kernel dimensions and the type and occurrence of kernel damage in rice. *Australian Journal of Agricultural Research*, *42*(3), 485-496.

Teluguntla, P., Thenkabail, P. S., Xiong, J., Gumma, M. K., Congalton, R. G., Oliphant, A., and Massey, R. (2017). Spectral matching techniques (SMTs) and automated cropland classification algorithms (ACCAs) for mapping croplands of Australia using MODIS 250-m time-series (2000–2015) data. *International Journal of Digital Earth*, *10*(9), 944-977.

Timsina, J., and Humphreys, E. J. A. S. (2006). Performance of CERES-Rice and CERES-Wheat models in rice–wheat systems: A review. *Agricultural systems*, *90*(1-3), 5-31.

Timsina, J., Godwin, D., Humphreys, E., Yadvinder-Singh, Bijay Singh, Kukal, S. S. and Smith, D. (2008). Evaluation of options for increasing yield and water productivity of wheat in Punjab, India using the DSSAT-CSM-CERES-wheat model. *Agricultural Water Management*., , 95, 1099–1110.

Tripathy, R., Chaudhari, K.N., Mukherjee, J., Ray, S.S., Patel, N.K., Panigrahy, S and Parihar, J.S. (2013). Forecasting wheat yield in Punjab state of India by combining crop simulation model WOFOST and remotely sensed inputs. *Remote Sensing letters*. 4(1): 19-28.

U.S. Department of Agriculture. FY (2021). Performance Report; U.S. Department of Agriculture: Washington, DC, USA, 2021.

Vikhe, S. D., and Patil, K. A. (2016). Land use/land cover classification and change detection using geographical information system: a case study. *International Journal of Civil Engineering and Technology*, *7*(3), 329-336.

Vilayvong, S., Banterng, P., Patanothai, A., and Pannangpetch, K. (2015). CSM-CERES-Rice model to determine management strategies for lowland rice production. *Scientia Agricola*, *72*, 229-236.

Wang, L., Dong, Q., Yang, L., Gao, J., and Liu, J. (2019). Crop classification based on a novel feature filtering and enhancement method. *Remote Sensing*, *11*(4), 455.

Watson, D.J. (1947). Comparative physiological studies in the growth of field crops. In: Variation in net assimilation rate and leaf area between species and varieties, and within and between years. *Annals of Botany*, 11:41-76.

Wilhelm, W. W., Ruwe, K., and Schlemmer, M. R. (2000). Comparison of Three Leaf Area Index Meters in a Corn Canopy. *Crop Science, 40*. doi:10.2135/cropsci2000.4041179x

Willmott, C.J., Ackleson, S.G., Davis, R.E., Feddema, J.J., Klink, K.M., Legates, D.R., O'Connell, J., Rowe, C.M., (1985). Statistics for the evaluation and comparison of models. *Journal of Geophysical Research*, 90, 8995–9005.

Xavier, A.C and Vettorazzi, C.A. (2004). Mapping leaf area index through spectral vegetation indices in a subtropical watershed. *International Journal of Remote Sensing*. 25(9): 1661-1672.

Xiao, X., He, L., Salas, W., Li, C., Moore Iii, B., Zhao, R., and Boles, S. (2002). Quantitative relationships between field-measured leaf area index and vegetation index derived from vegetation images for paddy rice fields. *International Journal of Remote Sensing*, *23*(18), 3595-3604.

Xiong, W., Balkovic, J., van der Velde, M., Zhang, X., Izaurralde, R. C., Skalský, R., and Obersteiner, M. (2014). A calibration procedure to improve global rice yield simulations with EPIC. *Ecological modelling*, *273*, 128-139.

Yan, G., Hu, R., Luo, J., Weiss, M., Jiang, H., Mu, X., and Zhang, W. (2019). Review of indirect optical measurements of leaf area index: Recent advances, challenges, and perspectives. *Agricultural and forest meteorology*, *265*, 390-411.

Yang, X., Brown, H.E., Teixeira, E and Moot, D.J. (2021). Development of a lucerne model in APSIM next generation: 1 phenology and morphology of genotypes with different fall dormancies. *European Journal of Agronomy*. 130: 126372.

Yi, Z., Jia, L., and Chen, Q. (2020). Crop classification using multi-temporal Sentinel-2 data in the Shiyang River Basin of China. *Remote Sensing*, *12*(24), 4052.

Yu, Y., Wang, J., Liu, G., and Cheng, F. (2019). Forest Leaf Area Index inversion based on landsat OLI data in the Shangri-La City. *Journal of the Indian Society of Remote Sensing*, 47, 967–976.

Yuan, S., Peng, S. and Li, T. (2017). Evaluation and application of the ORYZA rice model under different crop managements with high yielding rice cultivars in central China. *Field Crops Research*, 212(1), 115–125; doi:10.1016/j.fcr.2017.07.010.

Zhao, Y., Potgieter, A. B., Zhang, M., Wu, B., and Hammer, G. L. (2020). Predicting wheat yield at the field scale by combining high-resolution Sentinel-2 satellite imagery and crop modelling. *Remote Sensing*, 12, 1024.

Zheng, B., Myint, S. W., Thenkabail, P. S., and Aggarwal, R. M. (2015). A support vector machine to identify irrigated crop types using time-series Landsat NDVI data. *International Journal of Applied Earth Observation and Geoinformation*, *34*, 103-112.

Zhong, X. Y., Li, Q. P., Yang, F., Chen, D., He, L. H., Yang, Z. P., and Ren, W. J. (2022). Higher solar radiation and lower temperature enhance biomass production and grain yield of rice under high-altitude condition. *Archives of Agronomy and Soil Science*, *68*(12), 1664-1680.

Zhou, X., Zheng, H. B., Xu, X. Q., He, J. Y., Ge, X. K., Yao, X., and Tian, Y. C. (2017). Predicting grain yield in rice using multi-temporal vegetation indices from UAV-based multispectral and digital imagery. *ISPRS Journal of Photogrammetry and Remote Sensing*, *130*, 246-255.

https://www.isric.org

https://www.telangana.gov.in/

https://sites.google.com/a/irri.org/oryza2000/

https://agri.telangana.gov.in/

APPENDICES

APPENDIX-I

Mean weekly meteorological data during the crop growing season in Elbaka village

SMW*	Sunshine hours	Max Temperature °C	Min. Temperature °C	Rainfall (mm)
22	21.6	40.1	28.4	0.3
23	17.7	32.5	24.6	13.0
24	19.4	33.3	23.8	8.7
25	17.8	31.5	23.5	1.8
26	21.6	40.1	28.4	17.7
27	17.7	32.5	24.6	0.2
28	19.4	33.3	23.8	16.2
29	17.8	31.5	23.5	27.1
30	16.3	30.3	23.6	4.4
31	19.0	32.2	23.1	0.0
32	13.5	29.5	24.9	0.5
33	14.6	29.8	24.4	3.9
34	8.1	25.7	24.0	5.9
35	12.9	30.0	25.7	23.7
36	16.1	31.9	25.1	15.5
37	16.4	34.1	27.0	0.4
38	13.9	29.8	24.6	7.5
39	16.8	31.9	24.0	28.1
40	17.0	32.0	24.0	0.0
41	15.3	32.2	25.3	0.0
42	16.4	32.6	24.3	10.5
43	15.9	31.6	23.4	0.0

Mean weekly meteorological data during the crop growing season in Gangipalli Village

SMW*	Sunshine hours	Max Temperature ℃	Min. Temperature ℃	Rainfall (mm)
22	22.6	41.2	28.4	1.0
23	17.7	32.5	24.6	4.7
24	19.4	33.0	23.5	13.5
25	17.8	31.2	23.2	1.0
26	15.6	30.5	24.4	8.9
27	19.7	32.8	23.0	8.7
28	13.9	30.3	25.4	16.2
29	15.9	30.9	24.5	10.9
30	8.8	26.0	24.0	17.8
31	12.4	29.6	25.6	0.0
32	15.3	31.2	25.1	0.3
33	16.6	34.2	26.9	4.4
34	13.5	29.4	24.5	9.6
35	16.7	31.6	23.8	18.8
36	16.1	31.4	24.0	13.0
37	15.2	32.0	25.2	0.6
38	16.7	32.7	24.1	7.6
39	15.9	31.7	23.5	15.4
40	17.0	34.3	24.5	0.0
41	17.7	35.7	24.4	0.0
42	19.1	34.9	20.9	5.6
43	18.5	33.9	20.0	0.0

Mean weekly meteorological data during the crop growing season in Rukmapur and Vedurugattu Village

SMW*	Sunshine hours	Max Temperature ℃	Min. Temperature ℃	Rainfall (mm)
22	22.3	42.1	29.6	0.7
23	17.0	33.8	26.5	5.9
24	19.8	34.3	24.5	11.4
25	15.3	32.7	26.8	0.5
26	17.0	32.6	25.3	14.7
27	20.3	34.3	23.9	6.9
28	10.1	30.2	27.6	10.5

29	13.3	31.8	27.3	13.2
30	8.8	27.4	25.4	16.3
31	12.4	30.9	26.9	0.0
32	16.6	34.1	26.9	2.4
33	15.8	34.6	28.0	2.7
34	13.3	30.6	25.8	6.5
35	14.0	31.3	25.7	17.7
36	12.3	30.1	25.8	23.8
37	15.9	34.3	26.8	1.0
38	17.0	34.4	25.5	5.9
39	14.2	31.8	25.3	13.7
40	15.0	34.5	26.8	1.7
41	15.6	34.7	25.9	0.1
42	17.6	34.7	22.8	1.6
43	17.1	33.3	21.4	0.0

Mean weekly meteorological data during the crop growing season in Durshed Village

SMW*	Sunshine hours	Max Temperature ℃	Min. Temperature ℃	Rainfall (mm)
40	16.41	34.26	24.84	1.29
41	17.05	34.06	23.27	0.00
42	15.66	32.87	23.10	3.97
43	17.91	32.89	19.43	0.00
44	16.22	32.16	20.34	0.19
45	17.09	31.74	17.80	0.00
46	13.43	32.29	23.20	0.54
47	13.56	32.46	22.66	0.37
48	15.37	31.21	18.08	0.00
49	15.65	31.92	17.93	0.00
50	15.31	30.24	16.63	0.00
51	16.81	28.69	12.16	0.00
52	15.23	30.43	16.93	0.00
1	15.32	29.34	16.06	0.00
2	12.15	27.69	19.41	4.11
3	28.24	17.36	0.61	3.00
4	29.27	15.66	0.00	4.00
5	18.44	30.41	14.46	0.00
6	30.19	16.56	0.00	6.00
7	17.63	29.77	16.86	0.00
8	32.71	18.39	0.00	8.00

9	19.45	32.62	18.83	0.00
10	20.05	33.51	19.67	0.00
11	22.54	36.83	20.26	0.00
12	20.23	36.36	23.54	0.00
13	21.22	37.56	24.13	0.00
14	20.21	35.87	24.21	0.00
15	20.75	36.30	24.41	0.00
16	22.38	39.80	26.33	0.00
17	22.48	39.90	26.50	0.21

Mean weekly meteorological data during the crop growing season in Nagnur Village

SMW*	Sunshine hours	Max Temperature ℃	Min. Temperature ℃	Rainfall (mm)
40	14.97	33.06	25.23	1.29
41	16.07	32.94	23.33	0.00
42	15.08	32.30	23.11	3.97
43	17.48	31.77	18.94	0.00
44	15.40	32.21	21.57	0.19
45	15.83	31.64	19.69	0.00
46	12.78	32.13	23.87	0.54
47	12.96	32.60	23.67	0.37
48	14.44	31.45	19.86	0.00
49	14.77	32.08	19.62	0.00
50	14.63	29.96	17.49	0.00
51	16.76	27.34	10.91	0.00
52	14.18	29.11	17.35	0.00
1	14.60	27.83	15.74	0.00
2	10.91	26.51	19.93	4.11
3	27.17	16.70	0.61	28.24
4	27.84	15.20	0.00	29.27
5	18.13	29.14	13.66	0.00
6	28.83	16.60	0.00	30.19
7	17.36	28.90	16.30	0.00
8	31.36	18.74	0.00	32.71
9	18.51	32.23	19.72	0.00
10	19.55	32.74	19.56	0.00
11	21.30	34.30	19.50	0.00
12	19.15	35.30	23.86	0.00
13	20.03	36.40	24.40	0.00

14	18.79	35.30	25.23	0.00
15	19.48	35.74	25.29	0.00
16	20.52	38.14	26.83	0.00
17	20.61	38.31	27.03	0.21

Mean weekly meteorological data during the crop growing season in Renikunta Village

SMW*	Sunshine hours	Max Temperature °C	Min. Temperature °C	Rainfall (mm)
40	16.84	34.01	24.10	0.00
41	18.31	34.40	21.91	0.19
42	16.83	33.41	22.10	4.84
43	18.10	33.14	19.40	0.00
44	16.27	32.33	20.44	0.64
45	16.80	31.50	18.00	0.00
46	12.98	31.51	23.03	2.30
47	13.15	31.80	22.54	0.00
48	15.42	31.53	18.28	0.00
49	16.09	32.17	17.40	0.00
50	15.79	31.06	16.56	0.00
51	17.24	29.07	11.70	0.00
52	15.33	31.41	17.74	0.00
1	15.48	29.86	16.27	0.00
2	12.67	28.44	19.44	2.81
3	3.00	28.45	14.08	27.17
4	4.00	29.06	15.90	27.84
5	18.36	30.21	14.39	0.00
6	6.00	30.23	16.49	28.83
7	18.07	30.09	16.57	0.00
8	8.00	31.25	17.99	31.36
9	19.60	32.55	18.58	0.00
10	20.28	33.46	19.30	0.00
11	21.79	35.41	19.93	0.00
12	20.56	36.41	23.23	0.00
13	21.18	37.00	23.63	0.00
14	20.97	36.21	23.64	0.00
15	21.15	36.43	24.09	0.00
16	21.95	39.09	26.13	0.00
17	22.24	38.93	25.83	0.00

Mean weekly meteorological data during the crop growing season in Malkapur Village

SMW*	Sunshine hours	Max Temperature °C	Min. Temperature °C	Rainfall (mm)
40	14.79	33.03	25.39	4.33
41	16.31	33.21	23.33	0.44
42	15.25	32.29	22.94	7.03
43	17.41	32.34	19.63	0.00
44	15.63	31.84	20.87	0.00
45	16.53	31.36	18.33	0.00
46	12.82	31.67	23.37	2.09
47	13.15	32.26	23.04	0.00
48	14.71	30.86	18.81	0.00
49	15.08	31.80	18.77	0.00
50	14.71	29.94	17.37	0.00
51	16.29	28.40	12.90	0.00
52	14.39	30.00	17.91	0.00
1	14.83	29.41	16.97	0.00
2	11.58	27.47	20.01	9.56
3	28.24	17.36	0.61	3.00
4	29.27	15.66	0.00	4.00
5	18.10	30.84	15.46	0.00
6	30.19	16.56	0.00	6.00
7	17.08	30.37	18.29	0.00
8	32.71	18.39	0.00	8.00
9	19.53	33.05	19.17	0.00
10	19.74	33.84	20.41	0.00
11	21.81	36.21	20.66	0.00
12	20.39	36.83	23.90	0.00
13	21.45	38.11	24.36	0.00
14	19.95	36.31	24.96	0.00
15	22.16	38.39	24.83	0.00
16	22.71	40.54	26.69	0.00
17	21.95	39.77	26.91	0.00

APPENDIX-II

Questionnaire for crop data collection

Farmer details Name and address Contact no	
Location of Plot	
Area of land holding	
Previous crop sown	
Soil type	
Soil nutrient status	
Variety name and duration	
Date of transplanting /sowing	
Irrigation details No. of irrigations Stages of irrigation	
Fertilizer details Rate of application Stage of application with quantity	
Organic amendments (if any applied)	
Pest and disease attack (if any) Name and quantity of insecticides/ pesticides used	
Date of harvesting	
Yield (Kg/ha)	
Soil health card Details	

APPENDIX-III

GEE code for downloading NDVI values of karimnagar in Kharif season

```
function addNDVI(image) {
var ndvi = image.normalizedDifference(['B8', 'B4']).rename('ndvi')
return ndvi
}

//Sentinel2
var aug_1 = ee.ImageCollection('COPERNICUS/S2_SR')
.filterDate('2021-08-01','2021-08-02')
//.filter(ee.Filter.lt('CLOUDY_PIXEL_PERCENTAGE',20))
//.map(maskS2clouds)
.filterBounds(table).map(addNDVI).max().clip(table);

var aug_2 = ee.ImageCollection('COPERNICUS/S2_SR')
.filterDate('2021-08-06','2021-08-07')
//.filter(ee.Filter.lt('CLOUDY_PIXEL_PERCENTAGE',20))
//.map(maskS2clouds)
.filterBounds(table).map(addNDVI).max().clip(table);

var aug_3 = ee.ImageCollection('COPERNICUS/S2_SR')
.filterDate('2021-08-11','2021-08-12')
//.filter(ee.Filter.lt('CLOUDY_PIXEL_PERCENTAGE',  20))
//.map(maskS2clouds)
.filterBounds(table).map(addNDVI).max().clip(table);
```

```
var aug_4 = ee.ImageCollection('COPERNICUS/S2_SR')
.filterDate('2021-08-16','2021-08-17')
//.filter(ee.Filter.lt('CLOUDY_PIXEL_PERCENTAGE',  20))
//.map(maskS2clouds)
.filterBounds(table).map(addNDVI).max().clip(table);

var aug_5 = ee.ImageCollection('COPERNICUS/S2_SR')
.filterDate('2021-08-21','2021-08-22')
//.filter(ee.Filter.lt('CLOUDY_PIXEL_PERCENTAGE',  20))
//.map(maskS2clouds)
.filterBounds(table).map(addNDVI).max().clip(table);
var aug_6 = ee.ImageCollection('COPERNICUS/S2_SR')
.filterDate('2021-08-26','2021-08-27')
//.filter(ee.Filter.lt('CLOUDY_PIXEL_PERCENTAGE', 20))
//.map(maskS2clouds)
.filterBounds(table).map(addNDVI).max().clip(table);
var aug_7 = ee.ImageCollection('COPERNICUS/S2_SR')
.filterDate('2021-08-30','2021-08-31')
//.filter(ee.Filter.lt('CLOUDY_PIXEL_PERCENTAGE',  20))
//.map(maskS2clouds)
.filterBounds(table).map(addNDVI).max().clip(table);
var sep_1 = ee.ImageCollection('COPERNICUS/S2_SR')
.filterDate('2021-09-05','2021-09-06')
//.filter(ee.Filter.lt('CLOUDY_PIXEL_PERCENTAGE',  20))
//.map(maskS2clouds)
.filterBounds(table).map(addNDVI).max().clip(table);
var sep_2 = ee.ImageCollection('COPERNICUS/S2_SR')
```

```
.filterDate('2021-09-10','2021-09-11')
//.filter(ee.Filter.lt('CLOUDY_PIXEL_PERCENTAGE',  20))
//.map(maskS2clouds)
.filterBounds(table).map(addNDVI).max().clip(table);
var sep_3 = ee.ImageCollection('COPERNICUS/S2_SR')
.filterDate('2021-09-15','2021-09-16')
//.filter(ee.Filter.lt('CLOUDY_PIXEL_PERCENTAGE',  20))
//.map(maskS2clouds)
.filterBounds(table).map(addNDVI).max().clip(table)
var sep_4 = ee.ImageCollection('COPERNICUS/S2_SR')
.filterDate('2021-09-20','2021-09-21')
//.filter(ee.Filter.lt('CLOUDY_PIXEL_PERCENTAGE',  20))
//.map(maskS2clouds)
.filterBounds(table).map(addNDVI).max().clip(table)
var sep_5 = ee.ImageCollection('COPERNICUS/S2_SR')
.filterDate('2021-09-25','2021-09-26')
//.filter(ee.Filter.lt('CLOUDY_PIXEL_PERCENTAGE',  20))
//.map(maskS2clouds)
.filterBounds(table).map(addNDVI).max().clip(table)
var sep_6 = ee.ImageCollection('COPERNICUS/S2_SR')
.filterDate('2021-09-30','2021-10-01')
//.filter(ee.Filter.lt('CLOUDY_PIXEL_PERCENTAGE', 20))
//.map(maskS2clouds)
.filterBounds(table).map(addNDVI).max().clip(table)
var oct_1 = ee.ImageCollection('COPERNICUS/S2_SR')
.filterDate('2021-10-05','2021-10-06')
//.filter(ee.Filter.lt('CLOUDY_PIXEL_PERCENTAGE',  20))
```

```
//.map(maskS2clouds)
.filterBounds(table).map(addNDVI).max().clip(table)
var oct_2 = ee.ImageCollection('COPERNICUS/S2_SR')
.filterDate('2021-10-10','2021-10-11')
//.filter(ee.Filter.lt('CLOUDY_PIXEL_PERCENTAGE',   20))
//.map(maskS2clouds)
.filterBounds(table).map(addNDVI).max().clip(table)
var oct_3 = ee.ImageCollection('COPERNICUS/S2_SR')
.filterDate('2021-10-15','2021-10-16')
//.filter(ee.Filter.lt('CLOUDY_PIXEL_PERCENTAGE',   20))
//.map(maskS2clouds)
.filterBounds(table).map(addNDVI).max().clip(table)
var oct_4 = ee.ImageCollection('COPERNICUS/S2_SR')
.filterDate('2021-10-25','2021-10-26')
//.filter(ee.Filter.lt('CLOUDY_PIXEL_PERCENTAGE',   20))
//.map(maskS2clouds)
.filterBounds(table).map(addNDVI).max().clip(table)
var oct_5 = ee.ImageCollection('COPERNICUS/S2_SR')
.filterDate('2021-10-30','2021-10-31')
//.filter(ee.Filter.lt('CLOUDY_PIXEL_PERCENTAGE',   20))
//.map(maskS2clouds)
.filterBounds(table).map(addNDVI).max().clip(table)
//var cropmask = ndvi_Nalgonnda.gt(0.5)
//Map.addLayer(cropmask)

Map.addLayer(table)
```

```
var stack =aug_1.addBands(aug_2).addBands(aug_3).addBands(aug_4)
.addBands(aug_5).addBands(aug_6).addBands(aug_7).addBands(sep_1).addBands(sep_2)
.addBands(sep_3).addBands(sep_4).addBands(sep_5).addBands(sep_6).addBands(oct_1)
.addBands(oct_2).addBands(oct_3).addBands(oct_4).addBands(oct_5)
var points = stack.reduceRegions({
collection: table2,
reducer: ee.Reducer.median(),
scale: 10,  // meters
crs: 'EPSG:4326',
})

Map.addLayer(points)
print(points)
Export.table.toDrive(
points,
"table2",
"table2",
"table2");
```

APPENDIX-IV

GEE code for downloading NDVI values of karimnagar in Rabi season

```
var table = ee.FeatureCollection("users/Roja/karimanagar"),
table2 = ee.FeatureCollection("users/Roja/rabi_polygons");
function addNDVI(image) {
var ndvi = image.normalizedDifference(['B8', 'B4']).rename('ndvi')
return ndvi
}
var Jan_1 = ee.ImageCollection('COPERNICUS/S2_SR')
.filterDate('2022-01-01','2022-01-15')
//.filter(ee.Filter.lt('CLOUDY_PIXEL_PERCENTAGE',20))
//.map(maskS2clouds)
.filterBounds(table).map(addNDVI).max().clip(table);

var Jan_2 = ee.ImageCollection('COPERNICUS/S2_SR')
.filterDate('2022-01-16','2022-01-31')
//.filter(ee.Filter.lt('CLOUDY_PIXEL_PERCENTAGE',20))
//.map(maskS2clouds)
.filterBounds(table).map(addNDVI).max().clip(table);

var Feb_1 = ee.ImageCollection('COPERNICUS/S2_SR')
.filterDate('2022-02-01','2022-02-15')
//.filter(ee.Filter.lt('CLOUDY_PIXEL_PERCENTAGE', 20))
//.map(maskS2clouds)
.filterBounds(table).map(addNDVI).max().clip(table);

var Feb_2 = ee.ImageCollection('COPERNICUS/S2_SR')
```

```
.filterDate('2022-02-16','2022-02-28')
//.filter(ee.Filter.lt('CLOUDY_PIXEL_PERCENTAGE',  20))
//.map(maskS2clouds)
.filterBounds(table).map(addNDVI).max().clip(table);

var Mar_1 = ee.ImageCollection('COPERNICUS/S2_SR')
.filterDate('2022-03-01','2022-03-15')
//.filter(ee.Filter.lt('CLOUDY_PIXEL_PERCENTAGE',  20))
//.map(maskS2clouds)
.filterBounds(table).map(addNDVI).max().clip(table);
var Mar_2 = ee.ImageCollection('COPERNICUS/S2_SR')
.filterDate('2022-03-16','2022-03-31')
//.filter(ee.Filter.lt('CLOUDY_PIXEL_PERCENTAGE',  20))
//.map(maskS2clouds)
.filterBounds(table).map(addNDVI).max().clip(table);
var Apr_1 = ee.ImageCollection('COPERNICUS/S2_SR')
.filterDate('2022-04-01','2022-04-15')
//.filter(ee.Filter.lt('CLOUDY_PIXEL_PERCENTAGE', 20))
//.map(maskS2clouds)
.filterBounds(table).map(addNDVI).max().clip(table);
var Apr_2 = ee.ImageCollection('COPERNICUS/S2_SR')
.filterDate('2022-04-16','2022-04-30')
//.filter(ee.Filter.lt('CLOUDY_PIXEL_PERCENTAGE',  20))
//.map(maskS2clouds)
.filterBounds(table).map(addNDVI).max().clip(table);
var May_1 = ee.ImageCollection('COPERNICUS/S2_SR')
.filterDate('2022-05-01','2022-05-15')
```

```
//.filter(ee.Filter.lt('CLOUDY_PIXEL_PERCENTAGE',  20))
//.map(maskS2clouds)
.filterBounds(table).map(addNDVI).max().clip(table);
var May_2 = ee.ImageCollection('COPERNICUS/S2_SR')
.filterDate('2022-05-16','2022-05-31')
//.filter(ee.Filter.lt('CLOUDY_PIXEL_PERCENTAGE',  20))
//.map(maskS2clouds)
.filterBounds(table).map(addNDVI).max().clip(table);
//var sep_4 = ee.ImageCollection('COPERNICUS/S2_SR')
//.filterDate('2021-09-20','2021-09-21')
//.filter(ee.Filter.lt('CLOUDY_PIXEL_PERCENTAGE',  20))
//.map(maskS2clouds)
//.filterBounds(table).map(addNDVI).max().clip(table)
//var sep_5 = ee.ImageCollection('COPERNICUS/S2_SR')
//.filterDate('2021-09-25','2021-09-26')
//.filter(ee.Filter.lt('CLOUDY_PIXEL_PERCENTAGE',  20))
//.map(maskS2clouds)
//.filterBounds(table).map(addNDVI).max().clip(table)
//var sep_6 = ee.ImageCollection('COPERNICUS/S2_SR')
//.filterDate('2021-09-30','2021-10-01')
//.filter(ee.Filter.lt('CLOUDY_PIXEL_PERCENTAGE',  20))
//.map(maskS2clouds)
//.filterBounds(table).map(addNDVI).max().clip(table)
//var oct_1 = ee.ImageCollection('COPERNICUS/S2_SR')
//.filterDate('2021-10-05','2021-10-06')
//.filter(ee.Filter.lt('CLOUDY_PIXEL_PERCENTAGE',  20))
//.map(maskS2clouds)
```

```
//.filterBounds(table).map(addNDVI).max().clip(table)
//var oct_2 = ee.ImageCollection('COPERNICUS/S2_SR')
//.filterDate('2021-10-10','2021-10-11')
//.filter(ee.Filter.lt('CLOUDY_PIXEL_PERCENTAGE',  20))
//.map(maskS2clouds)
//.filterBounds(table).map(addNDVI).max().clip(table)
//var oct_3 = ee.ImageCollection('COPERNICUS/S2_SR')
//.filterDate('2021-10-15','2021-10-16')
//.filter(ee.Filter.lt('CLOUDY_PIXEL_PERCENTAGE',  20))
//.map(maskS2clouds)
// .filterBounds(table).map(addNDVI).max().clip(table)
//var oct_4 = ee.ImageCollection('COPERNICUS/S2_SR')
//.filterDate('2021-10-25','2021-10-26')
//.filter(ee.Filter.lt('CLOUDY_PIXEL_PERCENTAGE',  20))
//.map(maskS2clouds)
//.filterBounds(table).map(addNDVI).max().clip(table)
//var oct_5 = ee.ImageCollection('COPERNICUS/S2_SR')
//.filterDate('2021-10-30','2021-10-31')
//.filter(ee.Filter.lt('CLOUDY_PIXEL_PERCENTAGE',  20))
//.map(maskS2clouds)
// .filterBounds(table).map(addNDVI).max().clip(table)
//var cropmask = ndvi_Nalgonnda.gt(0.5)
//Map.addLayer(cropmask)

Map.addLayer(table)

var stack =Jan_1.addBands(Jan_2).addBands(Feb_1).addBands(Feb_2)
```

```
.addBands(Mar_1).addBands(Mar_2).addBands(Apr_1).addBands(Apr_2).addBands(May_1)
.addBands(May_2)
var points = stack.reduceRegions({
collection: table2,
reducer: ee.Reducer.median(),
scale: 10,  // meters
crs: 'EPSG:4326',
})
Map.addLayer(points)
print(points)
Export.table.toDrive(
points,
"table2",
"table2",
"table2");
```